BRNO UNIVERSITY OF TECHNOLOGY

VYSOKÉ UČENÍ TECHNICKÉ V BRNĚ

FACULTY OF ELECTRICAL ENGINEERING AND COMMUNICATION

FAKULTA ELEKTROTECHNIKY
A KOMUNIKAČNÍCH TECHNOLOGIÍ

DEPARTMENT OF RADIO ELECTRONICS

ÚSTAV RADIOELEKTRONIKY

TEXTILE INTEGRATED WAVEGUIDE COMPONENTS

KOMPONENTY NA BÁZI VLNOVODU INTEGROVANÉHO DO TEXTILU

DOCTORAL THESIS
DISERTAČNÍ PRÁCE

AUTHOR   Ing. Miroslav Cupal
AUTOR PRÁCE

SUPERVISOR   prof. Dr. Ing. Zbyněk Raida
ŠKOLITEL

BRNO 2020

ABSTRACT

The thesis is focused on the research of structures based on the Textile Integrated Waveguide (TIW). Attention is turned to the electrical characterization of textile materials (textile substrates, yarns) to be used for the implementation of textile-integrated antennas, reconfigurable and active circuits. The thesis deals with the design of multilayer transitions between a microstrip line on a conventional substrate and textile-integrated lines. Second, a concept of the textile-integrated switch is presented. The switch is controlled by conductive posts which are connected or disconnected by DC driven PIN diodes to form open or closed walls. Finally, the design methodology for textile-integrated circularly polarized antennas operating in ISM bands up to 24 GHz is proposed.

All the design procedures were verified by simulations and measurements of real samples manufactured by screen-printing using a silver polymer paste. For bonding semiconductor components, conductive silver adhesives were used. Screen-printed components were compared with reference structures manufactured from a self-adhesive copper foil.

KEYWORDS

Textile integrated waveguide (TIW), 3D knitted fabric, conductive yarn, screen-printing, conductive adhesive, circularly polarized antenna, reconfigurable switch, transition from conventional to textile-integrated line.

ABSTRAKT

Práce je zaměřena na výzkum struktur založených na vlnovodu integrovaném do textilu (TIW). Pozornost je věnována elektrické charakterizaci textilních materiálů (textilní substráty, nitě), které jsou využívány při implementaci antén, rekonfigurovatelných a aktivních obvodů integrovaných do textilu. Práce se zabývá návrhem vícevrstvých přechodů mezi mikropáskovým vedením na konvenčním substrátu a vedeními integrovanými do textilu. Dále je prezentován koncept přepínače integrovaného do textilu. Přepínač je řízen vodivými sloupky, které vytvářejí otevřenou či zavřenou stěnu prostřednictvím stejnosměrně ovládaných PIN diod. Na závěr je formulována metodika návrhu kruhově polarizovaných antén integrovaných do textilu, jež jsou určeny pro práci v ISM pásmech až do 24 GHz.

Všechny postupy návrhu byly ověřeny simulacemi a měřeními reálných vzorků, které byly vyrobeny sítotiskem stříbrnou polymerovou pastou. Polovodičové komponenty byly k obvodům přilepeny vodivým stříbrným lepidlem. Komponenty vyrobené sítotiskem byly porovnávány s referenčními strukturami, které byly realizovány pomocí samolepicí měděné fólie.

KLÍČOVÁ SLOVA

Vlnovod integrovaný do textilu (TIW), 3D tkaná textilie, vodivá nit, sítotisk, vodivé lepidlo, kruhově polarizovaná anténa, rekonfigurovatelný přepínač, přechod z konvenčního vedení na vedení integrované do textilu.

DECLARATION

I declare that I have written the Doctoral Thesis titled "Neural Modeling of Electromagnetic Fields in Cars" independently, under the guidance of the advisor and using exclusively the technical references and other sources of information cited in the thesis and listed in the comprehensive bibliography at the end of the thesis.

As the author I furthermore declare that, with respect to the creation of this Doctoral Thesis, I have not infringed any copyright or violated anyone's personal and/or ownership rights. In this context, I am fully aware of the consequences of breaking Regulation § 11 of the Copyright Act No. 121/2000 Coll. of the Czech Republic, as amended, and of any breach of rights related to intellectual property or introduced within amendments to relevant Acts such as the Intellectual Property Act or the Criminal Code, Act No. 40/2009 Coll., Section 2, Head VI, Part 4.

Brno, the 25th of February 2020   ………………………………….

                                                                          Author's signature

ACKNOWLEDGEMENT

Brno   ………………..   …………………………
                                                                       Miroslav Cupal

Contents

Introduction

The integration of electronic devices into clothing and textile materials became popular in the late 1990s with the spread of wearable devices and local body area networks. The first textile antennas and other textile components were designed for military, space and healthcare applications. Researchers and companies were focused on the characterization of textile materials, development of conductive textiles, conductive yarns, and complete textile electronic solutions.

The majority of textile-integrated electronics (TIE) can be found in wearable applications. Attention is paid to manufacturing technologies, integration to clothes, biological effects, influence of human body on antenna parameters, launder-ability, abrasion, mechanical stability, etc. Nevertheless, TIE can be also integrated into upholstery in homes, cars, trains or airplanes. The dissertation thesis deals with the non-wearable exploitation of TIE and is dominantly focused on vehicular applications.

The role of the textile substrate is played by the three-dimensional (3D) knitted fabrics. The 3D fabric is used as an equivalent of a conventional microwave substrate. As an equivalent of a substrate-integrated waveguide (SIW), a textile-integrated waveguide (TIW) can be created and can be used as a fundamental building block of textile-integrated structures.

TIW can be integrated into textile covers of seats and textile upholstery of trains, airplanes and buses to create a local communication network. TIW can provide services for passengers or can be used as a backup for control and sensor systems. Each seat in a vehicle can contain a tablet, a sensor network for passenger's personal use and other electronic components to be connected. TIW can create a wired local network within the seat and further communication can be provided by a wireless link. Textile antennas and textile microwave components seem to be a promising way to implement the described local networks.

Next to the wireless interface, attention is turned to the development of textile-to-substrate transitions enabling to create also a wired connection of TIE.

Implementation of TIE can become a part of the manufacturing process of textile materials. Such multi-functional fabrics can be then used not only for attenuating mechanical vibrations, providing thermal insulation and conventional utility properties but also can yield communication and sensory resources. The use of multi-functional textile materials can significantly reduce manufacturing and assembling costs.

The dissertation thesis is mainly aimed to research technologies to be used for the design and implementation of advanced TIW and TIW-based radio-frequency (RF) components. Attention is turned to the development of new components for industrial, scientific and medical (ISM) bands 2.4 GHz, 5.8 GHz and 24 GHz.

1 State of the Art

In the open literature, the reader can find several papers focused on the characterization of textile materials, on manufacturing textile-integrated electronics (TIE), and textile-integrated components (antennas, waveguides, sensors). Papers mostly deal with wearable electronics and the operation close to a human body. Available publications mainly cover the following areas:

- Textile-integrated sensors and electronics,
- Textile-integrated switches and buttons,
- Textile-integrated energy solutions,
- Textile-integrated antennas and microwave components,
- Textile-integrated lights and screens,
- Manufacturing technologies of TIE.

The *State of the Art* is divided into the following parts:

- Textile electronics, the general use and technologies of wearable applications,
- Textile-integrated microwave components,
- Textile-integrated high-frequency antennas,
- Textile-integrated switches,
- Textile-to-conventional line transitions.

1.1 Textile electronics

Clothing, military applications, space products and healthcare systems belong to the main application areas of textile electronics. A heating layer integrated into clothing was the first exploitation of e-textiles. Conductive fibers were knitted into a conventional textile material and were fed by a current to heat the user [1].

These days, more than 300 000 results can be found when searching for the keyword *textile electronics* in the open literature. Most of textile electronic applications are designed for on-body systems and wearable applications, i.e. sensors for medical and sports systems, communication units for smartphones and other devices, localization and for the emergency services, etc. A brief description of basic textile electronic applications follows.

Textile sensors are very popular in the field of healthcare, rehabilitation, and sports. Those sensors can significantly improve the quality of life of elderly and handicapped people by measuring a wide range of health functions.

The sensors can be divided into two groups:

- **Sensors based on conductive yarns or printed technologies** [2, 3]. Conductive and piezo-electric yarns are used to measure electrocardiogram (ECG) signals and monitor

pressure [4], [3]. Conductive yarns are weaved into electrodes and piezo-electric yarns serve as sensors of pressure or tension.

- **Polymer sensors** [5], [6]. Organic polymers excel in low weight, elasticity, chemical resistance and easy processing. Those sensors can be formed into many shapes, can be manufactured by printing, sewing or knitting. The organic polymers can be produced as piezo-resistive, thermo-resistive and magneto-resistive materials. Sensors can be used for measuring ECG and magnetocardiogram (MCG), respiration, electrical impedance or temperature of skin [3, 6].

Textile pressure sensors and switches are the next application field of textile electronics. There are two basic concepts of the switches to control electronic devices:

- **Touch capacitive sensors** can be fabricated as a parallel-plate electrode system with an elastic dielectric layer in between, which changes its capacitance when touched [7, 8]. Alternatively, a soft capacitor fiber can be exploited [2].

- **An open circuit** is created by two electrodes on the surface of a fabric. The electrical circuit is closed by the user when connecting electrodes by a finger [7, 9].

As all the devices, wearable devices need a power supply for their proper work. Solar, thermal and mechanical harvesters can be used and integrated into textile materials similarly like small battery cells [1]. A technique for energy scavenging using piezoelectric nanowires grown radially to textile fibers was described in [10], and the successive research was presented in [11]. Photovoltaic energy can be harvested by flexible photovoltaic yarn cells. Using carbon nanotubes, flexible solar yarns can be constructed [12, 13]. Harvested energy can be stored in flexible battery cells [14] or even in textile energy storage [15].

1.2 Textile-integrated microwave components

The integration of microwave components into textile materials is related to antennas and successive high-frequency circuits. During past years, researchers integrated into diverse textile materials various antennas devoted to different applications and operating at different frequencies. Nevertheless, there is only a limited number of technologies to create conductive components of antennas on textile materials.

Embroidering is one of those manufacturing techniques. Dipoles, patches, and planar inverted F antennas (PIFA) were usually designed for ISM bands 2.4 GHz and 5.8 GHz using different fabrics and different yarns. Some planar monopole antennas for the UWB band were designed for frequencies up to 20 GHz [16]. Papers have been focusing on the manufacturing process and the comparison of conventional antennas and embroidered ones:

- A meandered asymmetric flare dipole on a polyester fabric was presented in [17]. The antenna operated at the frequency 500 MHz, the size of the antenna was 190 mm × 25 mm, and its performance was comparable with the metal version of the same antenna.

- The comparison of fabric dipole antennas operating at 2.4 GHz was presented in [18]. Two embroidered antennas (single-layer and double-layer ones) were compared with a silver-fabric antenna. The gain of the silver-fabric antenna was about 6 dB higher than the gain of the embroidered antenna.

- A circularly polarized spiral antenna designed for the band 420 MHz belongs to more complex antennas [19]. The antenna was fed by a microstrip transmission line.

- Comparison of antennas created on different fabrics and manufactured with the use of various conductive threads is relatively common. Nevertheless, [20] compares the patch antenna designed for 2.4 GHz, which was embroidered using different stitch directions. Due to the losses in conductive threads, the gain of the embroidered patch antennas is lower than the gain of equivalent FR4 antennas.

- The 2.4 GHz PIFAs made from different meshes of conductive threads on different textile materials was presented in [21]. The antennas were compared with the conventional metallic PIFA.

In case of high-frequency components, textile-material printing is an interesting approach since printing technologies allow to achieve a good precision compared with sewing and embroidering. There are two printing methods to be used for manufacturing antennas:

- **The inkjet-printing.** The fabrication of inkjet-printed antennas is difficult because the surface has to be smooth enough and the textile material cannot allow the ink to penetrate. Therefore, the direct inkjet-printing on the textile is rare and was described for a limited number of materials and simple planar antennas [22, 23]. Planar dipoles were printed on Kapton, on a stretchable polyurethane (PU) fabric and on polyester / cotton fabrics with and without interface layers. The efficiency of dipoles varied from 74 % to 31 % depending on materials, interface layers and the number of printed conductive layers.

  In further papers, antennas were inkjet-printed on an interface layer. The interface layers were often made from ultra-violet (UV) durable polymers or polyurethanes, which were screen-printed on textile substrates. The textile substrates stayed flexible after screen-printing the interface layer, their surfaces were smoothened and became impermeable for silver inks [24, 25].

- **The screen-printing.** In textile industry, the screen-printing is used for creating logos and pictures on T-shirts and other products. The screen-printing can be applied directly to a textile material. The screen-printing can be used for manufacturing antennas for different applications and services. In [26], 14 different woven textile substrates and two silver conductive pastes were compared to be used for screen-printing. As shown in [26], the screen-printing pastes can also penetrate into the textiles in some cases. The square resistances were measured and compared in [26], and values between 0.02 $\Omega/\square$ and 0.15 $\Omega/\square$ were obtained. Moreover, the change of the square resistance after 5 000 abrading cycles was described in [26]. The resistance varied from 580% in the worst case to 6% in the best case. The maximum square resistance was smaller than 0.40 $\Omega/\square$. And [26] moreover shows that washing can be an issue: the resistance can grow from ~0.1 $\Omega/\square$ to ~10 $\Omega/\square$.

  A screen-printed patch antenna was presented in [27]. The antenna was printed on two different substrates – on [100% polyester] and on [20% cotton + 80% polyester]. The antenna was printed by pastes with square resistances 0.015 $\Omega/\square$ and 0.025 $\Omega/\square$. The antennas were fabricated with a protective cover layer and without the layer. The antennas were washed 20 times and the reflection coefficient at the antenna input was measured after each 5th cycle. The antenna was well protected up to the 20th washing cycle.

Connecting a sub-miniature-version A (SMA) connector to a textile-integrated antenna is the next issue. Connectors can lose the electrical connection or can become disconnected.

The wearable ultrahigh frequency (UHF) radio-frequency identification (RFID) tag antenna was designed in [28] using a cotton fabric and a cotton / polyester one. The tag was screen-printed by a silver conductive paste. The printed tag was covered by different protective layers (epoxy, silicone, latex, etc.). The realized gain and the theoretical reading range of the antenna were computed.
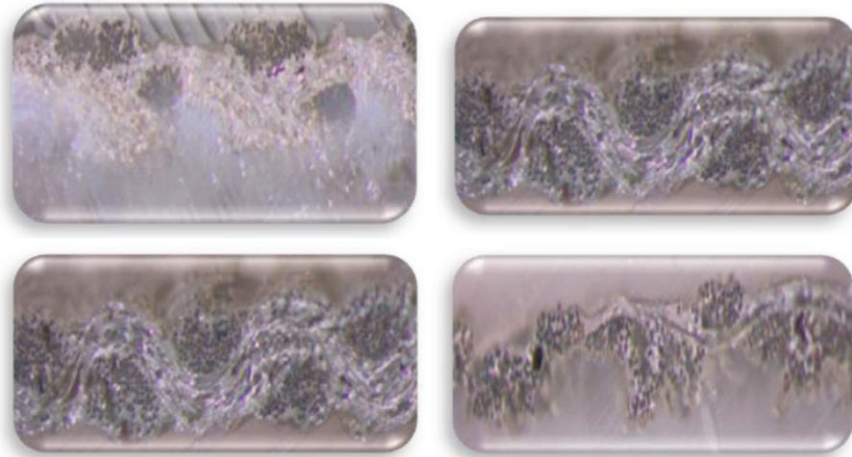
Figure 1 Cross section view of textile penetrated by screen-printed paste.
Adopted from [26].

1.3 Textile-integrated high-frequency antennas

As shown in previous chapters, the majority of papers is focused on manufacturing TIE using different textile materials (polyester, cotton and their combinations) as substrates and different materials for creating conductive layouts. Copper foils are often used for the first prototyping and manufacturing reference structures to be compared with printing technologies.

TIE is intended to integrate into clothing both standalone high-frequency (planar) components and combined on-chip elements. Since high-frequency components (filters, feeding lines, etc.) are rather large at commonly used ISM, Wi-Fi and Bluetooth (BT) frequencies, research in the field of RF components is dominantly focused on the design and implementation of planar textile antennas.

Textile integrated waveguides (TIW) are a textile version of conventional substrate integrated waveguides (SIW) with some specific properties. Unlike a microstrip line or a coplanar waveguide, TIW is a closed system. TIW can be therefore touched by the human and even bent with a minimal affection to parameters. TIW allows microwave components (antennas and filters) to be coupled with. TIW can be manufactured by all commonly used technologies like printing, plating or embroidering. Nevertheless, embroidering is not suitable for creating more complicated structures containing slots or transitions. Therefore, more complicated TIW antennas are usually manufactured from an electrically conductive textile (ECT), from a copper foil, by screen-printing

or inkjet-printing [23, 29, 30]. Manufacturing of top and bottom conductive walls of TIW structures is going to be described in following paragraphs.

In the open literature, three ways of manufacturing sidewalls of TIW were described:

- **Metal eyelets.** Eyelets have a good electrical conductivity and stability. On the other hand, their dimensions are relatively large [31].

- **Conductive yarns.** Relatively high resistivity of yarns is the main disadvantage of sewing sidewalls by yarns. The usual resistivity varies from 10 Ω/m to 100 kΩ/m [32], [33].

- **Electrically conductive textile** (ECT)**.** The textile substrate is cut to form a dielectric filler of the waveguide, and this filler is completely covered by ECT. Unfortunately, manufacturing is rather demanding, and TIW is not integrated into a textile substrate completely.

TIWs, TIW-based components (filters, antennas) and their properties were presented in [31], [33]. The described TIW was designed for the frequency 2.4 GHz using a textile material with $\varepsilon_r = 1.45$, $\tan \delta = 0.017$ and thickness $h = 3.94$ mm. The TIW was connected to a SMA connector by a conventional microstrip-to-TIW transition. Sidewalls were created by eyelets and conductive layers by a copper ECT. The average value of transmission coefficient was $S_{21} = -2$ dB.

The substrate integrated folded waveguide (SIFW) is a double-layer version of SIW [31]. The layers inside the waveguide are partly separated by a conductive wall and partly are adjoint. That way, dimensions of the structure can be reduced. As shown in [31], SIFW can be used for the design of a bandpass filter: the operation frequency was 2.4 GHz and the insertion loss at 2.45 GHz was 2.3 dB.

Finally, [31] presented a cavity backed patch antenna designed for the frequency 2.4 GHz with the gain 5.93 dBi and the efficiency 74%. The presented results show that TIW components designed for the ISM band 2.4 GHz can reach reasonable parameters.

A wearable textile shielded stripline for broadband application was presented in [34]. The stripline was put inside the shield created by a TIW structure from a silver-plated conductive textile and a conductive yarn with resistance 1 Ω/mm. The stripline was connected to a SMA connector. The transmission coefficient S_{21} was measured from 0 to 8 GHz and decreased with frequency. On average, the transmission coefficient varied from -0.2 dB to -1.1 dB and decreased up to -2 dB during structure banding.

A wearable quarter-mode textile antenna was presented in [35]. The antenna was based on a quarter-mode TIW (QMTIW), used eyelets for creating sidewalls of the TIW and was designed for the ISM band 2.4 GHz. Top and bottom conductive surfaces were manufactured from a copper-plated polyester ECM. Thanks to QMTIW, the antenna size was minimized. The antenna gain was 4.2 dBi and the efficiency in free space was 82%.

In [36], a textile microstrip-fed cavity antenna designed for the ISM band 2,4 GHz was presented. The cavity was created by eyelets, the H-shaped slot was etched in the top conductive layer and the microstrip feeder was placed on the bottom. The free-space gain of the antenna was 3.9 dBi and the efficiency 68%. The front-to-back ratio of the antenna was about 20 dB. Feeding on the bottom is a disadvantage because the microstrip can be affected by surroundings. The

described antenna was completed by solar energy-harvesting system; the effect on antenna parameters was presented in [37]. The solar system generated the power from 100 μW to 400 μW.

In [33], a TIW for the ISM band 5.8 GHz was presented. The sidewalls were created from a conductive yarn with conductivity 10 Ω/m and TIW was fed by a coaxial probe. The average transmission coefficient S_{21} was −2.3 dB for 135 mm long TIW. The TIW was tested for tension, bending and torsion with a small decrease of S_{21} (about 0.6 dB).

A design of a HMTIW antenna was presented in [38]. The sidewalls of the antenna were manufactured by two technologies – using a conductive yarn and a seam compression. In case of seam compression, conductivity of sidewalls was higher, and efficiency of the antenna was better. Nevertheless, the seam compression shifted the resonance frequency of the antenna.

1.4 Textile-integrated switches

TIW can be used both as a backup of conventional metallic cables and as a building component of reconfigurable communication networks in cars, buses and airplanes. TIW is a textile version of a conventional SIW. SIWs are designed on microwave substrates like Arlon or Rogers which have low losses, are not flexible, their weight and cost is relatively high (with respect to coaxial cables).

Textile-integrated switches can be a part of a TIW network to switch among applications, frequency bands or antennas with different radiation patterns. In the open literature, no TIW switches have been described yet. Therefore, an overview of conventional SIW switches is provided.

Depending on the switching method, conventional SIW switches can be divided into three groups:

- **Mechanically driven switch** was designed in [39] for V and W bands. A T-divider was a fundamental building block of the switch with 4 metalized via holes in each arm. These holes were mechanically short-circuited to mirror the electromagnetic (EM) wave. If not short-circuited, the via holes were *invisible* for the EM wave.

- **Magnetically driven switch** based on a ferrite-loaded SIW shifted the cutoff frequency of the L-folded SIW (LFSIW). The shift of the cutoff frequency was considered as switching. The LFSIW is formed by folding a SIW along its longitudinal axis. The LFSIW switch [40] was designed for the frequency 10 GHz and its bandwidth was 1.1 GHz. The isolation was 20 dB and the insertion loss was below 1 dB.

- **Electronically driven switch** with PIN diodes was used for shorting via holes in arms of the SIW divider [41], for shorting slots [42] or for switching between the HMSIW structure and the SIW one [43]. Finally, stubs can be shorted and opened [44].

Since mechanic switches need nonflexible materials and magnetic materials can be hardly integrated into textile materials, attention is paid to electrically driven SIW switches.

A switchable T-divider with via holes short-circuited by PIN diodes [41] had 3 via holes in each branch to create a mirror. The insertion loss was lower than 2.5 dB in the open branch and the isolation was higher than 10 dB. The slot on the top layer was used to create an attenuating impedance.

Switches based on HMSIW were presented in [43, 44]. In [44], stubs were connected to the virtual wall of the HMSIW and were short-circuited or open-circuited by PIN diodes. If short-circuited, the virtual wall was damaged and the HMSIW had a high attenuation. In [43], a HMSIW was connected with a common SIW wall by PIN diodes. Connecting the second wall to the HMSIW, the cutoff frequency of the structure was changed, and the attenuation became high.

1.5 Textile-to-conventional line transitions

As shown in [25], even relatively complicated devices can be printed on textile materials or thin film interposers. But:

- Soldering on textile substrates (with printed electronics, especially) is very complicated.

- Some components (transceivers, e.g.) need an additional shield which is difficult to be manufactured from textile materials.

- Majority of textile antennas, which are designed for personal or local area networks, are expected to be fed by a coaxial cable. But coaxial cables integrated into clothes are impractical from the viewpoint of users.

Therefore, transitions between conventional microwave substrates (Arlon, Rogers, FR4) and textile materials have to be developed.

In the thesis, attention is paid to two-layer transitions between a SIW and a microstrip transmission line (MTL) on a conventional substrate. In [25], advanced electronics was on a conventional substrate, an antenna and a micro-controller unit (MCU) were on a polyethylene terephthalate (PET), interposer, and a transition between a transceiver and an antenna was not solved.

Transitions between MTL on a ceramic substrate and MTL on a textile one were published in [45, 46]. These transitions had a metallic connection between those two MTLs. The first MTL had characteristic impedance 50 Ω and the second one 75 Ω.

In [47, 48], a connection by *Snap-On* buttons was investigated and compared with other methods to be used for connecting microstrips. A connection of microstrips on a non-flexible substrate and a flexible one was shown in [49]: the force to keep the connection was given by permanent magnets.

TIWs are usually fed by coaxial cables. According to author's best knowledge, a two-layer transition between TIW and MTL has not been published yet. As demonstrated in [50], a two-layer transition between MTL and SIW can be created with the transmission $S_{21} \approx -1.8$ dB at the frequency 5 GHz.

1.6 Conclusions

The *State of the Art* results in the following conclusions:

- Basic textile integrated elements, electronic components and sensors are well described in the open literature. Publications comprise various textile materials playing the role of the printed-circuit board (PCB) and different technologies to create electronic components

(embroidering, several types of printing). Various structures designed for ISM bands up to 5.8 GHz are presented. In order to investigate frequency limits of textile electronics, an antenna for the ISM band 24 GHz is designed and characterized in the thesis.

- Despite all the efforts, integration of advanced electronics (transceivers, e.g.) to textile materials is difficult and is done impractically by coaxial cables. Therefore, the thesis deal with the transitions between conventional substrates and textile materials.

- TIW structures are very practical because a closed system is created. There are many papers on TIWs and TIW-based antennas but more complicated components like textile-integrated filters, switches or reconfigurable structures have not been described yet. Therefore, the thesis is focused on more complicated textile elements and their configurability.

Considering these conclusions, objectives of the dissertation thesis are formulated in the following chapter.

2 Objectives

The previous part showed the progress in the integration of electronics into textile materials and in techniques of manufacturing textile-integrated microwave components. Many textile antennas for ISM bands 2.4 GHz and 5.8 GHz were presented in the open literature as an isolated part of electronic systems without any connection to the transmitter or receiver. Only a limited number of advanced components (couplers, switches) was described. Considering these facts, three objectives of the dissertation thesis can be formulated.

Objective 1

Design methodology for transitions between MTL on a conventional (non-flexible) substrate and a textile (flexible) substrate will be formulated with emphasis on the transition between two MTLs and between MTL and TIW. The transitions between two MTLs at two frequencies, and the transition between TIW and MTL will be designed and experimentally verified.

Objective 2

Methodology of the integration of advanced and reconfigurable microwave components into textile materials will be formulated. In the thesis, a TIW-based switch with PIN diodes will be described. The switch can be used for switching two antennas with different radiation patterns.

Objective 3

Methodology of the synthesis of a TIW antenna for the ISM band 24 GHz will be formulated. The antenna can be used for future wireless communication systems in public transportation and can be integrated into textile upholstery of vehicles.

3 Textile-to-Conventional Line Transitions

Textile materials can be considered as low-permittivity substrates for frequency range from 0 GHz to 60 GHz [51]. Therefore, dimensions of 50 Ω transmission lines and antennas are larger compared to conventional microwave substrates (Arlon, Rogers, FR4) of the same thickness. Next, thickness of textile substrates usually ranges from 0.5 mm to 5 mm [1], and the width of the microstrip can be from 2 mm to 15 mm for 50 Ω MTL [46, 48] when considering a common relative permittivity of the textile. The problem can be solved by microstrips with a higher characteristic impedance (up to 100 Ω) [52]. Nevertheless:

- The width of 100 Ω MTL on a 3D knitted fabric 3D041 is 5 mm and connecting a transmitter or a receiver is still difficult.

- Transmitters and receivers are designed for 50 Ω impedances. The use of 100 Ω transmission lines leads to mismatch and additional losses.

3.1 Design of MTL-to-TIW transition

A two-layer transition between TIW and MTL on a conventional substrate is based on a current probe which is used for feeding waveguides or SIWs. This transition can connect electronics on a conventional substrate and textile-integrated antennas. Antennas can be designed on a textile substrate without difficulties. Some subsystems like RF circuits are too small and sensitive for manufacturing precision and have to be designed on a conventional PCB. The transition allows to connect TIW working with the dominant TE_{10} mode and MTL with a different characteristic impedance on a conventional substrate. The mechanical connection between TIW and PCB is given by a metal wire used as a current probe. Moreover, the connection can be supported by additional mechanic supports. Hence, a strong connection protected against mechanical damage can be created.

The design of the transition is similar to the design of a current (coaxial) transition between a coaxial cable (connector) and TIW. The coaxial cable is only replaced by MTL. The shorting pin connects the end of the MTL and the bottom conductive wall of TIW (see Figure 2). The waveguide part is designed by rules given by [53], and the width of the microstrip is given by its characteristic impedance [54].

The distance between the short-circuited termination of TIW and the shorting pin l_{dp1} is an important parameter. The proper distance has to be $\lambda_g/4$ where λ_g is the wavelength in TIW (the pin is in the maximum of electric field).

On the top side of TIW and on the ground side of MTL, a circular slot is created. The slot is centered around the shorting pin and its diameter can be calculated as the diameter of

a corresponding coaxial cable [54]. The bandwidth of the transition can be increased by a circular ring around the shorting pin which compensates its inductance [55].
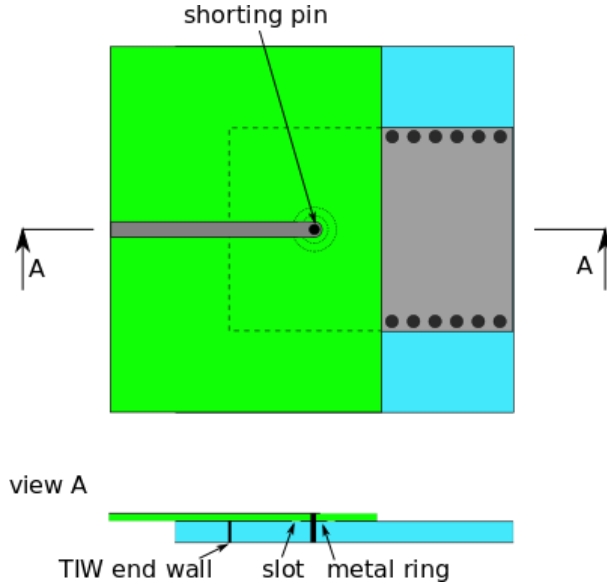
Figure 2 Top view and cross section view of MTL-to-TIW transition.

The shorting pin has two main functions:

- Excitation of electromagnetic field inside TIW;
- Mechanical connection between the top PCB and the bottom textile material.

The circles with the diameters d_{in} and d_{out} create a *coaxial* probe with the same impedance as the top MTL. If relative permittivity of the top conventional layer is high and relative permittivity of the bottom textile layer is small, recalculations used for coaxial cable impedances can be applied.

According to [53], TIW can be designed as a rectangular waveguide with effective width w_{ef}:

$$w_{ef} = w - 1.08\frac{d^2}{s} + 0.1\frac{d^2}{w}$$

(1)

$$\frac{s}{d} = 2.5$$

(2)

Here, d denotes the diameter of vias, s is the distance between two neighboring vias and w is the physical width of TIW.

3.2 Design procedure and results of simulations

Using rules given in the previous section, two transitions were designed:

- For UWB frequency band around 8 GHz;
- For ISM band 5.8 GHz.

Transitions were designed for the textile substrate 3D097 ($\varepsilon_{r1} = 1.22$, tan $\delta_1 = 0.002$, $h_{hs1} = 2.6$ mm) and two different conventional substrates. For the UWB band, we used Arlon 25N ($\varepsilon_{r2} = 3.38$, tan $\delta_2 = 0.0025$, $h_{s2} = 0.762$ mm). For the ISM band, we used FR4 ($\varepsilon_{r3} = 4.2$,

$\tan \delta_3 = 0.02$, $h_{s3} = 1.52$ mm). The FR4 was chosen because this material is often used for the construction of electronic devices. The design procedure is the same for both the transitions:

- MTL on the conventional substrate is designed;
- TIW with short-circuited termination is designed;
- Wavelength in TIW is calculated, shorting pin is installed in the distance $\lambda_g/4$ from the termination;
- Circular slot around shorting pin is designed (the same impedance as MTL);
- Circular metal ring around shorting pin is designed (initial radius is half of the slot radius).

The designed transition is shown in Figure 3, dimensions of transitions are given in Table 1.

Table 1 Dimensions of MTL-to-TIW transitions for ISM and UWB bands.

dim [mm]	w_{siw}	l_w	d	d_p	d_1	d_2	w_p	h_{s1}	h_{s2}	s
ISM	50	19.1	0.3	1.0	2.0	5.2	2.8	2.6	1.52	2.0
UWB	23	13.2	0.3	2.0	2.0	4.6	1.7	2.6	0.76	2.0
ISM (75 Ω)	50	19.1	0.3	0.4	2.1	4.0	1.3	2.6	1.52	2.0
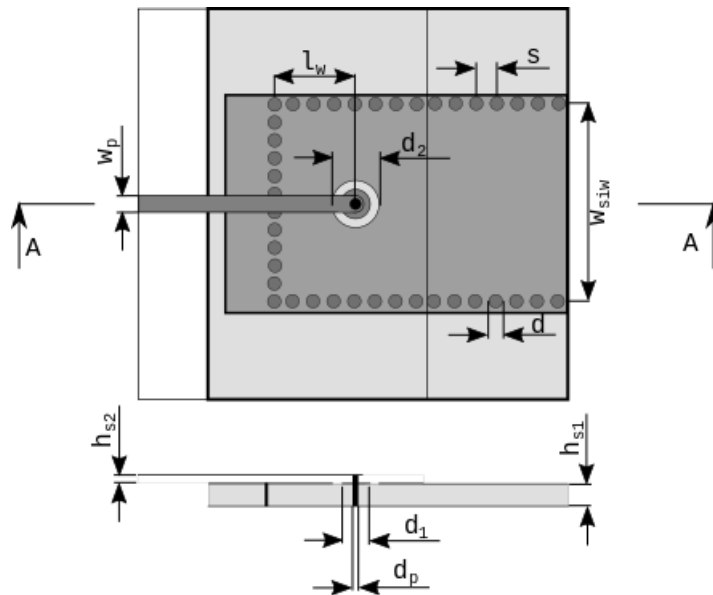
Figure 3 MTL-to-TIW transition with dimensions.

Now, attention is turned to outputs of simulations of the ISM 5.8 GHz transition. The top MTL was designed on FR4 and the bottom TIW on the 3D textile 3D097. The transition was simulated with SMA connected to MTL and the waveguide port at the end of TIW. The reflection coefficient was $S_{11} = -24.2$ dB and the transmission $S_{21} = -0.32$ dB.

Since the diameter of the conductive thread was $d = 0.3$ mm and the wall was sewed by hand, the distance between stitches was $s = 2$ mm. This relatively long distance caused a parasitic radiation among stitches and decreased performance of the transition. The difference between the transitions simulated with continuous sidewalls and with stitched ones is shown in Figure 4. The differences are $\Delta S_{21} = 0.98$ dB and $\Delta S_{11} = 3.32$ dB.
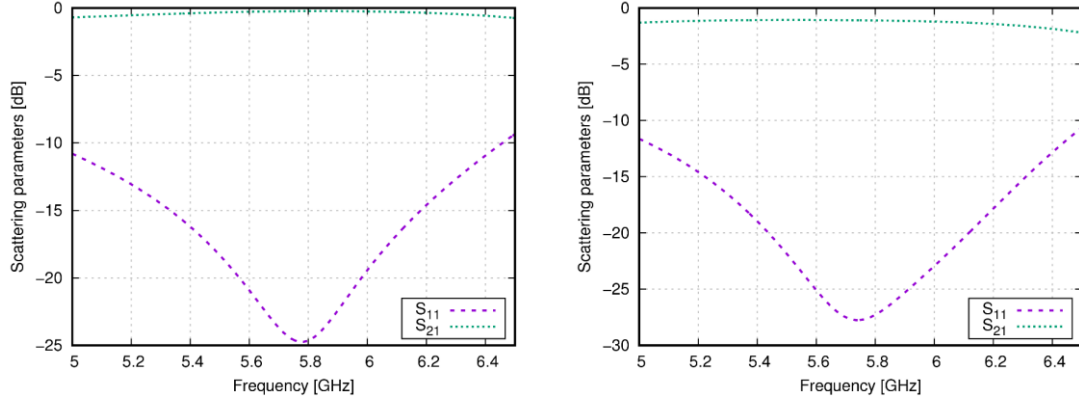
Figure 4 MTL-to-TIW transition for ISM band: simulated reflection and transmission coefficient for continuous sidewalls (left) and stitched sidewalls (right).

Figure 5 shows results of parametric analyses performed on important parts of the transition. During parametric analyses, the reflection coefficient and the transmission one were observed.

Diameter of the circular slot d_2 was changed from 4.4 mm to 6.0 mm and the transmission varied from −0.20 dB to −0.37 dB. The results showed that the variation of d_2 can improve performance but the variation of the diameter of the metal ring changed the transmission only for about 0.17 dB.

The variation of the distance between the end of TIW and the shorting pin caused that the maximum of the transmission moved to another frequency. When varying the diameter of the shorting pins from 0.4 mm to 1.6 mm with the step 0.4 mm, the transmission changed from −0.21 dB to −0.78 dB (the larger radius of the pin, the better performance).

Parametric analyses showed that the performance of the designed transition can be improved by varying important parameters. Especially, the diameter of the shorting pin is critical.

The MTL-to-TIW transition can be designed even for microstrips with the characteristic impedance which differs from 50 Ω. In order to approve the concept, the transition was designed for the microstrip with the characteristic impedance 75 Ω. Performance of the designed transition was verified by simulations. The transition was designed according to rules described in the previous section. Dimensions of the transition are given in Table 1. Frequency responses of reflection and transmission coefficient of this transitions are shown in Figure 6. The reflection coefficient is $S_{11} = -25.47$ dB and the transmission coefficient is $S_{21} = -0.11$ dB.
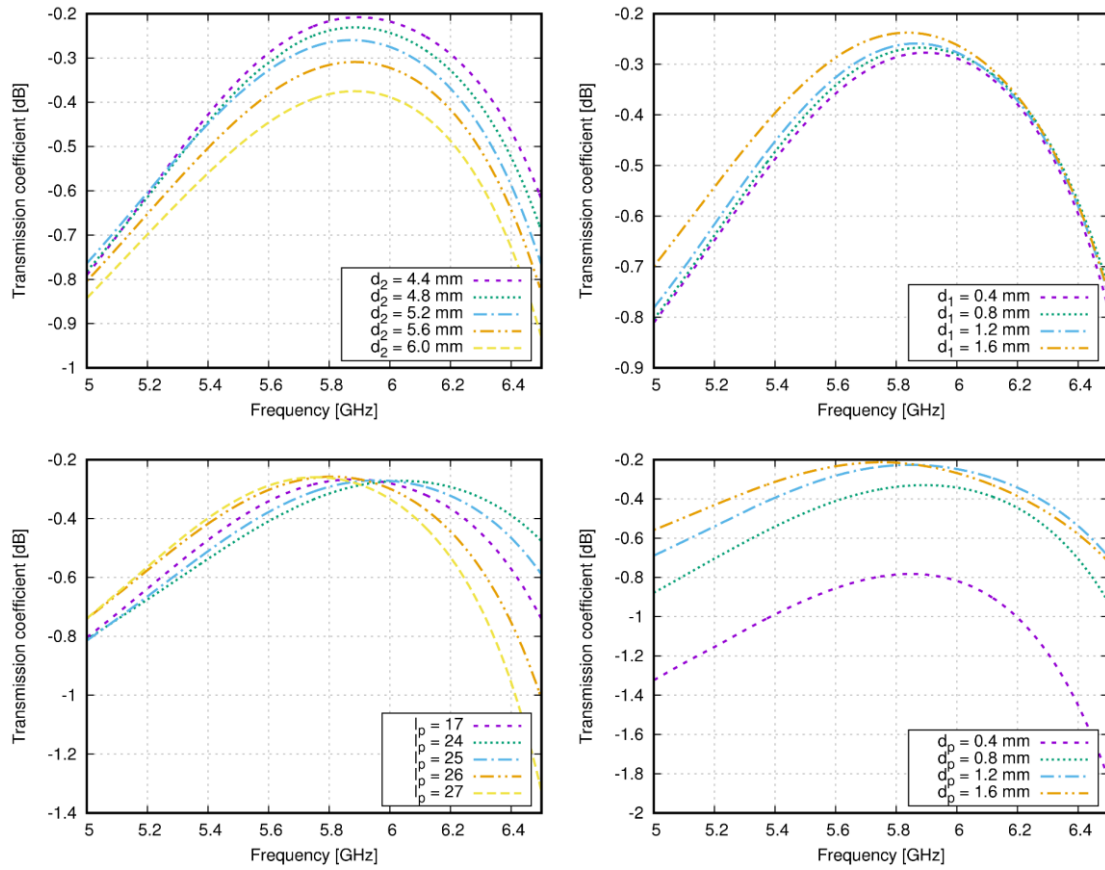
Figure 5 MTL-to-TIW transition for ISM band: parametric analysis of the transmission coefficient when varying d_2 (top, left), d_1 (top, right) d_p (bottom, right) and l_p (bottom, left).
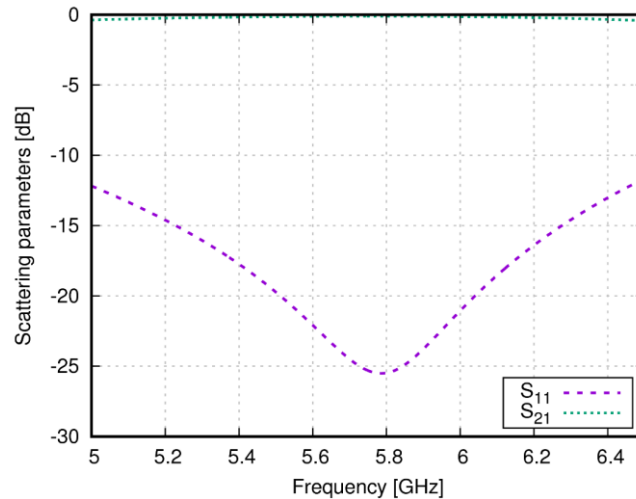
Figure 6 MTL-to-TIW 75 Ω transition: reflection and transmission coefficient.

The MTL-to-TIW transition for the UWB band-group 6 was designed without a circular ring in the slot because the pin diameter was increased according to previous parametric simulations (see Table 1). The transition was simulated with stitched sidewalls. As the conventional substrate, Arlon 25N with thickness 0.762 mm was used.

3.3 Results of measurements

For the experimental verification, two transitions operating in the ISM band 5.8 GHz and two transitions operating in the UWB band were manufactured and connected by TIW (see Figure 7). Manufacturing and technological details are provided in Chapter 6.

Figure 7 Photographs of manufactured MTL-to-TIW transitions (ISM left; UWB right).

Results of simulations and measurements of these transitions are shown in Figure 8 and Figure 9. The ISM transition has the simulated insertion loss 2.32 dB (the measured one is 3.12 dB) and the simulated reflection coefficient at the SMA input is $S_{11} = -19.22$ dB (the measured one is −17.23 dB). The maximum of the transmission is shifted to a lower frequency than 5.8 GHz. The minimum of the reflection coefficient is shifted to a frequency lower for about 100 MHz.

The UWB transitions were optimized to maximize the bandwidth where $S_{11} < -10$ dB. The insertion loss varies for less than 3 dB in the band-group 6. Results of measurements show that the reflection coefficient is higher than −10 dB in a lower part of the UWB band and the insertion loss varies from 1.1 dB to 4.3 dB.
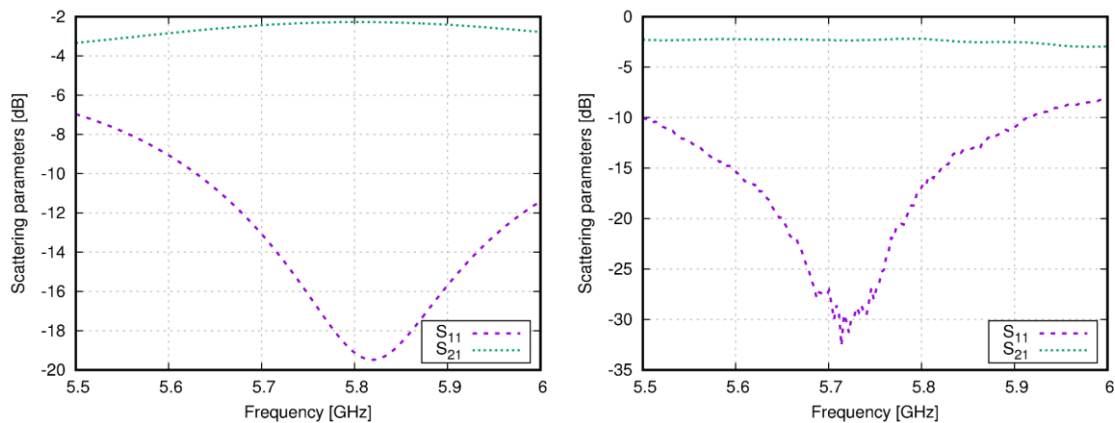
Figure 8 MTL-to-TIW transition for ISM band: simulated S parameters (left) and measured S parameters (right). Configuration from Figure 7.
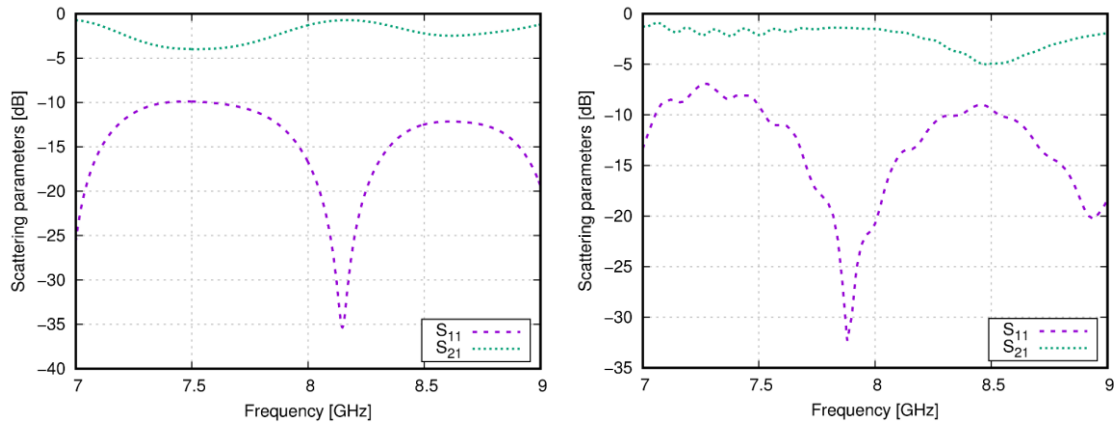
Figure 9 MTL-to-TIW transition for UWB band: simulated S parameters (left) and measured S parameters (right). Configuration from Figure 7.

3.4 Conclusions

The methodology of the design of multilayer transitions between MTL on a conventional substrate and TIW was presented. The designed transitions were simulated, and results were verified by measurements.

The conclusions are as follows:

- TIW can be used in combination with other devices integrated into other substrates.

- The presented MTL-to-TIW transition is suitable for narrow-band applications (for ISM bands, e.g.).

- The transition can be also used for wide-band applications with a higher insertion loss and a higher value of reflection coefficient.

4 Textile-Integrated Switches

Since TIW are relatively bulky and are not suitable for wearable applications, attention is turned to non-wearable structures (bed sheets, upholstery, seat covers, etc.). In all those textile structures, TIW can play the role of a transmission line. TIW can be used as a high-speed communication bus for media streaming in cars, buses and airplanes. TIW-based systems can create a backup communication bus for sensors or emergency systems.

The chapter is aimed to describe the design of a TIW switch, which is expected to transmit the power from the input 1 to the output 2, or the output 3.

The design of textile-integrated components is specific due to the manufacturing technology. Tolerances of textile materials are very limited. The resistance of conductive textiles and yarns is relatively high compared with copper, gold or even with aluminum. The yarns or eyelets have fixed dimensions and properties. Due to these reasons, the textile-integrated switch has to be designed step by step. All the steps are described in the following paragraphs.

4.1 Textile-integrated T-divider

The design of the textile-integrated T-divider is similar to the design of a SIW T-divider with some manufacturing limitations. The width of the waveguide is given by the formulas (1) and (2) on the page 12. The width of the waveguide is 35 mm for the operation frequency 5.8 GHz, the cutoff frequency $f_{off} = 3.9$ GHz and the 3D textile with the height 3.4 mm and the relative permittivity 1.2. The length of waveguide branches was chosen to be 20 mm.

The T-divider has an inductive post in the center. The conductivity and the diameter of the post are very important. Both these parameters affect the reflection at the input port and the insertion loss between the input port and the output ports. Figure 10 to Figure 13 show the frequency dependence of S_{11} and S_{21} with the radius and the conductivity of the inductive post as parameters, respectively.

Obviously, the diameter of the inductive post plays an important role. The value of S_{11} varies between −37 dB and −13 dB and S_{21} between −3.50 dB and −3.18 dB. Since the diameters of conductive yarns are limited, the inductive post can be constructed as follows:

- To use more yarns in parallel. The method is complicated for manufacturing, the precision of the diameter is limited.

- To use a copper wire with a proper diameter. The method is easy for use and manufacturing, the precision of the diameter is good.

- To manufacture the conductive thread with the defined diameter. The tolerance of manufacturing the yarn with a given diameter is ±10%.

The conductivity of the central post varies from 10^2 S·m^{-1} to 10^6 S·m^{-1}. Since the conductive threads used for RF applications have the resistance between 10 Ω and 100 Ω, these threads were not suitable for creating the central inductive post and also switchable pins.
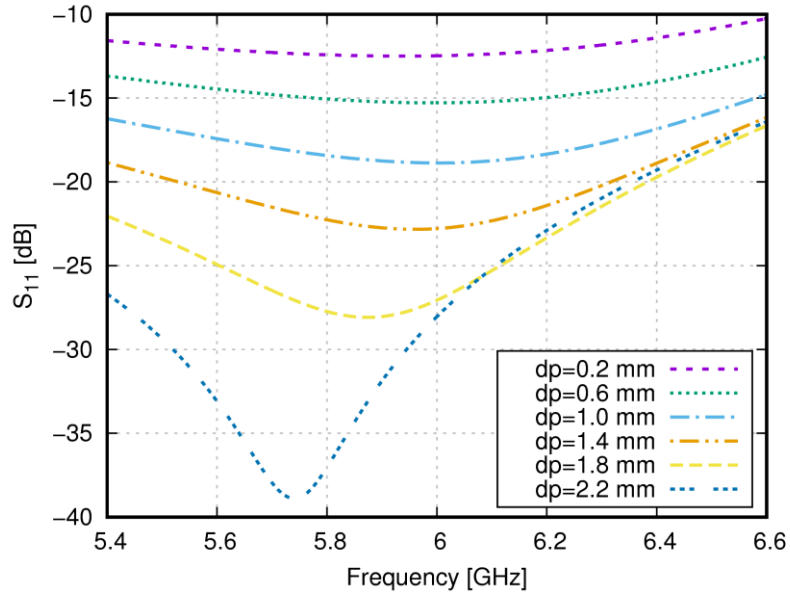
Figure 10 Frequency response of the reflection coefficient at the input port of the switch: radius of the inductive post as a parameter.
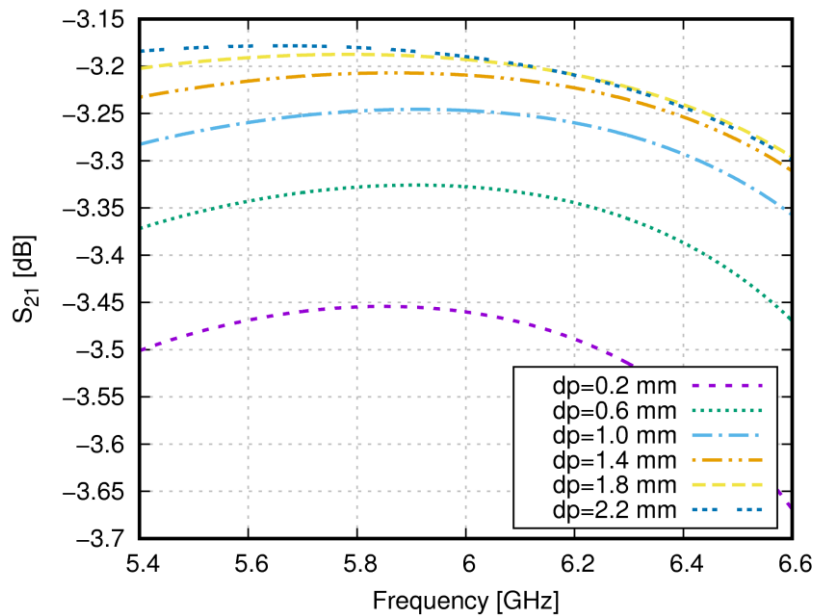
Figure 11 Frequency response of the transmission between the input port and the port 2: radius of the inductive post as a parameter.
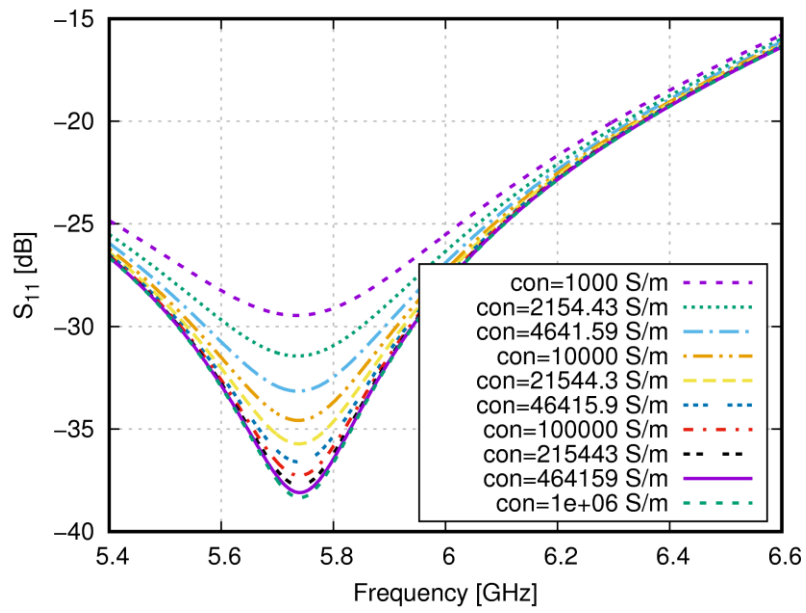
Figure 12 Frequency response of the reflection coefficient at the input port of the switch: conductivity of the inductive post as a parameter.
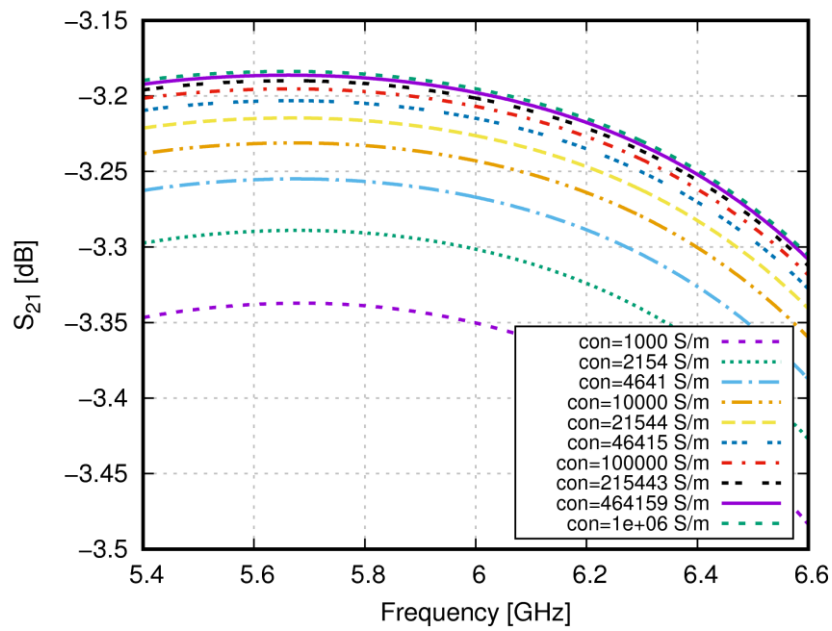
Figure 13 Frequency response of the transmission between the input port and the port 2: conductivity of the inductive post as a parameter.

4.2 Switch design and simulations

The TIW switch is based on a conventional T-divider with four switchable pins. These pins are separated from the top and bottom conductive layers by a circular gap and can be connected by PIN diodes.

Schematics of the designed T-divider is depicted in Figure 14. The strong inductive post is in the vertical axis of the divider. On the left-hand side and the right-hand side, switchable pins to be used for switching are installed.
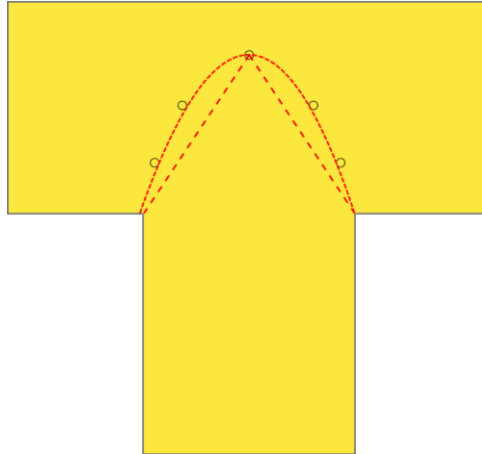
Figure 14 Position of the inductive post (on the top) and switchable pins
(on the left, on the right). Linear or parabolic distribution.

The diameter and the conductivity of switchable pins are important as well. Therefore, all the switchable pins are constructed from copper wires. Switchable pins are placed inside the TIW. Their positions with respect to the central post and inner corners of the divider are given by an equilateral triangle or by a part of a parabolic curve (see Figure 14). The distances between pins are the same.

The switch was simulated with perfectly electrically conductive (PEC) pins. Two pins on the right-hand side were fully connected to the top metal layer and the bottom one and closed the port no. 2. Two pins on the left-hand side were disconnected and opened the port no. 3.

Frequency responses of reflection and transmission coefficients are shown in Figure 15 for the parabolic distribution of switchable pins and in Figure 16 for the linear distribution of switchable pins. Responses for closed ports are very similar for both the distributions, but responses for open ports are different: S_{11} is for about -19 dB better and S_{31} is for about 0.5 dB better in case of the parabolic distribution.

The shape of the gap between the inductive post and conductive layers is a circular ring slot (see Figure 17). The radius of the ring slot affects parameters of the switch. The top slot and the bottom one can have a different radius. Using a simplified model of the switch without PIN diodes (the diodes were replaced by a conductive strip), parametric analyses were done for the diameter of the top slot, and the diameter of the bottom slot. The simplified switch is depicted in Figure 18 and transmissions to the open and closed port are depicted in Figure 19 and Figure 20.
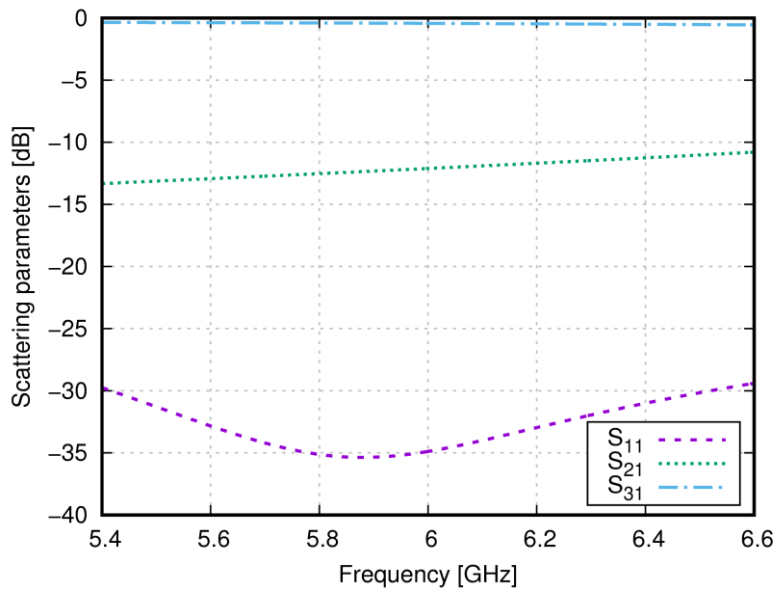
Figure 15 Frequency response of S-parameters of the switch: parabolic distribution of switchable pins.
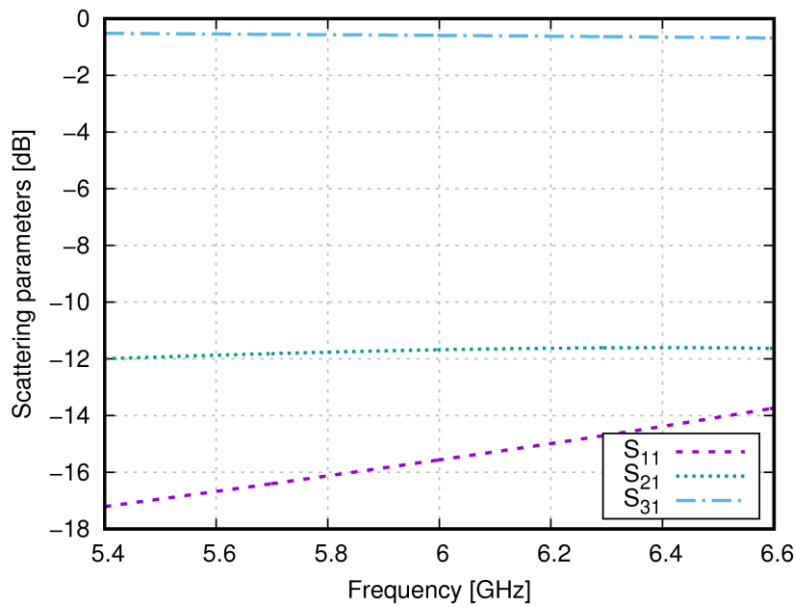
Figure 16 Frequency response of S-parameters of the switch: linear distribution of switchable pins.
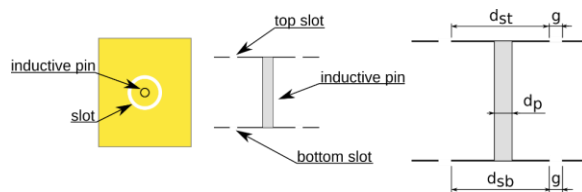
Figure 17 Design of switchable pins.
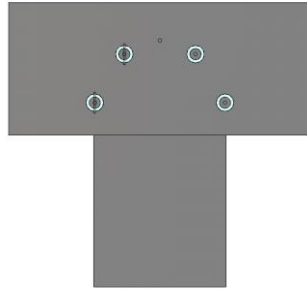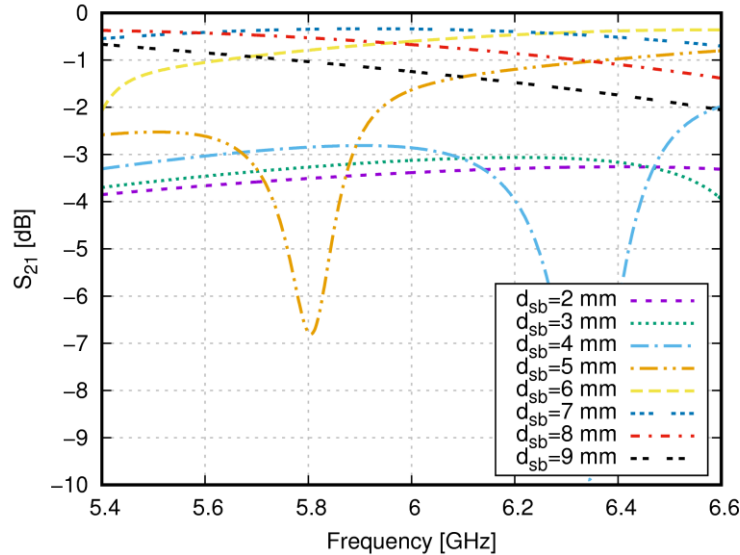
Figure 18 Switch without PIN diodes; sidewalls created by continuous PEC.
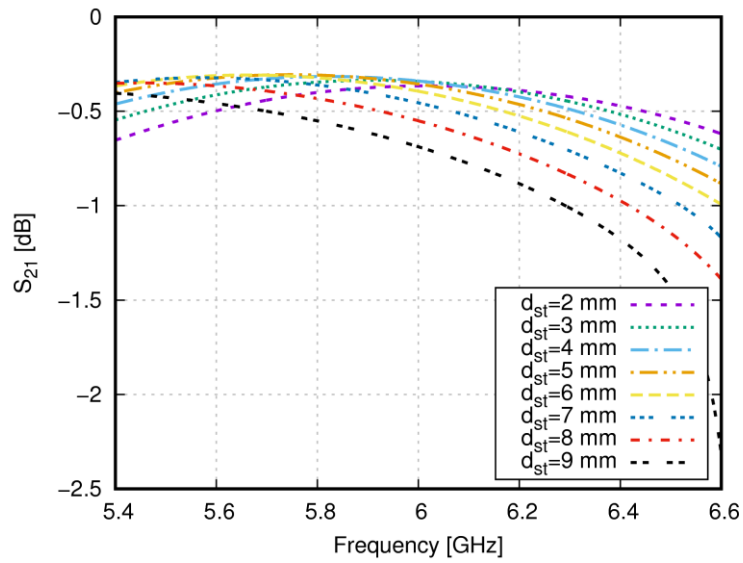
Figure 19 Frequency response of the transmission from the input port to the open port: diameter of the slot on the top d_{st} as a parameter.
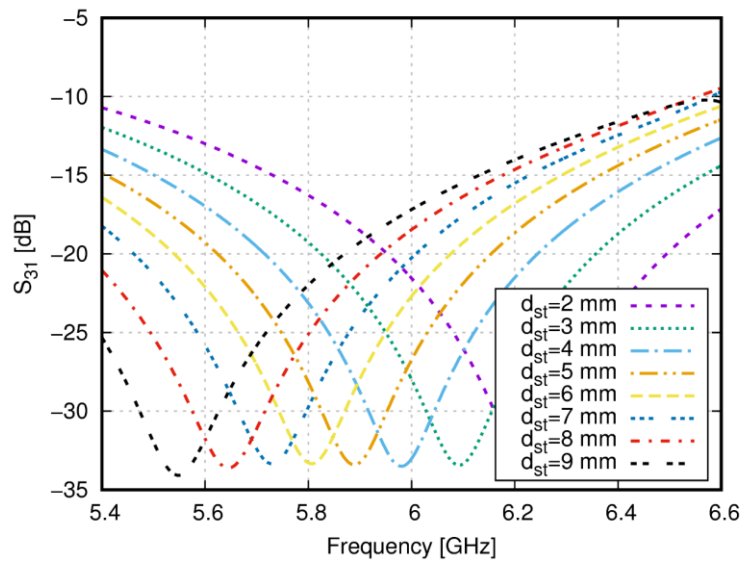
Figure 20 Frequency response of the transmission from the input port to the closed port: diameter of the slot on the top d_{st} as a parameter.

Frequency dependencies in Figure 19 to Figure 22 show the effect of diameters of slots on the top and the bottom of the switch on the transmission between the input port and the open port or the closed one. The simplified switch used for parametric analyses is shown in Figure 18. The width of the waveguide was 35 mm and switchable pins were placed on the part of a parabolic curve. Two switchable pins on the left-hand side were connected to the metal layer by conductive strips and two pins on the right-hand side were disconnected. During the parametric analyses, the inner diameter of the top and bottom slots was changed (dimension d_{st} and d_{sb}) and the width of slots (g) was constant (dimensions are shown in Figure 17).

Figure 21 Frequency response of the transmission from the input port to the open port: diameter of the slot on the top as a parameter.
Inner diameter of the bottom slot d_{sb} varied during parametric analysis.
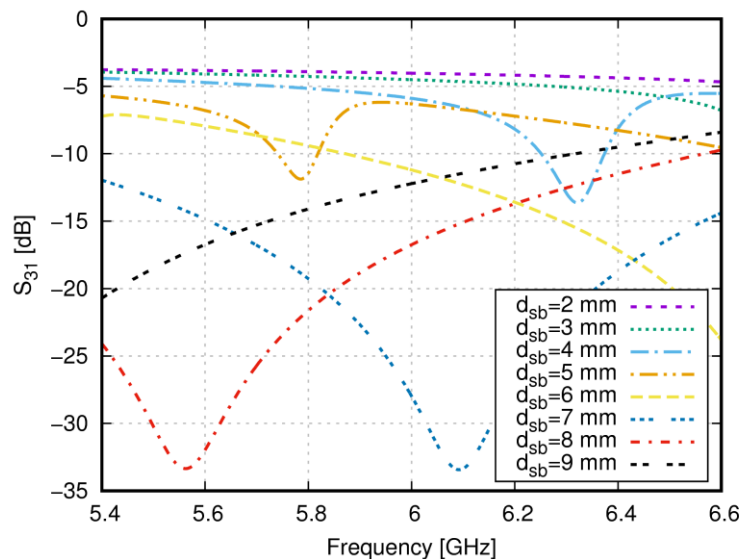
Figure 22 Frequency response of the transmission from the input port to the closed port: diameter of the slot on the top as a parameter.
The inner diameter of the bottom slot d_{sb} varied during parametric analysis.

During the first simulation, the slot on the top had the diameter $d_{st} = 1$ mm and the diameter of the slot on the bottom d_{sb} was changed. During the second simulation, the diameter of the slot on the bottom was set to $d_{sb} = 3$ mm and diameter of the slot on the top d_{st} was changed. Figure 21 and Figure 22 show that the diameter of the bottom slot is critical for the proper function of the TIW switch.

Results of parametric analyses show that the diameters of the top and the bottom circle around pins are very important parameters. The diameter d_{sb} should vary between 6 mm and 9 mm and the diameter of the top ring d_{st} should be between 5 mm and 7 mm if the diameter of the bottom ring is chosen to be 7 mm. Since these diameters influence the parasitic capacitance and inductance of the pin, the right diameters depend on the diameter of pins and parasitic properties of used PIN diodes. Table 2 shows that the diodes used in [41, 44] have lower capacitance and inductance than diodes used in [43], but these diodes are in a small package and cannot be used for textile manufacturing. Therefore, the PIN diodes BAR64-02 were used. Their maximum operation frequency is 6 GHz.

Table 2 Parameters of equivalent circuit components of PIN diodes.

PIN	R ON (Ω)	R OFF (kΩ)	C (pF)	L (nH)	Ref.
BAR64-02	2.1	3.0	0.20	0.80	[43]
HPND-4038	1.5	--	0.06	0.15	[41]
GC4941-12	1.5	--	0.06	--	[44]
MA4AGFCP910	5.0	--	0.02	--	[42]

The equivalent circuit of PIN diodes is shown in Figure 23 for the ON state and the OFF state. Results given by these equivalent circuits correspond to S-parameters given in the datasheet. PIN diodes are connected between the ring around the switchable pin and the top conductive layer. The PIN is connected to the driving voltage.

More diodes can be used per one switchable pin to improve the performance. One, two and three diodes were simulated, and results were compared (see Figure 24 and Figure 25).
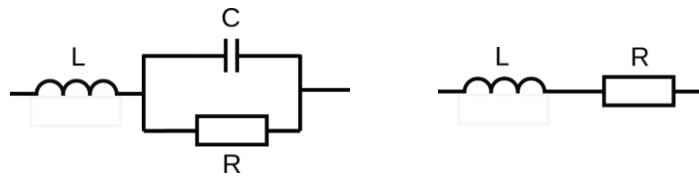
Figure 23 Equivalent circuit of PIN diode.
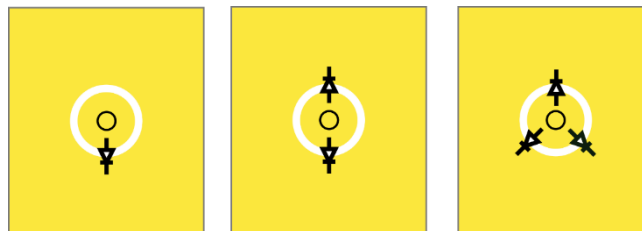
Figure 24 Connection of the different number of PIN diodes.
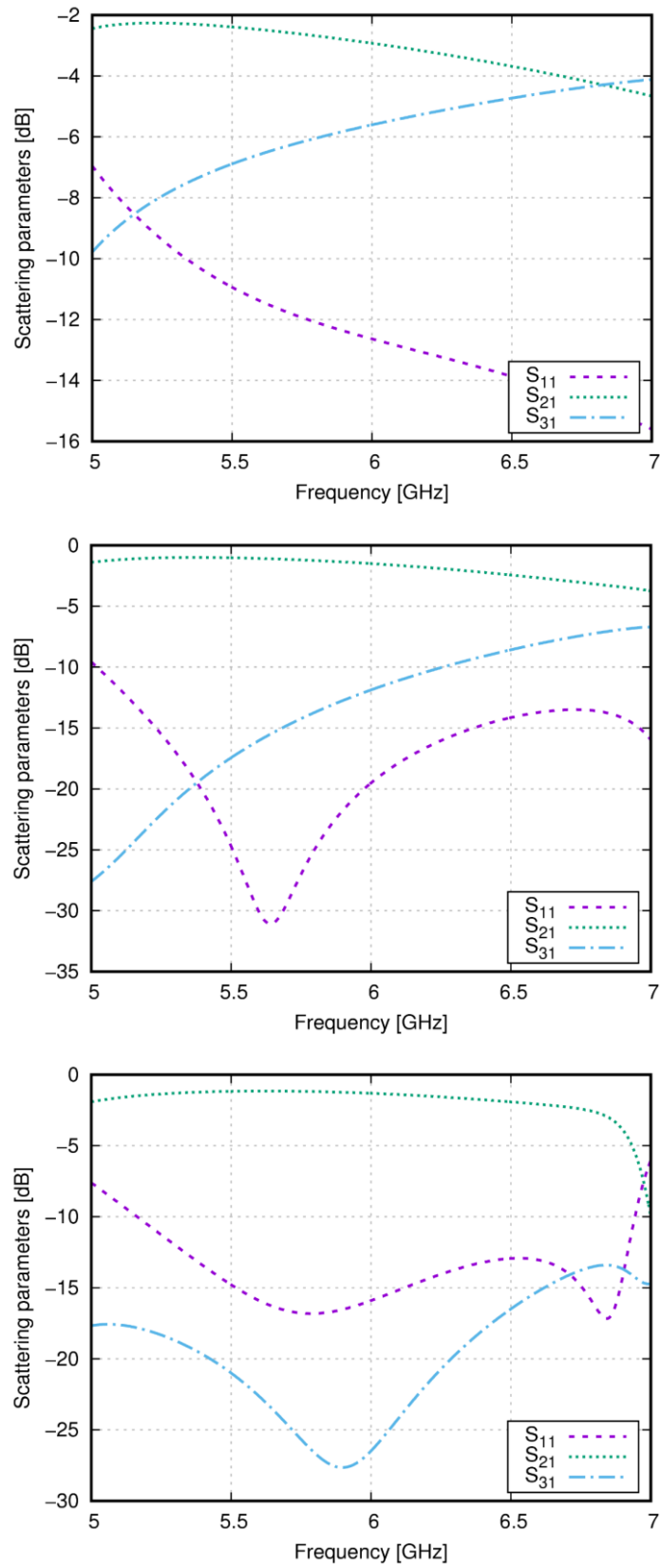
Figure 25 Frequency responses of S-parameters of the simulated switch with one (top), two (center) and three (bottom) PIN diodes connected to switchable posts.

Figure 25 shows that the parameters of the switch depend on the number of PIN diodes connected to switchable pins. All simulations were done with the same dimensions and setting. The switch with one PIN diode per pin had $S_{11} = -12.10$ dB, $S_{21} = -2.73$ dB and $S_{31} = -5.73$ dB. As shown in [41], one PIN diode per pin can be used, but parameters of used PIN diodes have to be much better than BAR64-02 has. Insertion loss of the open port is similar to cases with two and three PIN diodes. Due to the parallel combination of three PIN diodes, the switch has a very low transmission to the closed port (about -28.22 dB) but S_{11} is -17.12 dB. The switch with two PIN diodes has $S_{11} = -19.98$ dB but the transmission to the closed port is -23.25 dB.

4.3 Switch manufacturing and measurements

The TIW switch was designed for the 3D textile substrate 3D041 produced by SINTEX. The height of the 3D textile was 3.4 mm, relative permittivity 1.2 and the loss tangent $\tan \delta = 0.002$. Top and bottom conductive layers were screen-printed by a silver paste. The screen printing was chosen for the following reasons:

- The manufacturing process is compatible with the standard PCB technology.
- The precision of manufacturing is comparable to the standard PCB technology.
- The silver paste is well conductive.
- The PIN diodes or metal wires can be soldered or glued to the screen-printed silver paste.

Sidewalls of the TIW were sewed by the conductive silver thread ELITEX® Art, SC 110/f34_PA/Ag with the diameter 0.3 mm and the resistivity 18 Ω/m. The thread is suitable for hand and machine sewing. Since TIW was connected to a standard vector network analyzer (VNA), the transmission between TIW and SMA was designed. The width of the 50 Ω microstrip was 15 mm and the width of the TIW was 35 mm. The tapered transition between microstrip and TIW can be calculated by the equation given in [56].
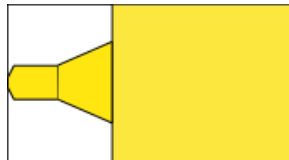
Figure 26 Transition MTL to TIW.

Since the height of the substrate was 3.4 mm, the losses of the transition were relatively high (see Figure 27**Figure 27** Simulated frequency response of S-parameters of the transition between the SMA connector and TIW.) and degraded parameters of the TIW switch. The insertion loss at 5.8 GHz was 1.27 dB for the optimized transition.
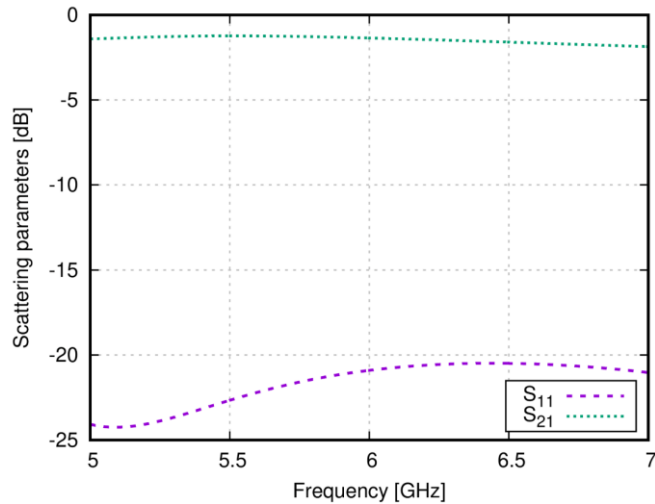
Figure 27 Simulated frequency response of S-parameters of the transition between the SMA connector and TIW.
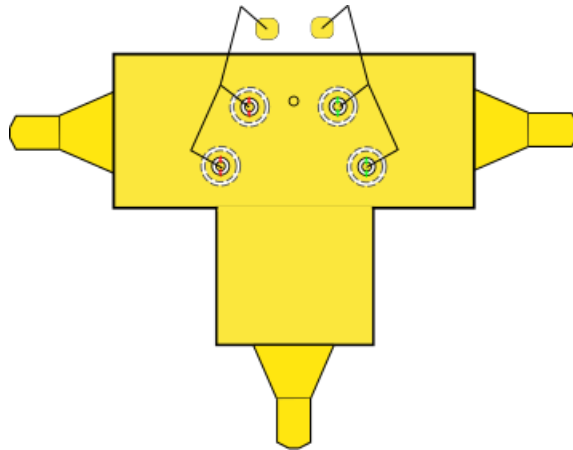
Figure 28 TIW switch with transitions to SMA connectors.

The switch was measured using a two-port VNA. The VNA was connected by SMA connectors to the input port and one of the switchable ports. The unconnected port was ended by a 50 Ω resistor. Switchable pins were connected to the driving voltage −5 V for the open port (diodes OFF) and +1.1 V for the closed port (diodes ON). The current was limited by a series resistor to the maximum recommended value 80 mA. The manufactured switch is shown in Figure 29.
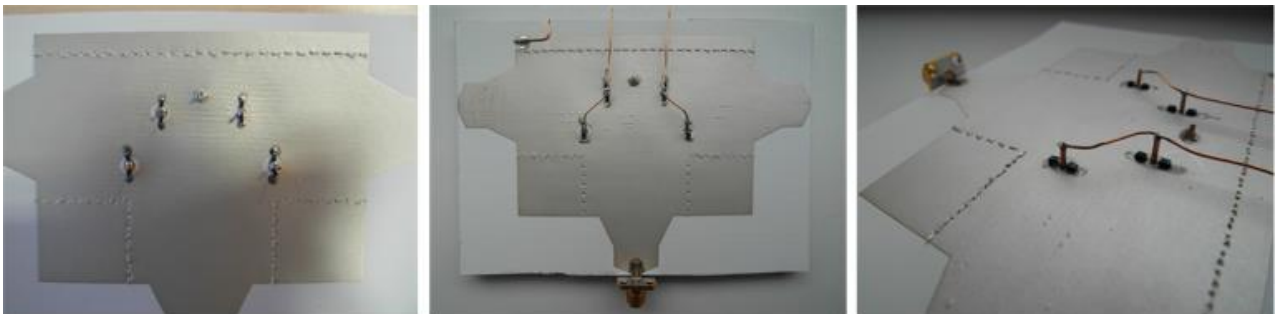
Figure 29 Photos of the screen-printed textile-integrated switch.

Simulated and measured results of the complete switch are depicted in Figure 30. The switch was simulated with SMA-to-TIW transitions and diodes replaced by the equivalent circuit. The reflection coefficient of the simulated switch was −13.30 dB (measured −14.60 dB) at the frequency 5.8 GHz and losses of the open port were 5.10 dB (measured 6.21 dB). The simulated isolation of the closed port was 14.92 dB (measured 15.63 dB). Obviously, measured data corresponds well with simulations.

4.4 Conclusions

The methodology of the design of the textile-integrated switch was presented in this Chapter. The design was verified by simulations and measurements. The design procedure can be divided into the following steps:

- The textile-integrated T-divider is designed with the fixed post in the longitudinal axis of the divider.

- Switchable conductive posts are installed into the divider following the linear or parabolic trajectory. The trajectory is defined by the center post and internal corners of the T-divider.

- Suitable PIN diodes are selected. The selection is limited by the operation frequency (parasite properties) and technology of creating metal layers.

- Top and bottom slots around switchable pins and the fixed post are designed. The bottom slots are recommended to be of the double size compared to top ones, approximately. The width of the slot is given by manufacturing technology (precision) and used PIN diodes. The parasitic properties of the diodes can be compensated by increasing the number of diodes.

These design rules were used for designing the textile-integrated switch for the ISM band 5.8 GHz. The switch was fed via SMA-to-TIW transitions by tapered microstrip lines on each port. Figure 27 shows that this transition was not ideal for this type of the textile material and degraded properties of the switch (see Figure 30).
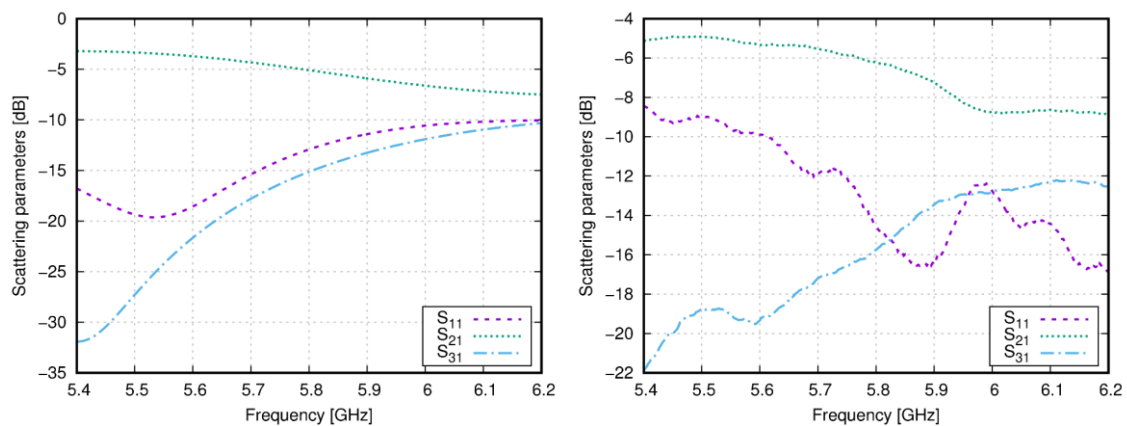
Figure 30 Frequency responses of S11, S21 and S31 of the TIW switch: simulated (left) and measured (right).

5 Circularly Polarized Textile-Integrated Antennas

The circularly polarized textile-integrated antenna is based on a concept of a circular patch antenna fed by the microstrip from the bottom side and with the cross slot inside the circular patch [57]. The role of the radiating element is played by a circular ring slot in the top metal layer of TIW. Inside the circular ring slot, a cross slot rotated for about 45° is etched to excite the circular polarization. The polarization of the antenna can be changed by the rotation of the cross slot.

The antenna is designed in two versions. The first version is more complicated for manufacturing at frequencies above 20 GHz, especially. The second version is easy to be manufactured because the most critical parts of the first version were eliminated. Hence, the second version is suitable even for higher frequencies above 20 GHz and a lower precision of manufacturing. Both versions of the antenna have similar properties; the first version has a better axial ratio (AR).

5.1 Design of textile-integrated antennas

The textile-integrated circularly polarized slot antenna is an analogy of an antenna integrated into a conventional substrate. The design rules are the same both for SIW and TIW, but different technical limitations have to be considered (the diameter of conductive threads, the thickness and permittivity of textile substrates, the precision of manufacturing conductive layers, etc.).

The design of the antenna can be divided into two parts. First, the TIW has to be designed. Second, the radiating element has to be developed and its position has to be optimized. Design equations provide basic dimensions of radiating slots for further optimization.

The radiating element is depicted in Figure 31. The antenna consists of a circular ring slot and a cross slot inside. The circumference of the ring slot is given by the wavelength of the radiated wave. The circumference should equal to the wavelength of the radiated wave. The middle radius of the ring slot can be calculated by [58]:

$$r = \frac{c}{2\pi f_c \sqrt{\varepsilon_r}} \qquad (3)$$

where c is velocity of light in vacuum, f_c is frequency of operation and ε_r is relative permittivity of the textile substrate.

The width of the slot is given be the requested characteristic impedance of the slot.

The cross slot can be divided into two arms. The first arm is longer and the second one is shorter. The length of the longer arm is given by the radius of the circular ring slot and its width. There is a small conductive strip between the circular ring slot and these arms (see Figure 31). This thin strip improves the axial ratio of the antenna.

The length of the shorter arm is given by:

$$l_{c2} = r/4 \qquad (4)$$

where r is the middle circumference of the ring slot given by (3).
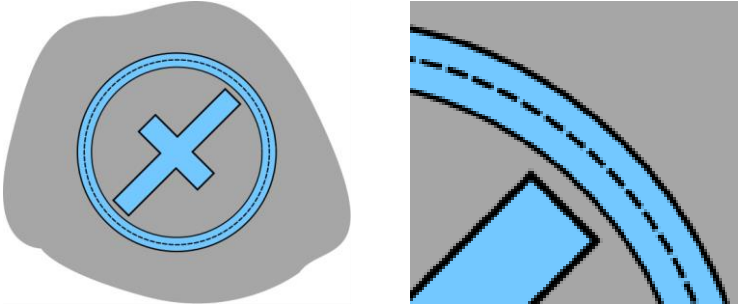
Figure 31 Version 1 of the radiating element (left),
detail of the conductive strip between the ring slot and the cross slot (right).
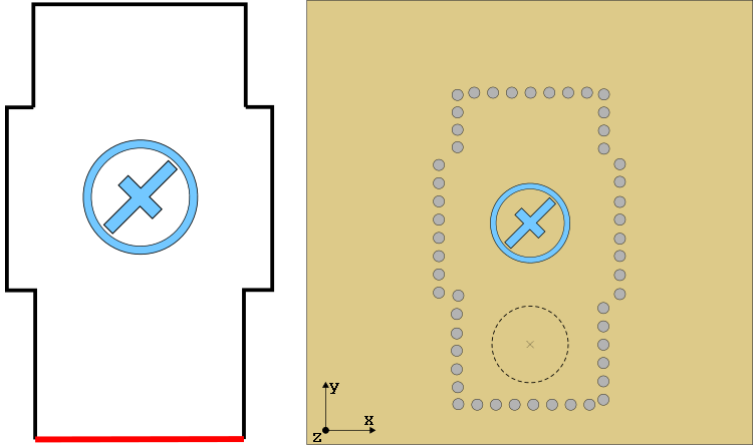
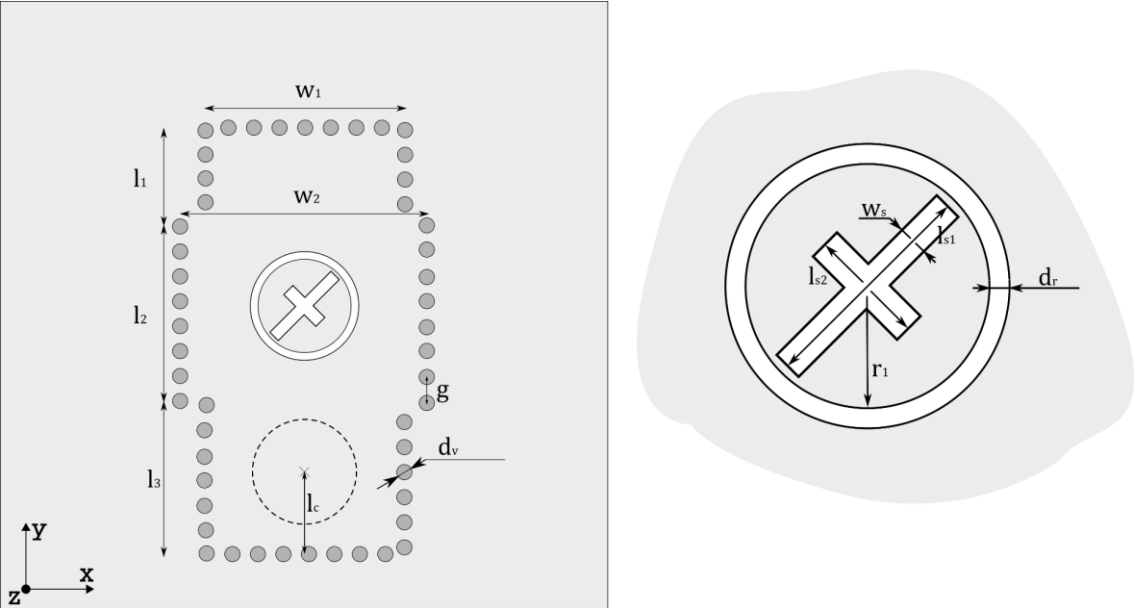**Figure 32** Version 1 of the antenna: simplified model (left), full model (right).

Figure 33 Version 1 of the textile-integrated antenna.
The whole antenna (left), the radiating slot (right).

First, TIW has to be designed by a conventional approach as a cascade of textile-integrated waveguides of two widths (the version 1, Figure 33 and Figure 34). The cutoff frequency of the narrower part of the TIW has to be 72,5 % of the operational frequency and the cutoff frequency of the wider part of the TIW has to be 58.3% of the operational frequency. This wider part close to the radiating ring creates more constant field distribution in the slot and improves radiation parameters of the antenna.

The distance between the short-circuited end of the TIW and the center of the radiating slot has to be determined. This distance should equal to half of the wavelength at the operating frequency. The length of the wider part of TIW equals to 0.4 of wavelength and the slot is placed to the center of the wider part of TIW. These simple rules allow the antenna to achieve good radiation parameters.
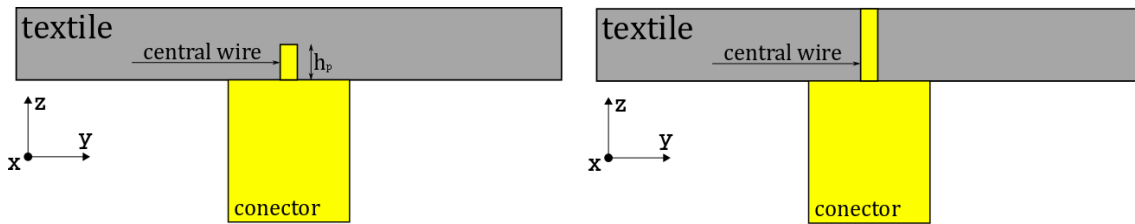
Figure 34 Coaxial excitation of TIW feeder: SMA not connected to top wall (left),
SMA connected to top wall (right).

The TIW feeder is recommended to be excited by a coaxial probe from the bottom. Figure 34 shows two possible ways of the excitation. The thickness of the 3D textile is usually higher than the thickness of conventionally used substrates. For this reason, the conventional transition between TIW and the coaxial does not work, and the conventional transition between the rectangular waveguide and the coaxial probe is a proper solution. This type of transition is relatively hard to be integrated into the textile because the diameter of the central wire of the SMA connector is 1.27 mm. Moreover, placing the central wire to a correct position is challenging also.

Due to the limited manufacturing precision of textile technologies, the design of the antenna has to be simplified:

- The thin strip between the ring slot and the cross slot is removed. The width of the strip is about 0.2 mm at 24 GHz and touches limits of manufacturing precision.

- The width of TIW is unified keeping the larger width.

Version 2 of the antenna is depicted in Figure 35 (the radiating slot) and Figure 36 (the whole antenna). Version 2 of the antenna was designed considering screen-printing. Dimensions of version 2 of the antenna are given in Table 3.
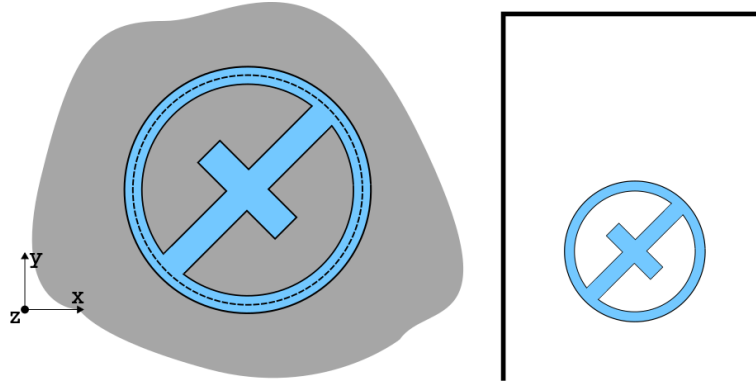
Figure 35 Version 2 of the radiating element with missing conductive strip (left),
TIW feeder with unified width (right).
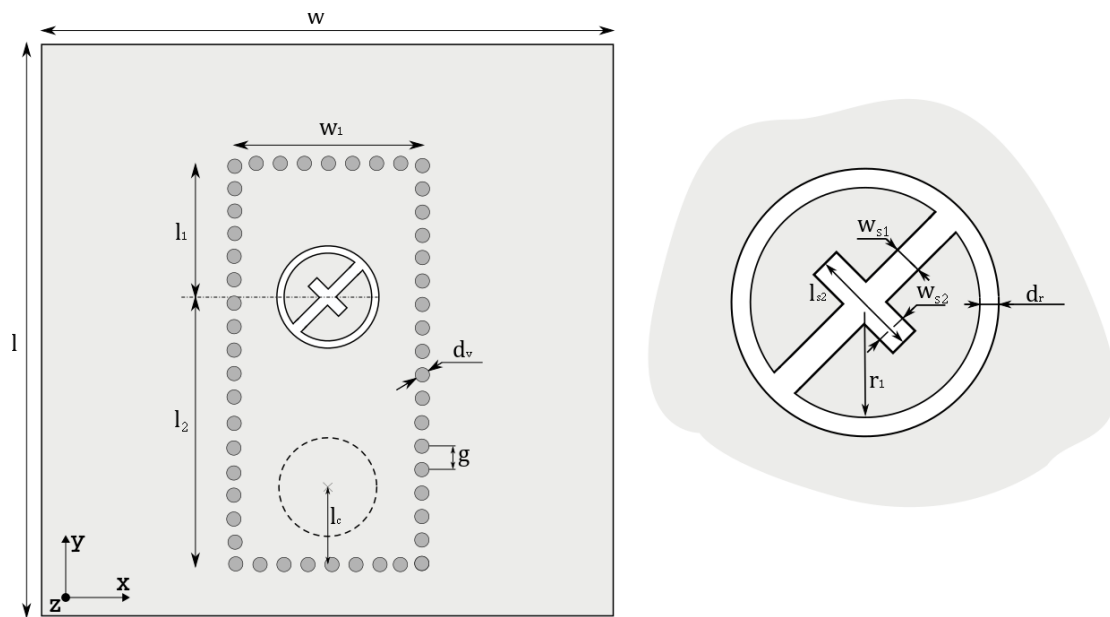
Figure 36 Version 2 of the textile-integrated antenna.
The whole antenna (left), the radiating slot (right).

Table 3 Dimensions of version 2 of the textile-integrated antenna.

Param. [mm]	l_1	l_2	w_1	d_v	g	l_c	w_{s1}	w_{s2}	l_{s2}	r_1	d_r
5.8 GHz	25.8	55.7	40.82	0.3	1.2	22.6	2.5	2.7	12.3	9.8	2.5
24 GHz	5.86	11.30	10.20	0.3	1.2	3.23	0.42	1.28	1.79	1.76	0.65

Table 4 Dimensions of version 1 of the textile-integrated antenna.

Param. [mm]	l_1	l_2	l_3	w_1	w_2	d_v	g	l_c	w_{s1}	w_{s2}	l_{s1}	l_{s2}	r_1	d_r
24 GHz	6.00	7.00	3.93	7.74	9.70	0.30	1.00	3.23	0.46	0.51	3.40	1.75	1.85	0.27

5.2 Simulation, implementation and measurement of TIW antennas

Textile-integrated antennas are constructed on textile substrates by screen-printing the conductive layers and sewing the sidewalls; hence conductivities are different.

The textile substrate is inhomogeneous; consists of vertical textile fibers from different materials in free space. The substrate can be affected by humidity or mechanical pressure during manufacturing. The thickness of the textile substrate can vary for about ±0.2 mm. Sidewalls can be manufactured using eyelets [36] or conductive threads [37] with limited accuracy. The resistance of threads vary from 10 Ω to 10 kΩ.

Simulations of textile-integrated structures are therefore rather difficult since the conventional simulation software is not adopted for such complex and random structures. Open literature shows that textile-integrated antennas can be simulated as SIW antennas on conventional microwave substrates. In next paragraphs, simulations of textile-integrated antennas designed for the ISM band 24 GHz are described using conventional simulation software and conventional principles.

Version 1: simulation

The antenna was simulated in CST Microwave Studio. Simplified simulations considered continuous metal sidewalls of TIW and feeding by a waveguide port connected to TIW directly (the red line in Figure 32). The antenna was optimized for resonance frequency 24 GHz and axial ratio lower than 3 dB in the frequency range from 24.00 GHz to 24.25 GHz.

The principle of antenna operation is demonstrated by electric and magnetic field distribution in TIW and in the plane of the slot (see Figure 37). The electric field is visualized for three cases:

- The ring slot is covered by PEC;
- The cross slot is covered by PEC;
- All slots are uncovered.

Figure 38 shows the rotation of the electrical field in the slot in a different time (phase).
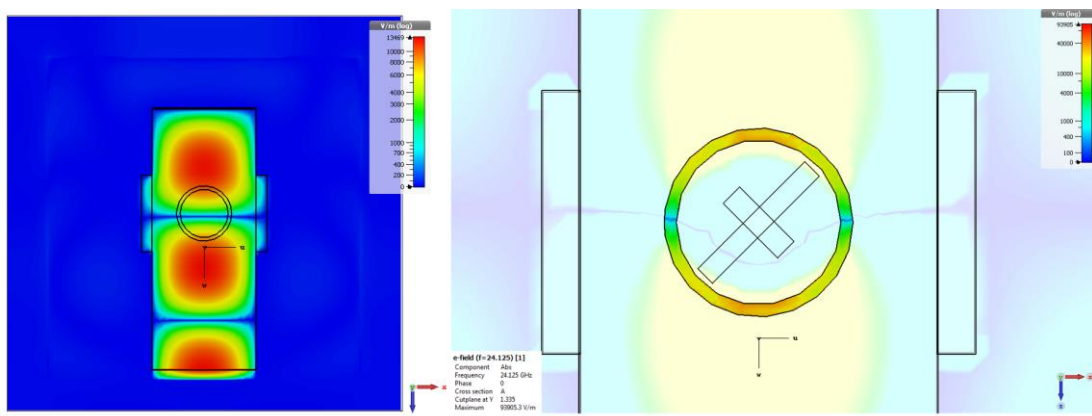
Figure 37 Electrical field in TIW (left), electrical field in the ring slot (right).
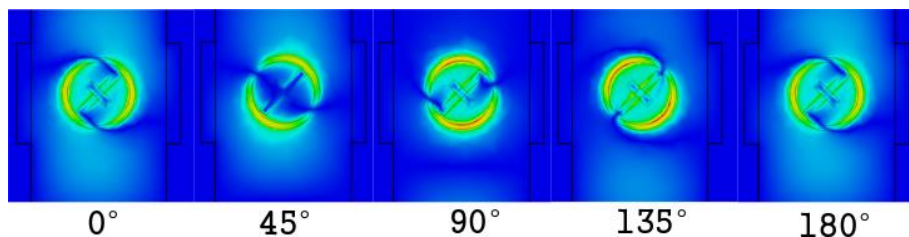
Figure 38 Rotation of E-filed in the ring slot with the cross slot inside.

The frequency response of the reflection coefficient of the simulated version 1 antenna with full sidewalls and the waveguide port connected directly to the waveguide is depicted in Figure 39. The impedance bandwidth of the antenna for $S_{11} < -10$ dB is 11.05 % (23.18 GHz to 25.83 GHz).

The AR bandwidth of the version 1 (see Figure 40) is lower than the impedance bandwidth, reaches 327 MHz and covers the whole ISM band. The antenna was not optimized for the best parameters because the model is strongly simplified.
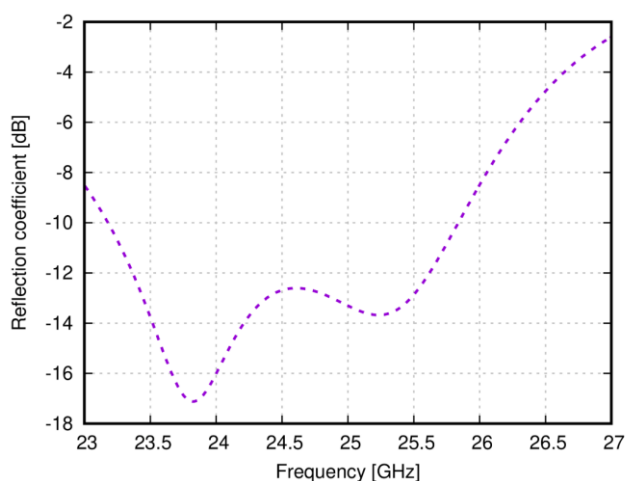
Figure 39 Simulated frequency response of reflection coefficient of the version 1 antenna: continuous walls and waveguide port.
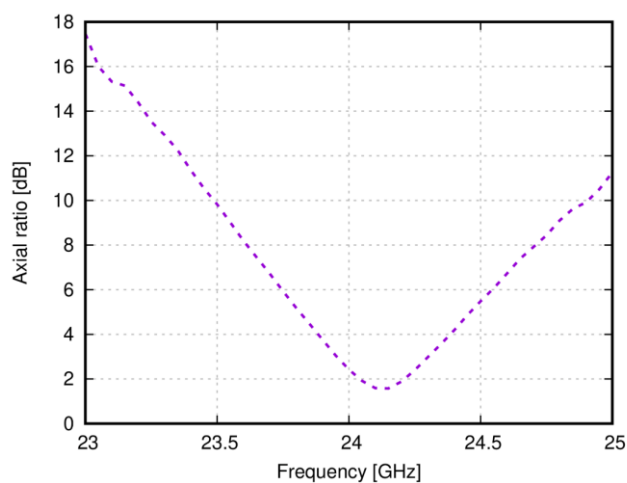
Figure 40 Simulated frequency response of axial ratio of the version 1 antenna: continuous walls and waveguide port.

Radiation patterns of the version 1 antennas are shown in **Figure 41** and **Figure 42**. The width of the main lobe is 101° in the XZ plane and 100.7° in the YZ plane. The maximal gain is 6.61 dBi and the maximum is shifted to directions 17° and 23°. The gain in the front direction is 5.53 dBi.
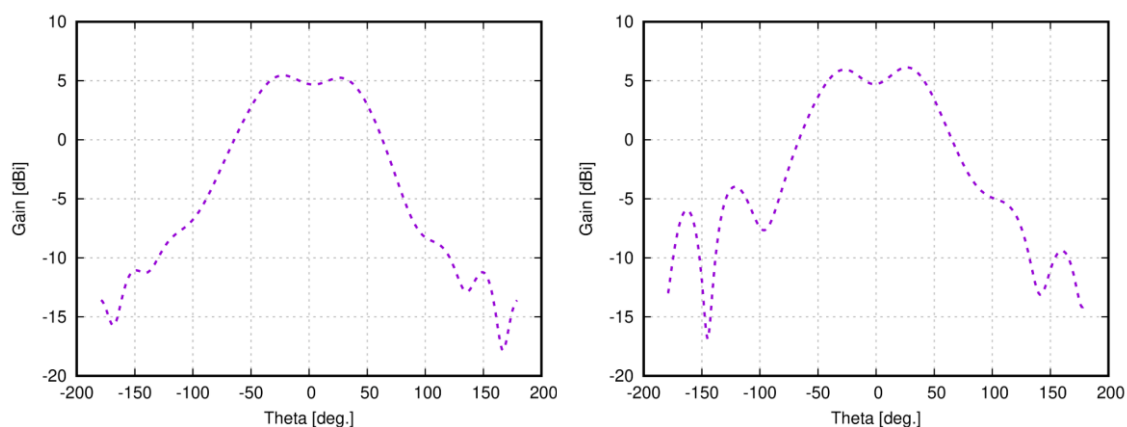
Figure 41 Simulated radiation patterns of the version 1 antenna
with the waveguide port: XZ plane (left) and YZ plane (right).
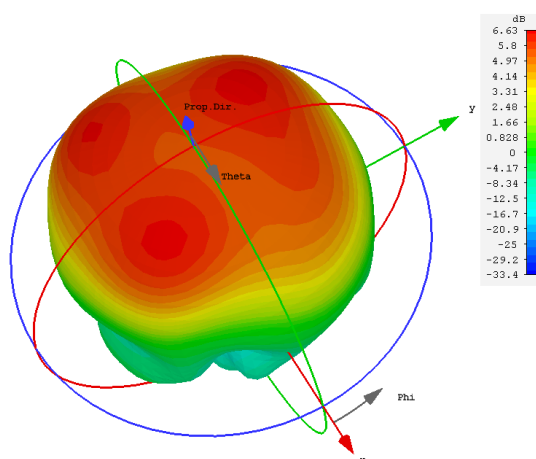
Figure 42 Simulated 3D radiation pattern of the version 1 antenna
with the waveguide port.

In the full model of the version 1 antenna (Figure 32 right), continuous sidewalls were replaced by posts from the conductive thread and TIW was excited by the coaxial probe. Instead of the coaxial probe, we can use a conventional waveguide operating at the frequency 24 GHz. Strips, microstrips, and coplanar waveguides cannot be used at this frequency on the textile substrate of a given thickness.

A precise SMA connector is used to excite the waveguide in the optimum position. Since TIW meets objectives of a rectangular waveguide, the SMA center pin is not connected to the top side of the TIW (see Figure 34).

The antennas were simulated as idealized models, where the conductive material is represented by PEC and the TIW structure is replaced by full walls. Location of the excitation is the same for

both the antennas. The length of the used probe (in case the central pin is not connected to the top conductive layer) is 1.95 mm and the 3D textile 3D097 ($h = 2.6$ mm) is used as a substrate.

Frequency responses of reflection and transmission coefficients are depicted in Figure 43 (the center pin of the coaxial probe is not connected to the top conductive layer of TIW) and Figure 44 (the center pin is connected to the top conductive layer). The transmission coefficient of the non-connected transition is −0.16 dB and the reflection coefficient is −21.5 dB at the frequency 24 GHz. The transmission coefficient is −4.14 dB and reflection coefficient is −2.23 dB for the connected central wire.
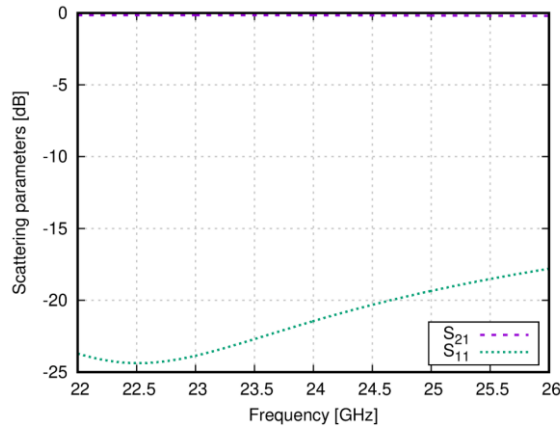
Figure 43 Simulated frequency responses of S-parameters of the version 1 antenna: center pin is not connected to conductive top wall of TIW ($h = 2.6$ mm, $f = 24$ GHz).
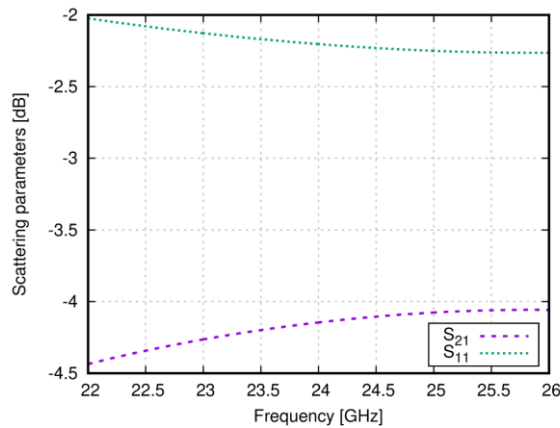
Figure 44 Simulated frequency responses of S-parameters of the version 1 antenna: center pin is connected to conductive top wall of TIW ($h = 2.6$ mm, $f = 24$ GHz).

All the sidewalls are hand-made, and the precision of the sewing is very low. Therefore, parametric analyses were performed to test influence of selected critical dimensions of radiating elements and TIW feeders on manufacturing tolerances. During parametric analyses, we changed the length of arms of the cross slot l_{s1} and l_{s2}, the width of arms w_s and the width of the radiating circular slot d_r. Those parameters provide a good description of the antenna performance. The parameters are shown in Table 5 with their limits and the step. Frequency response of the reflection coefficient, the axial ratio and the gain were observed during parametric analyses.

Table 5 Variation of parameters of the version 1 antenna
during the parametric analysis.

Parameter	Limits	Step
d_r	0.10 – 0.40 mm	0.1 mm
l_{s1}	1.50 – 1.90 mm	0.1 mm
l_{s2}	0.70 – 1.10 mm	0.1 mm
w_2	0.50 – 1.50 mm	0.5 mm
w_s	0.10 – 0.40 mm	0.1 mm

In Figure 45, influence of the width of the circular ring slot d_r on antenna parameters is analyzed. Variation of the width of the ring slot influences the reflection coefficient at the input of the antenna. The reflection coefficient changes its magnitude and the frequency of resonance. The frequency of resonance is influenced because the inner radius of the slot stays constant and the outer radius varies. Magnitude of the minimum of the axial ratio varies for about 3 dB and the frequency of the minimum changes in range of 0.5 GHz. If the d_r equals to 0.4 mm, the gain is almost constant over frequency.
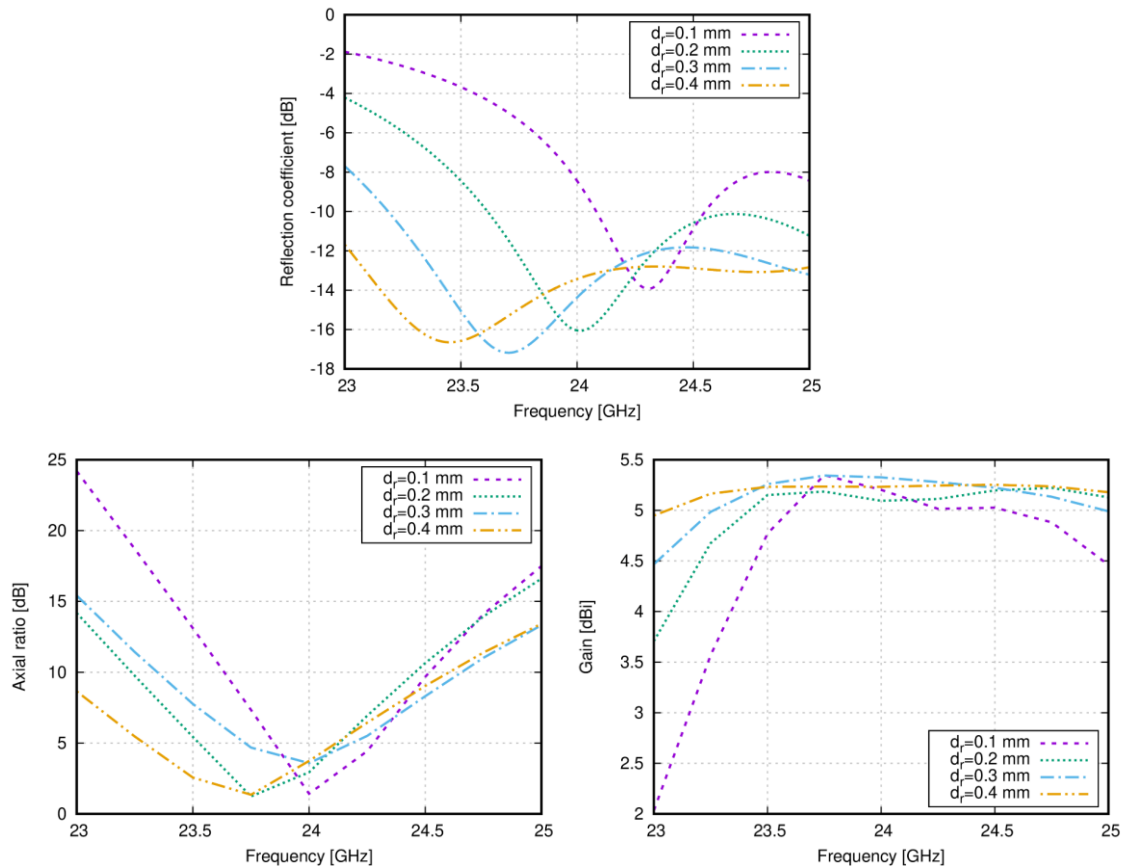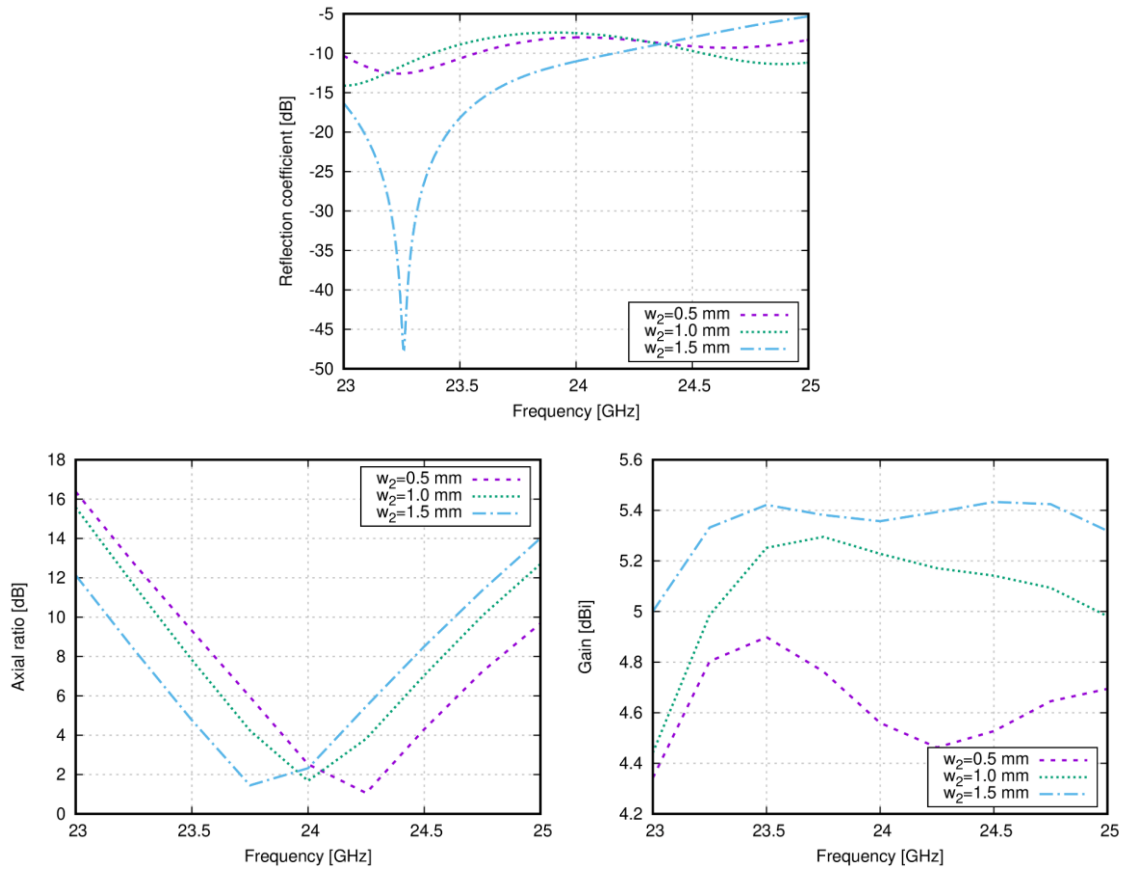

Figure 45 Frequency response of the reflection coefficient (top); frequency response of axial ratio (bottom left); frequency response of gain (bottom (right).
Width of the circular ring slot d_r varied during parametric analysis.
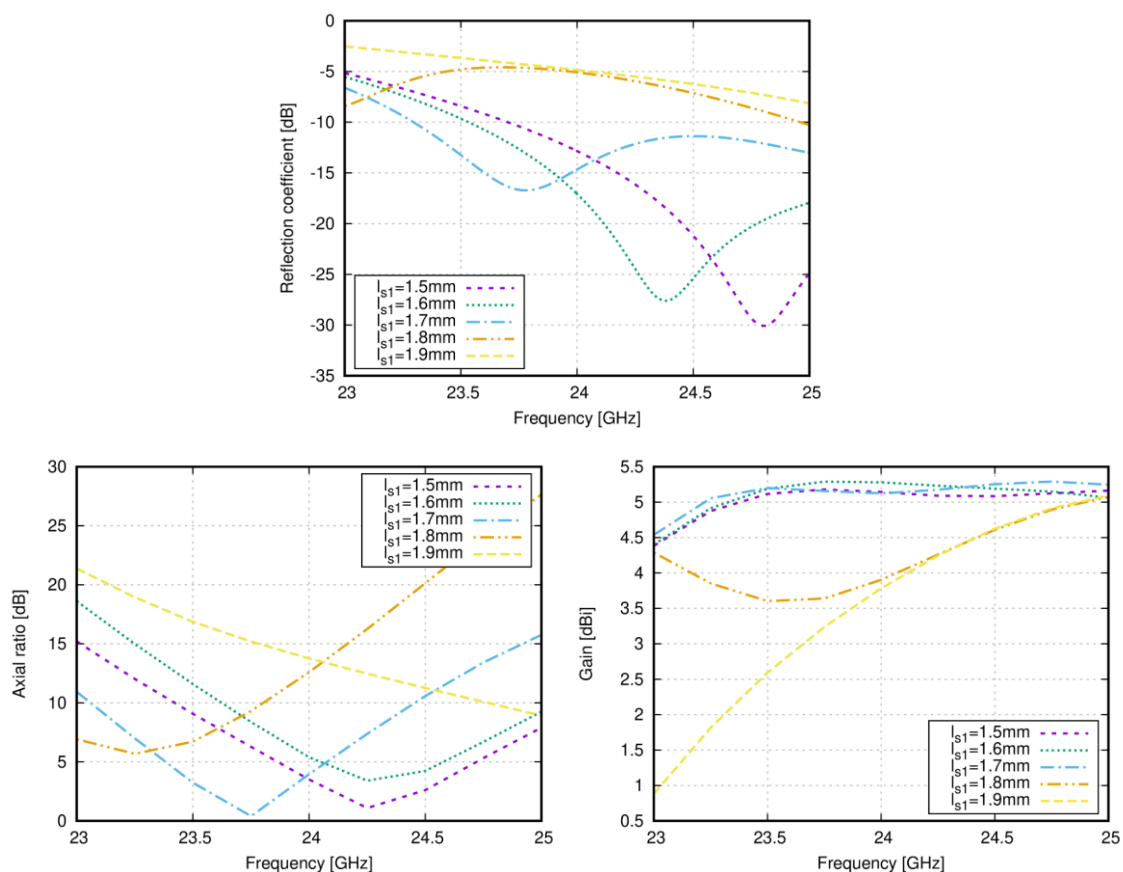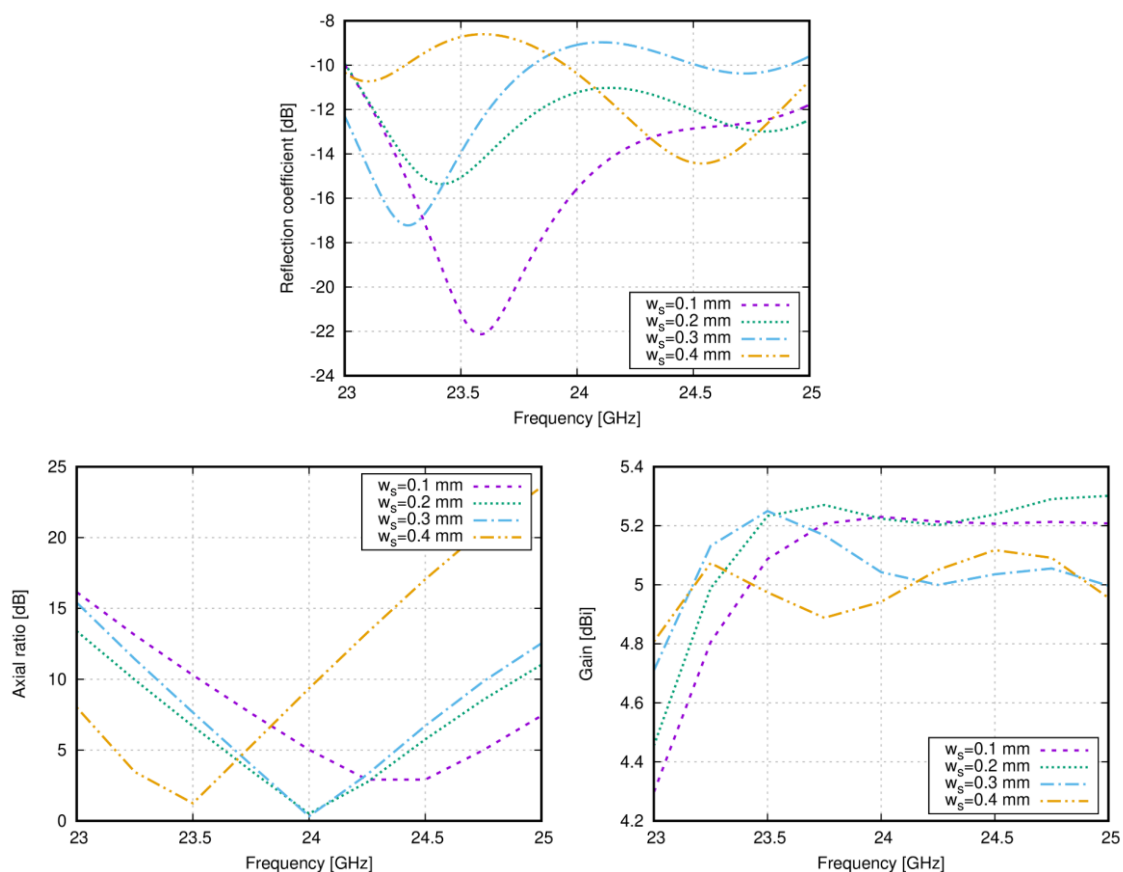
Figure 46 Frequency response of the reflection coefficient (top); frequency response of axial ratio (bottom left); frequency response of gain (bottom (right)).
Length of longest arm of cross slot l_{s1} varied during parametric analysis.

In Figure 46, influence of the length of longest arm of the cross slot l_{s1} on antenna parameters is analyzed. The parameter l_{s1} influences the frequency response of the reflection coefficient and the axial ratio. If the parameter l_{s1} is 1.9 mm, the cross-slot arm meets the ring slot and the antenna totally changes its parameters (the axial ratio, the gain). The minimum of the reflection coefficient varies from 23.8 GHz (1.7 mm) to 24.8 GHz. If the l_{s1} is in range from 1.5 mm to 1.7 mm, the gain stays practically the same (changes about 0.25 dB). The variation of l_{s2} does not influence the reflection coefficient of the antenna because the shortest arm is short and far away from the ring slot. The minimum of the axial ratio varies between 23.5 GHz and 24 GHz and the magnitude of the axial ratio is about 2 dB. The gain of the antenna varies from 4.8 dBi to 5.25 dBi. The changes of l_{s2} influence the shape of radiation patterns.
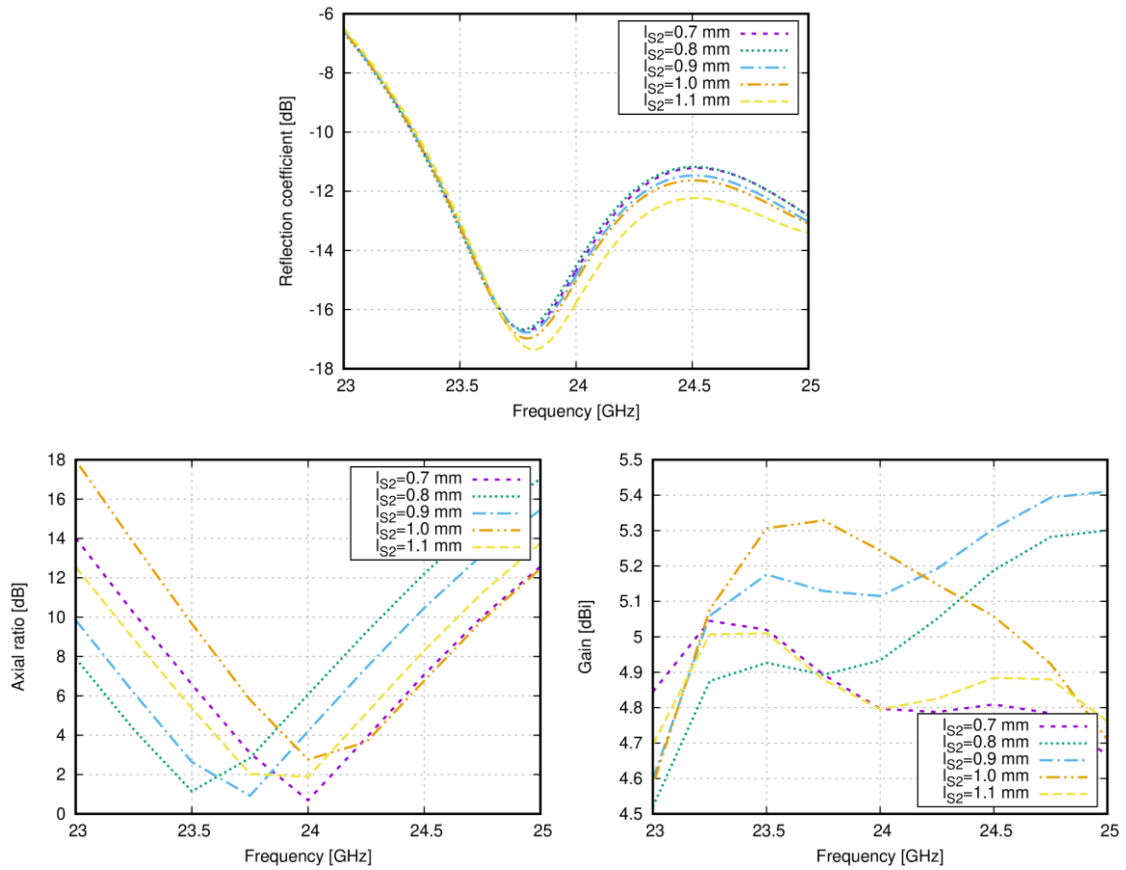
Figure 47 Frequency response of the reflection coefficient (top); frequency response of axial ratio (bottom left); frequency response of gain (bottom (right).
Length of shortest arm of cross slot l_{s2} varied during parametric analysis.

In **Figure 47**, influence of the length of shortest arm of the cross slot l_{s2} on antenna parameters is analyzed. Frequency response of the reflection coefficient is not influenced significantly. Frequency of the minimum of the axial ratio varies from 23.5 GHz to 24.0 GHz. And the maximum gain in the frequency band of operation is obtained for $l_{s2} = 1.0$ mm.

Figure 48 Frequency response of the reflection coefficient (top); frequency response of axial ratio (bottom left); frequency response of gain (bottom (right).
Width of wider TIW part w_2 varied during parametric analysis.

In Figure 48, influence of the width of the wider part of the TIW w_2 on antenna parameters is analyzed. The width of the TIW changes electromagnetic field distribution inside the waveguide, and the field in the slot is different too. The width of the TIW strongly influences frequency response of the reflection coefficient. On the other hand, changes of the frequency response of the axial ratio are relatively small (the minimum shift is about 0.5 dB) considering the difference is 1 mm. The gain varies from 4.6 dBi ($w_2 = 0.5$ mm) to 5.35 dBi ($w_2 = 1.5$ mm).

Figure 49 Frequency response of the reflection coefficient (top); frequency response of axial ratio (bottom left); frequency response of gain (bottom (right).
Width of cross slot w_s varied during parametric analysis.

In Figure 49, influence of the width of cross slot w_s on antenna parameters is analyzed. This width influences all antenna parameters, but the variation of the gain is relatively small. Dealing with frequency response of the reflection coefficient, the matching of the antenna is better if the width of the slot is small (simulated 0.1 mm) but this dimension is too small for the manufacturing process.

Now, let us turn the attention to the full model of the version 1 antenna. The full model was optimized for the ISM band 24 GHz (24.00 GHz to 24.25 GHz) and antenna parameters (reflection coefficient, axial ratio, radiation pattern, gain) were investigated in this band.

Frequency response of the reflection coefficient of the antenna is depicted in Figure 50. The impedance bandwidth of the antenna is 2.67 GHz comprising two main resonances (23.76 GHz and 25.69 GHz). The value of S_{11} is for about 2 dB higher compared with the simplified antenna (a waveguide port instead of the SMA feeding).

Frequency response of the axial ratio is shown in Figure 51. The AR bandwidth is 470 MHz and the minimal value of the AR is 1.39 dB at the frequency 24.24 GHz.
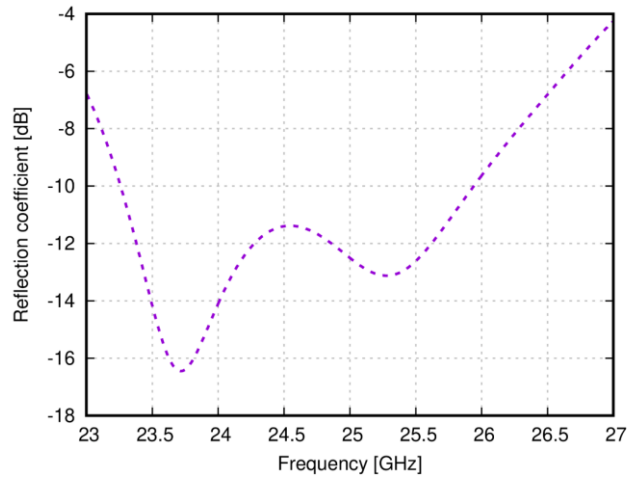
Figure 50 Simulated frequency response of reflection coefficient of version 1 antenna; feeding with connected SMA connector.
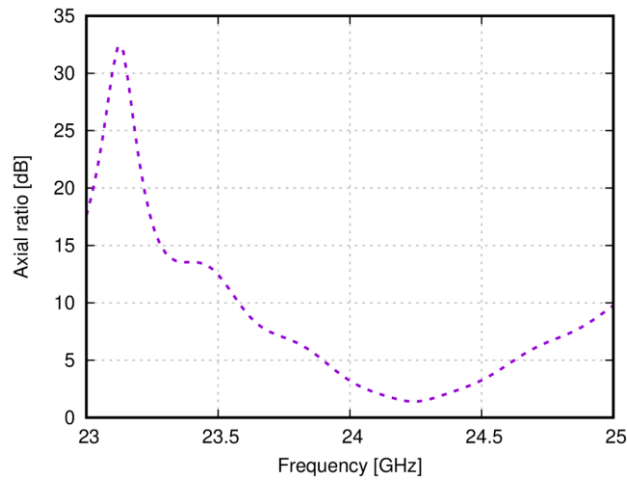
Figure 51 Simulated frequency response of axial ratio of version 1 antenna; feeding with connected SMA connector.
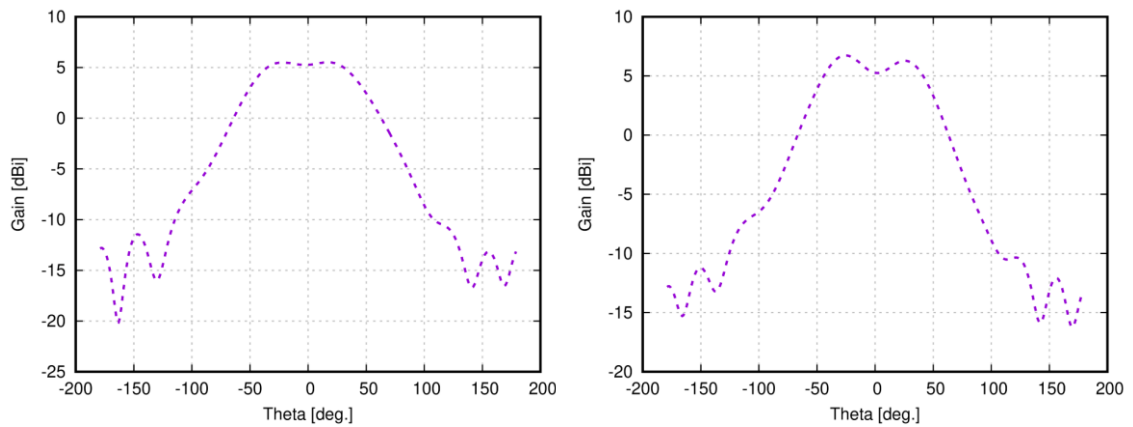
Figure 52 Simulated radiation patterns of version 1 antenna in XZ plane (left), YZ plane (right); feeding with connected SMA connector.

Figure 52 shows radiation patterns of the full model of the antenna. The main lobe is divided by small *gain gap* about 0.3 dB into two parts. The width of the main lobe is 102.3° in the XZ plane and 98.8° in the YZ plane. The maximum gain of the antenna is 6.77 dB and declines from the Z axis to the Y axis for −25°. The side lobe level of the simulated antenna is −18 dB.

Version 1: implementation and measurement

The antenna was fabricated from the 3D knitted fabric 3D097 produced by SINTEX. The relative permittivity of the fabric was 1.2 and the height was 2.6 mm. The conductive metal layers were manufactured by the PCB technology from a self-adhesive copper foil (the thickness 0.03 mm). The PCB technology allowed to achieve a good manufacturing precision which is important at the operation frequency 24 GHz.

The sidewalls of TIW were sewed by the conductive thread ELITEX 440 dtex produced by IMBUT. The resistivity of the thread was 15.52 Ω (for details, see Chapter 6). The precise connector was soldered to the bottom conductive copper foil. Photography of the manufactured antenna is depicted in Figure 53.

Figure 53 Photograph of the version 1 antenna for the ISM band 25 GHz;
manufactured from copper foil.

Antenna parameters (reflection coefficient, axial ratio, radiation patterns, gain) were measured by VNA ZVA-110 in an anechoic chamber. Dependencies in Figure 54 to Figure 56 show that the operation frequency of the antenna was shifted from 24 GHz to 22 GHz. This frequency shift was caused by under-etching of the cross slot and the ring slot. The requested length of the first arm of the cross slot was increased from 3.39 mm to 3.60 mm and the resonance frequency of the antenna was shifted to 22.3 GHz. The simulation model was therefore modified accordingly. Then, the measured data showed a good agreement with simulated ones.

Figure 54 shows that the measured value of reflection coefficient decreased for about 4 dB with respect to simulation. The bandwidth of the antenna was 800 MHz. This decrease was caused by a combination of several factors:

- Additional losses are given by conductivity of the used thread,
- Additional losses are given by humidity in the knitted fabric,
- The simulation model did not contain all changes of dimensions caused by under-etching.
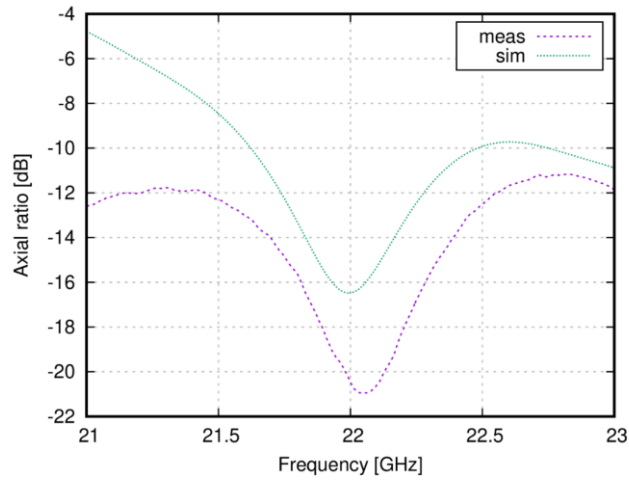
Figure 54 Version 1 antenna for the ISM band 25 GHz:
simulated and measured frequency response of reflection coefficient.
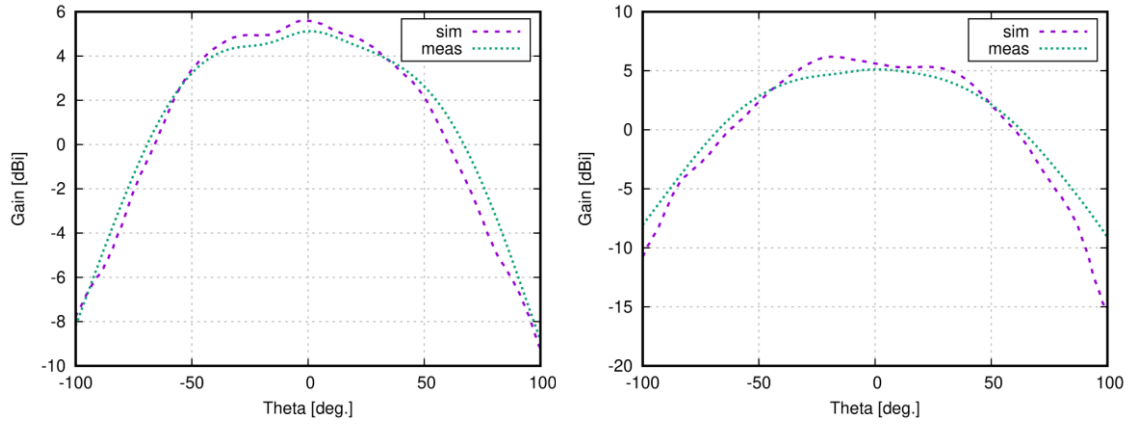
Figure 55 Version 1 antenna for the ISM band 25 GHz:
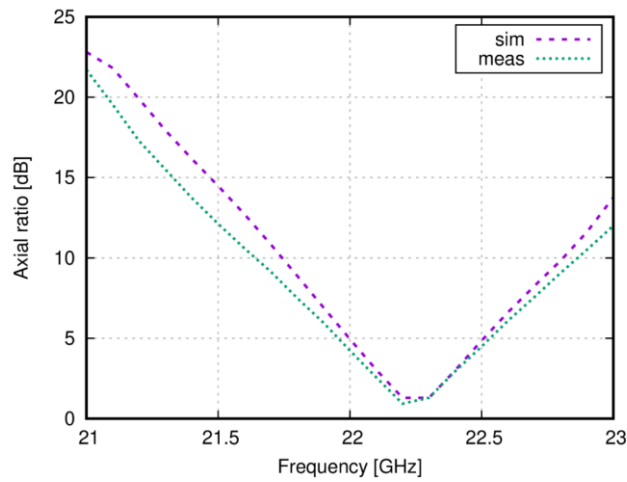simulated and measured radiation patterns in XZ plane (left) and YZ plane (right).

Figure 56 Version 1 antenna for the ISM band 25 GHz:
simulated and measurement frequency response of axial ratio.

Radiation patterns and the gain of the antenna are shown in Figure 55. The measured gain is 5.81 dBi at the frequency 22.20 GHz and the main lobe width in the XZ plane is 112° and in the YZ plane is 91°. Due to the configuration of the anechoic chamber, radiation patterns were measured only in the span from −100° to 100° in both planes.

Figure 56 shows frequency response of the axial ratio of the version 1 antenna. The minimal value of the AR is 0.93 dB at the frequency 22.20 GHz and the AR bandwidth is 386 MHz.

Version 2: simulations

The version 2 of the antenna was designed at two frequencies. The first one was the ISM band 5.8 GHz and the second one the ISM band 24 GHz. Both the antennas were designed by same procedure and optimized for typical impedance and axial ratio bandwidths and maximal radiation in the front direction.

Let us start with the 5.8 GHz antenna. Figure 57 shows frequency response of the reflection coefficient simulated in CST Microwave Studio. The designed antenna had the impedance bandwidth 682 MHz and two resonances close to frequencies 5.9 GHz and 5.7 GHz. The impedance bandwidth of the version 2 antenna is as wide as the version 1 antenna. The value of S_{11} at 5.8 GHz is −15.6 dB and is between resonances. In this simulation, no foil separating the conductive (screen-printed) surfaces and the textile substrate was considered.
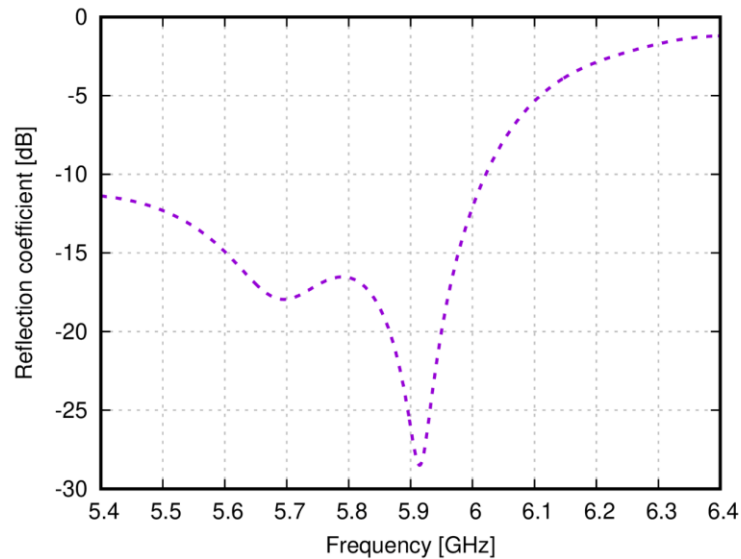
Figure 57 Frequency response of reflection coefficient of the version 2 antenna; simulated without foil.

The frequency response of axial ratio is shown in Figure 58. The minimal value of AR is 0.4 dB at the frequency 5.8 GHz. The axial ratio bandwidth (AR smaller than 3 dB) is 151 MHz. Even in that case, the foil separating the textile material and conductive surfaces was not considered.

Figure 59 shows radiation patterns of the antenna at the frequency 5.8 GHz in two planes. The maximum gain in the front direction is 4.92 dBi and the elevation angle of the maximum is 5° in the XZ plane. The maximum gain in the YZ plane is 4.96 dBi and the elevation angle is −23° in

the YZ plane. The main lobe width is 92.1° in the YZ plane and 87.5° in the XZ plane. The sidelobe level is −20 dB.
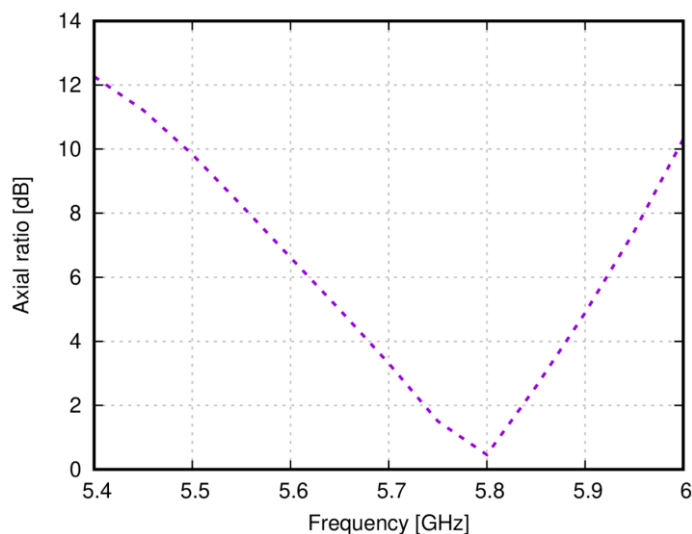
Figure 58 Frequency response of AR of the version 2 antenna; simulated without foil.
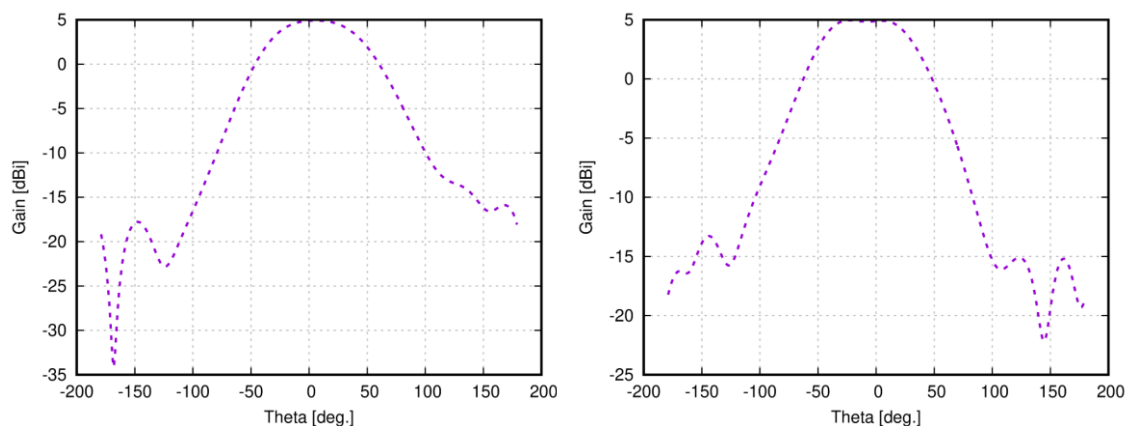
Figure 59 Radiation patterns of the version 2 antenna; simulated without foil in AR minimum.

Now, attention is turned to the antenna designed for the ISM band 24 GHz. The antenna is depicted in Figure 36 and the dimensions are given in Table 3. The antenna was simulated as the full-wave model in CST Microwave Studio. For the simulation, both the frequency-domain solver and the time-domain solver were used to verify results. The model was relatively complicated, including a thin layer of the DIGIFLEX MASTER foil.

Figure 60 shows frequency response of the reflection coefficient and the axial ratio in the Z direction. The impedance bandwidth of the antenna is wider than the depicted 2 GHz and is similar to the version 1 of the antenna.

The minimum of the axial ratio is 1 dB and the frequency of the minimum is 24 GHz. There are small differences between responses provided by the frequency-domain solver and the time-

domain solver. These differences can be caused by differences in meshes and solver errors. The axial ratio bandwidth is 967 MHz (T-solver) and 959 MHz (F-solver).

Radiation patterns are shown in Figure 61. The main lobe width is 104.7° in the XZ plane and 105.2° and in the YZ plane. The simulated gain of the antenna is 6.37 dBi and the main direction of the maximum is 4° in the XZ plane and 5° in the YZ plane. The front to back ratio of the antenna is 28.25 dB.
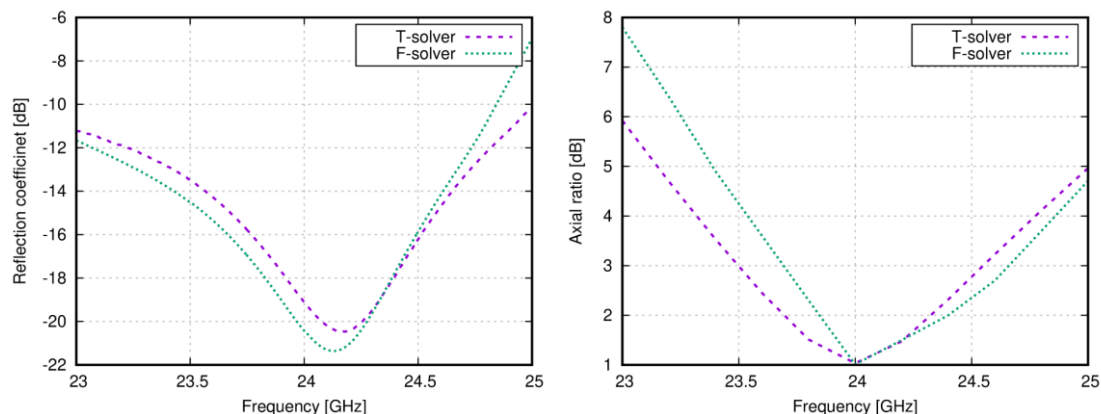
Figure 60 Frequency responses of reflection coefficient (left) and axial ratio (right) of version 2 antenna for the ISM band 24 GHz. Time-domain solver versus frequency-domain solver
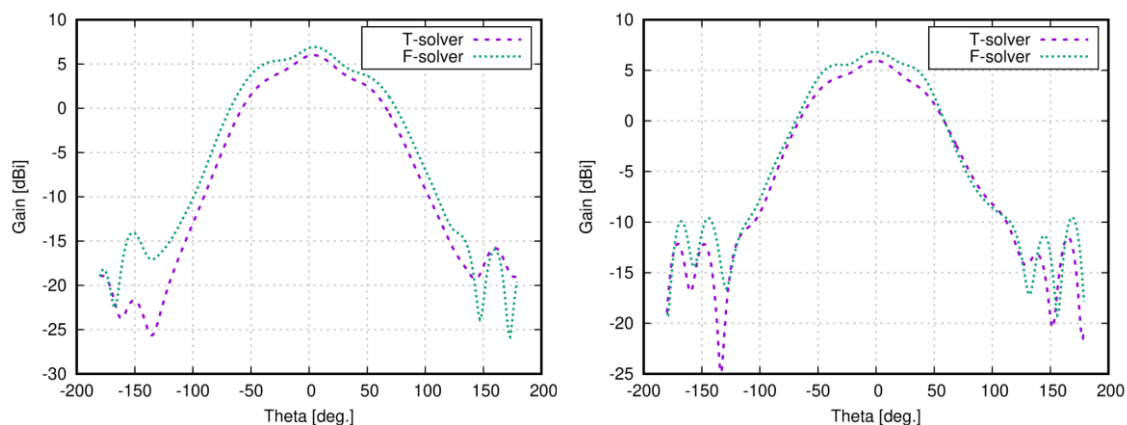
Figure 61 Radiation patterns of version 2 antenna at 24 GHz: the XZ plane (left), the YZ plane (right).

Parametric analyses are not presented because the second version of the antenna shows very similar characteristics as the version 1 antenna.

Version 2: implementation and measurement

Version 2 of the circularly polarized antenna was designed and manufactured for the ISB band 5.8 GHz and the ISM band 24 GHz. Antennas were designed on the 3D textile 3D097 with height 2.6 mm and relative permittivity 1.22. The selected 3D textile allows to create textile antennas even at frequencies above 20 GHz.

The antennas were manufactured by screen-printing, but an iron-on foil protecting the textile substrate against the penetration was not considered during the design and simulation of the antenna at 5.8 GHz. This inaccuracy in the model caused the frequency shift of antenna characteristics of the manufactured prototype.
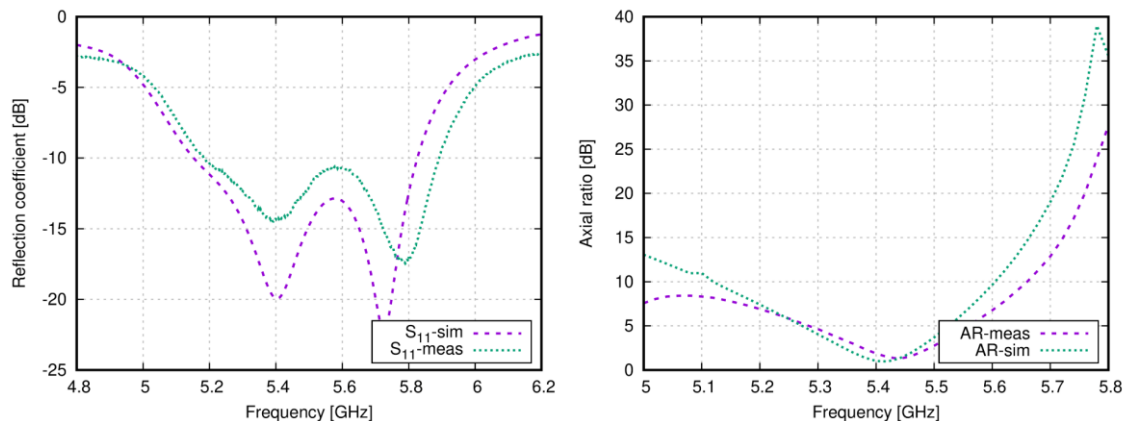
Figure 62 Version 2 antenna for ISM band 5.8 GHz: simulated and measured frequency responses of reflection coefficient (left) and axial ratio (right).

The resonant frequency of the antenna was shifted towards 5.4 GHz due the used foil. This explanation was supported by additional simulations with the foil and by comparisons with measured results.

The frequency response of the reflection coefficient is shown in Figure 62 (left). The measured bandwidth for $S_{11} < -10$ dB is 674 MHz. The AR bandwidth is 150 MHz for AR < 3 dB. The frequency response of the axial ratio is shown in Figure 62 (right) and the minimum value of AR is 1.27 dB at the frequency 5.45 GHz.
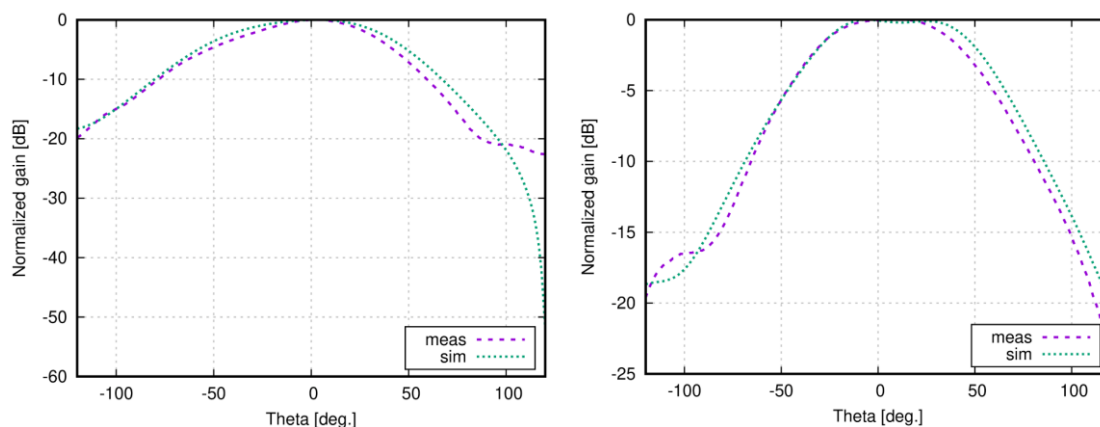
Figure 63 Measured normalized radiation patterns of version 2 antenna for ISM band 5.8 GHz: XZ plane(left), YZ plane (right).

The radiation patterns were measured in the XZ plane and the YZ plane in the span 240°. The left-handed circular polarization (LHCP) radiation patterns are shown in Figure 63. The measured width of the main lobe in the XZ plane is 86° and in the YZ plane is 94°. The gain of the measured antenna is 5.32 dBi and the elevation of maximum is –7° in the XZ plane and 3° in the YZ plane.

The difference between measured and simulated results can be caused by the measurement precision or by screen-printing (the real precision of printing on the textile is ±0.3 mm).

For the ISM band 24 GHz, two samples of the version 2 antenna were manufactured. First, the standard copper foil was used to fabricate conductive surfaces, and second, the screen-printing was applied. Both the conductive materials were placed on the DIGIFLEX MASTER foil. Using two fabrication technologies, manufacturing intolerances can be compared, and properties of the antennas can be verified.

The 3D textile material 3D097 played the role of the substrate of both the antennas. The precise SMA connector with the maximum operation frequency 24.5 GHz was used for feeding. Both versions of the antenna were manufactured considering the same source data and basic parameters were measured. The detailed description of the manufacturing process is given in Chapter 6.
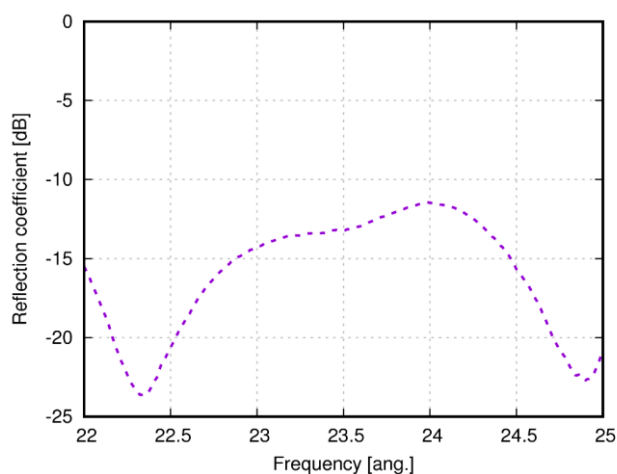
Figure 64 Measured frequency response of reflection coefficient at the input of version 2 antenna for ISM band 24 GHz (copper foil).

First, frequency response of the reflection coefficient at the input of the version 2 antenna for the ISM band 24 GHz was measured by the vector analyzer RS ZVA110 (see Figure 64). The result shows that reflections are lower than -10 dB with two modes of resonance at frequencies 22.4 GHz and 24,8 GHz. The S_{11} level at the band of interest varies from -12.15 dB to -13.08 dB.
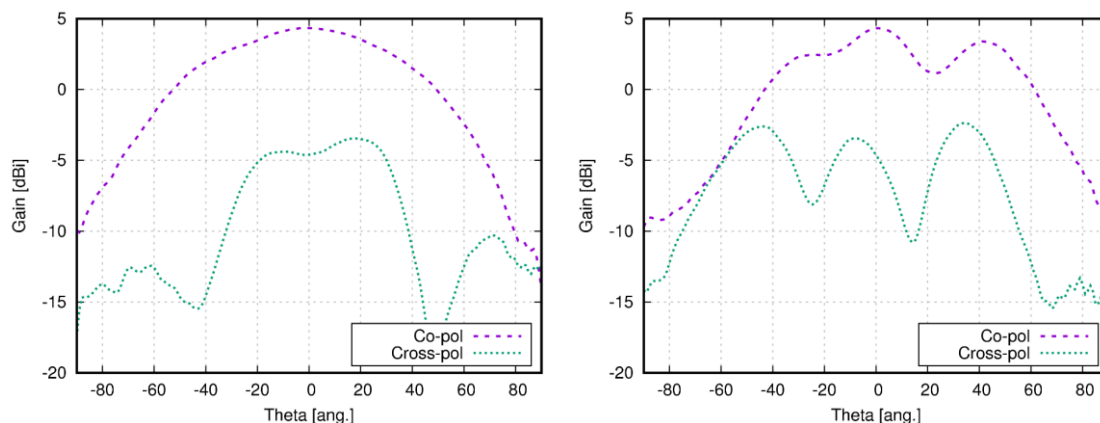
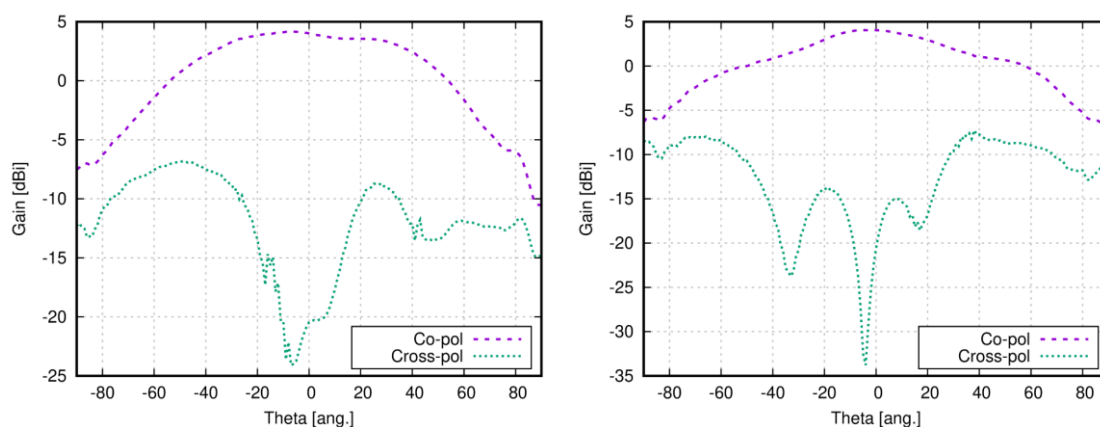**Figure 65** Measured radiation patterns of version 2 antenna for ISM band 24 GHz (copper foil): YZ plane (left); XZ plane (right).

Radiation patterns were measured in the XZ plane and the YZ plane (see Figure 65). The span of the measurement was 180° (−90°; +90°) because a good precision can be achieved in this limited span. The gain was measured by the method based on the comparison with the reference antenna. The measured beam width was 56° in the XZ plane and 84° in the YZ plane.

Frequency response of the axial ratio (Figure 66) was measured in the front direction (0°; 0°). The minimum magnitude of the AR ≈ 5.0 dB is at the frequency 23.90 GHz. Since the magnitude of the axial ratio is higher than 3 dB, the antenna radiates the elliptically polarized wave. The higher AR magnitude is caused by the manufacturing method (see Chapter 6).
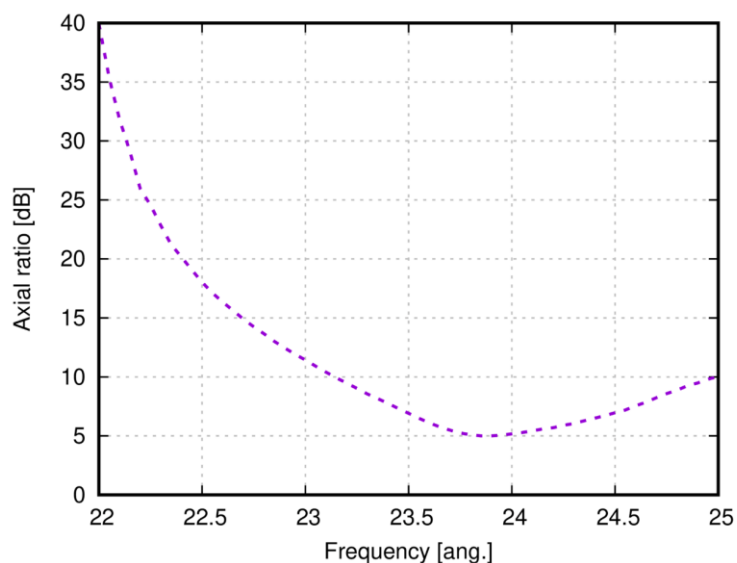
Figure 66 Frequency response of axial ratio of version 2 antenna
for ISM band 24 GHz (copper foil).
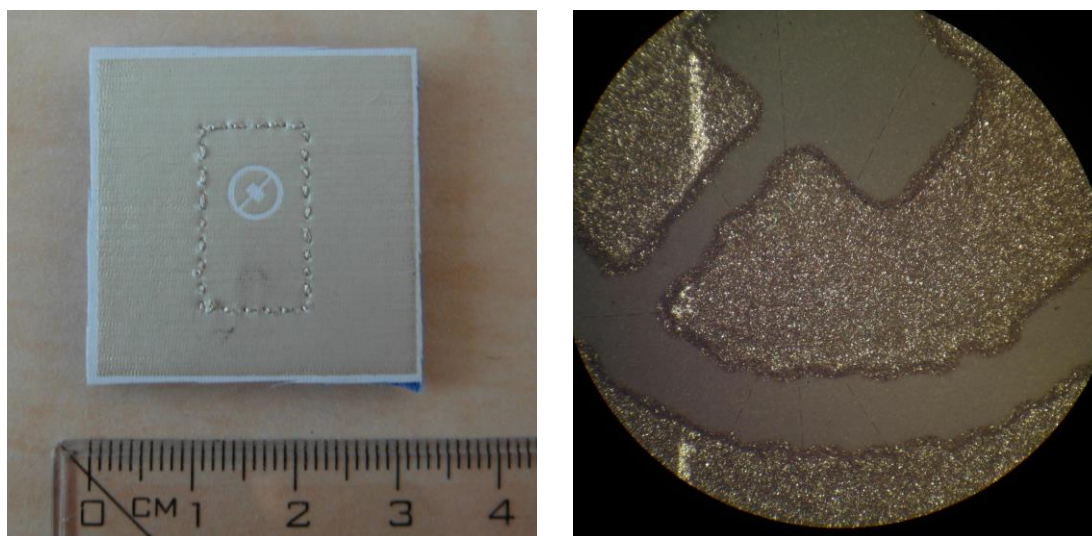
Figure 67 Photograph of the version 2 screen-printed antenna for the ISM band 24 GHz:
the macroscopic view (left), the microscopic view (right).

The antenna was printed on the DIGIFLEX MASTER foil by a silver polymer paste. In Figure 67, the macroscopic photo (left) and the microscopic one (right) are given. Since the viscosity of

the polymer paste is not high enough, the shape of the antenna layout is not sharp, and the width of the ring slot is not constant.

Measured frequency responses of the reflection coefficient and the axial ratio are shown in Figure 68. The minimum of reflection coefficient is shifted to the frequency 22.7 GHz and the shape differs from the copper antenna and the simulation. The impedance bandwidth of measured printed antenna is 3.02 GHz. Since the resonant frequency is shifted to lower frequency, also the minimum of the axial ratio is shifted to the frequency 22.25 GHz. The minimum magnitude of the axial ratio is 1.06 dB. The axial ratio bandwidth is 1.2 GHz.

Radiation patterns are shown in Figure 69 for the XZ plane and the YZ plane. The maximum of the gain declines for about –2° and –4°, respectively. The maximum gain is 4.2 dBi. The radiation patterns are measured in the minimum of the axial ratio (22.25 GHz). The width of the main lobe is 79° in the YZ plane and 95° in the XZ plane.
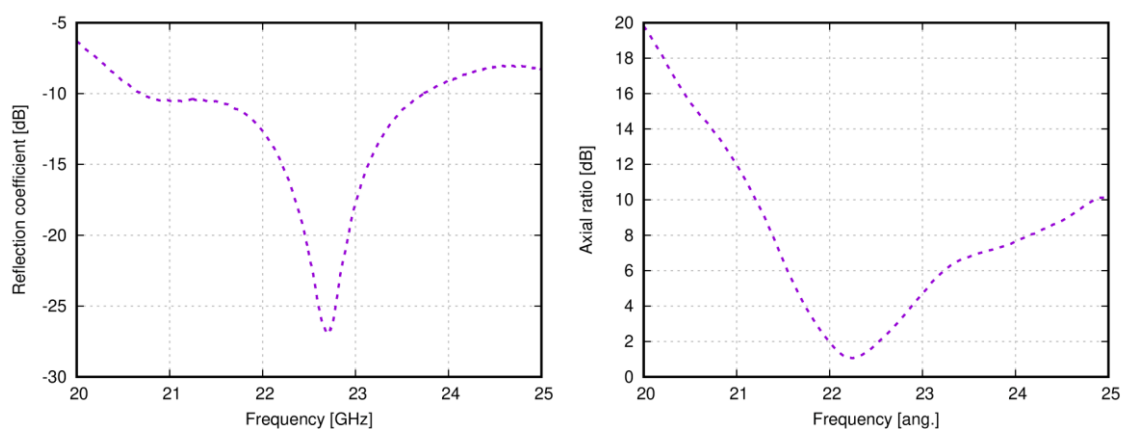
Figure 68 Measured frequency response of reflection coefficient (left) and axial ratio (right) of version 2 antenna for ISM band 24 GHz (screen printing).

Figure 69 Measured radiation patterns of version 2 antenna for ISM band 24 GHz (screen printing) at 22.25 GHz: YZ plane (left); XZ plane (right).

5.3 Conclusions

Two versions of the circularly polarized slot antenna were presented in this chapter. The First version of the antenna has been designed for ISM band 24 GHz and compared simulated and

measured results. Due to manufacturing under-etching, the resonance frequency of the antenna shifted to 22.3 GHz. The second version of the antenna was simplified and prepare for manufacturing by screen printing technology. Two versions of the antenna were manufactured. The first one was designed for ISM 5.8 GHz and the second for ISM band 24 GHz.

The resonance frequency of manufactured ISM 5.8 GHz antenna is shifted to lower frequency because the antenna was simulated without interlayer used for printing.

The version 2 of the antenna designed for the ISM band 24 GHz was manufactured using both the copper foil and screen printing. Both versions of the antenna were measured and compared with simulated data. The copper antenna is well matched at the frequency 24 GHz but the axial ratio is about 5 dB in the minimum. The resonant frequency of the screen-printed antenna is shifted to 22.7 GHz.

6 Technological Aspects

The technological aspects of manufacturing mm-wave structures on textile substrates have specific features comprising used materials, technologies and their precision which is about ±10% in the textile industry. Parameters of textile materials used as substrates, conductive surfaces or threads are given with a typical precision which is relatively low. Since the thesis deal with the design of TIW-based components and antennas, there are three main conductive objects to be characterized: textile substrates, conductive surfaces and conductive sidewalls.

3D textile materials, which are used as substrates in this work, were measured by the transmission line method and presented in [59]. Values of relative permittivity of selected textile substrates are shown in Table 6.

Table 6 Material properties of selected 3D textile substrates.

Material	Relative permittivity	Loses (tan δ)
3D041	1.22	0.0021
3D097	1.22	0.0019

Conductive surfaces are another interesting component of textile-integrated antennas and circuits. As described in the *State of the Art*, two manufacturing techniques are used in the thesis:

- **The self-adhesive copper foil**. The layout can be prepared compatibly with the standard PCB technology with the comparable precisions. The thickness of the copper foil is 0.035 mm and the glue is on its bottom side.

- **Screen printing**. A silver paste can be printed by screen printing technology to various surfaces (textiles, foams, etc.). Since the used 3D textile is porous, the silver paste penetrates into the textile substrate and does not create a conductive surface on the top of the textile only. Therefore, an iron-on foil is used to avoid the penetration of the silver paste and to smoothen the textile surface before printing. Thickness of the foil is 0.08 mm and relative permittivity 2.1. A corresponding layer has to be added to the simulation model to prevent shift of the resonant frequency.

6.1 Conductive threads

The sidewalls of TIW were shown in *State of the Art* to be implemented by various materials and technologies. Since the thesis is focused on advanced textile-integrated components, the construction of sidewalls is critical. The requirements follow:

- Good conductivity comparable with a conventional SIW;

- Good manufacturing precision and a small diameter;
- Possible hand sewing and machine manufacturing;
- Possibility to create various shapes (rectangles, circles, etc.).

Table 7 List of measured threads.

No.	Materials	Name	Linear mass density	Datasheet resistivity	Manufacturer
1.	PAD/carbon	F901	144 dtex		Shakespeare
2.	Stainless steel	Bekonix VN 14.1.9.00Z	110 tex	70	Bekaert
3.	PAD/silver	silver-stat	240 dtex	---	R-stat
4.	PAD/silver	X-static	160 dtex	---	NFT
5.	PAD/silver	Elitex 220 dtex	220 dtex	70	Imbut
6.	PAD/silver	Elitex 440 dtex	440 dtex	20	Imbut
7.	Stainless steel	Bekonix VN 12.1.2. 100Z	235 dtex	30	Bekaert
8.	Stainless steel	Bekonix VN 12.3..2.175S	760 dtex	9	Bekaert
9.	PES/Stainless steel	Bekonix BK 50/3	50/3Nm	---	Bekaert
10.	PES/Stainless steel	I-tech 20	312*3 dtex	---	Amann
11.	PES/Carbon	C-tech 80	111*3 dtex	---	Amann
12.	Silver	Schieldtex 235f	560 dtex	<100	Statex
13.	PAD/Silver	Shieldtex 110/34 dtex HC	10/34 dtex	<3000	Statex
14.	PAD/Silver	Shieldtex 110/34 dtex HC	117/17 dtex	<3000	Statex
15.	PAD/Silver	Silver-tech 120	90*3 dtex	360	Amann

Considering the above-given requirements, conductive threads or metal wires are used to create TIW sidewalls. Metal wires excel in a very high conductivity given by the metal the wire is produced from. Unfortunately, metal wires are hard to be used for sewing.

Conductive threads can be manufactured from different materials, with different thicknesses and conductivities. Conductive threads are usually composed from two types of materials – from a non-conductive fiber (cotton, polyester, etc.) and a conductive wire (silver, stainless steel, carbon, but also copper, nickel, etc.). Conductive threads are usually classified according to a used conductive material:

- **Carbon** (threads no. 1 and 11 in Table 7). Threads are dominantly used for protective clothes and EM shielding.

- **Stainless steel** (threads no. 2, and 7 to 10 in Table 7). Threads are manufactured from textile fibers and thin steel wires. Threads show a better conductivity compared to carbon threads.

- **Silver threads** (threads no. 3 to 6, and 12 to 15 in Table 7). Threads are manufactured from textile fibers which are enriched by silver particles. Silver threads show a very good conductivity even for a very thin thread (the diameter ~0.3 mm).

Instead of the diameter, threads are usually characterized by the linear mass density given in tex and dtex. The unit tex is used for natural-based fibers [60]

$$T(tex) = \frac{M(g)}{L(km)} \tag{5}$$

and the unit dtex is used for synthetic materials [60]

$$1dtex = \frac{M(g)}{L(10km)} \tag{6}$$

where *M* represents the weight of a sample and *L* is the length of this sample.

6.2 Measurement of threads and results

Conductive threads are produced by different manufacturers from different materials with various thicknesses. Obviously, mechanical parameters (elasticity) and electrical parameters (resistance) of those threads differ. Some threads can change its resistance depending on the tension (which is used for sensing mechanical tension or breath).
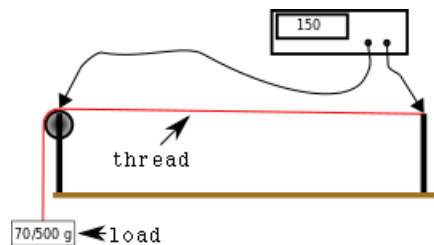
Figure 70 Measurement of threads.

The threads were measured by the RLC meter LCR-819 between two points (see Figure 70). The threads were stretched by loads 70 g and 500 g. The threads were measured at four frequencies – DC, 1 kHz, 10 kHz and 100 kHz. Each thread was measured five times on a different part to minimize the influence of inhomogeneities. Final values of resistivity of all measured threads are given in Table 7. If some values miss, the resistivity was not measured.

Carbon threads have the resistance ~100 MΩ and are suitable for manufacturing clothes which shield EM fields.

Two stainless-steel threads (Bekonix VN 12.3.2.175S and Bekonix BK50/3) have the resistance around ~1 kΩ; this higher resistance is given by the structure of threads. Other two stainless-steel threads (Bekonix VN 12.1.2. 100Z and Bekonix VN 12.3.2.175S) have the

resistance between ~10 Ω and ~40 Ω; these threads are well-conductive at DC and low frequencies, but their linear mass density is relatively high and it is difficult to sew with them.

Silver threads exhibit significant differences in resistance, but the resistance is relatively low for all the threads. The resistance ranges from ~10 Ω to ~1 kΩ, depends on the construction of threads and the amount of silver used. The threads ELITEX 220 dtex and ELITEX 440 dtex have the best resistance, their linear mass density is relatively low, and the threads are suitable both for manual and machine sewing.

The threads with the resistance lower than 100 Ω were chosen for further testing. The SIW was designed and sidewalls were sewed by tested conductive threads. The SIW was designed for a conventional FR4 substrate with relative permittivity 4.2 and tan δ = 0.02. The cutoff frequency was 5 GHz and the operation frequency 8 GHz. Diameter of metallized vias creating the sidewalls was 1 mm and the distance between two vias was 1 mm. Metalized vias of one testing sample were created by a conventional PCB technology and this sample was the reference for comparison.

Table 8 Measured resistivity of conductive threads.

	70 g				500 g			
	DC	1 kHz	10 kHz	100 kHz	DC	1 kHz	10 kHz	100 kHz
1.	7.7 M	2.54 M	2.5 M	697.7 k	------	------	------	------
2.	73.33	68.92	68.9	69.72	69.61	68.94	68.96	69.42
3.	226	228.8	228.6	229.4	234	232	232.2	233.2
4.	232	255.4	254.6	254.6	------	------	------	------
5.	72.26	72.42	74.92	63.60	NA	NA	NA	NA
6.	14.08	14.22	14.25	14.30	15.52	15.56	15.70	15.68
7.	50	36.2	37.46	31.8	38	29.88	29.8	29.86
8.	11	9.23	9.18	9.32	10.8	9.18	9.19	9.25
9.	3 k	4.04 k	2.228 k	13.34 k	1.6 k	1.904 k	1.666 k	1.53 k
10.	7 k	3.26 k	3.82 k	2.394 k	2.5 k	2.394 k	2.34 k	2.626 k
11.	> 200 M	>200 M	75.78 M	0.5 M	> 200 M	> 200 M	53.2 M	> 200 M
12.	15	13.88	13.95	13.95	14.11	13.32	13.64	13.67
13.	758	848	823.2	743	643	594.32	633	652
14.	141	140.8	140.5	140.24	148.1	149.8	149.6	149.8
15.	309	305.60	305.40	304	311	308	310	310

The threads 2, 5, 6, 7, 8 and 12 were selected to create the sidewalls of SIW, and the SIW was simulated in CST Microwave Studio. SIW was not optimize for the best S_{21} but it is only as a testing example. The cutoff frequency was s 5 GHz. The simulated results are shown in Figure 71. The transmission coefficient varies between −2 dB and −3 dB.

The simulated SIW manufactured in two samples − with metallized vias and empty holes. Through empty holes, conductive threads were laced to create sidewalls. Measured results are given in Figure 72. The transmission coefficient S_{21} for the copper wire is in a good agreement with simulation.

The silver threads 2, 5, 6 and 12 show a different DC conductivity and very similar transmissions when used as sidewalls of the FR4 SIW. The transmissions of SIW with sidewalls implemented by the thread 12 and the copper wire are in a good agreement. The thread 6 provides good results too, but there is a gap around 7 GHz; the transmission coefficient is around −2.5 dB. The threads 2 and 5 show worse parameters than previous ones; the transmission coefficient varies between −2.5 dB and −3 dB. All these threads are suitable for implementing conductive walls of TIW components.

In case of stainless-steel threads 7 and 8, the transmission coefficient of SIW rapidly changes with frequency: S_{21} is −6.4 dB for the thread 7 and −8.1 dB for the thread 8 at the frequency 7 GHz (see Figure 72). The threads 7 and 8 are harder than others and a conductive connection between the copper part of the waveguide and threads is not ideal.
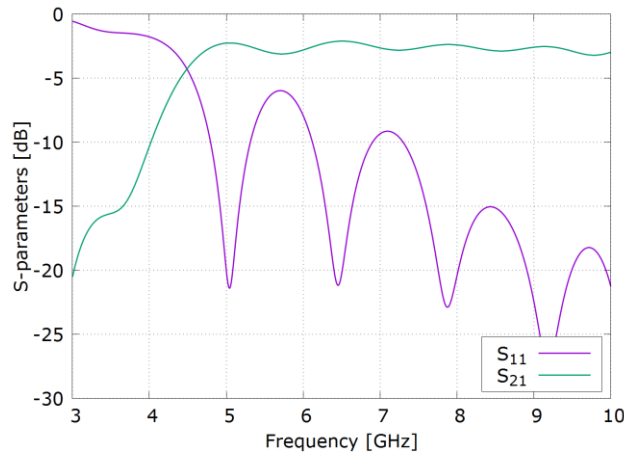
Figure 71 Simulated SIW characteristics for testing conductive threads.
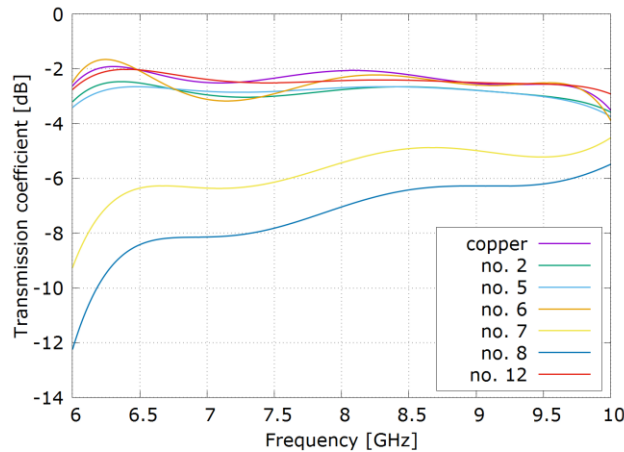
Figure 72 Frequency response of transmission coefficient of SIW
with sidewalls created from conductive threads.

6.3 Conclusions

The resistivity of fifteen conductive threads was measured and some threads were tested as sidewalls of SIW. The threads were loaded by two loads during the resistivity measurement to

achieve the same conditions for threads. Threads were measured by an RLC meter at four different frequencies. Threads, which have resistance lower than 100 Ohms, were used as sidewalls of SIW. This practical test shows that threads with a low DC resistivity are not any time the best choice for this type of application and the selection depend on the material of the thread and its construction.

For manufacturing TIW structures, threads no. 6 and 12 can be recommended. Both threads are PAD/silver based with a relatively high linear mass density, but the diameter of the thread number 6 is 0.3 mm and the diameter of the thread number 12 is 1 mm. Due to this reason, the thread no. 6 is suitable for more applications, machine sewing and hand sewing.

7 Summary

The dissertation thesis was aimed to extend possibilities of textile-integrated electronics. Attention was turned to high frequency circuits integrated into textile substrates, especially. The basic concepts of planar antennas and circuits were advanced to ensure a reliable operation in ISM bands 5.8 GHz and 24 GHz, and the band group 6 UWB band.

Textile-integrated electronics has been intensively researched for last 30 years. Nevertheless, only few products based on textile-integrated electronics is commercially available to operate without a plastic box or another protection. Research outputs in field of textile-integrated electronics are interesting but manufacturing and integration are difficult and expensive. Last but not least, the problems with durability of textile-integrated electronics in clothing have not been solved yet sufficiently. But clothing is not the only application field of textile-integrated electronics. Promising applications of textile-integrated electronics appear also in the area of homecare systems and vehicles.

In the thesis, attention is turned to vehicular applications (cars, busses, airplanes). Thanks to the textile-integrated electronics, purely textile upholstery and seat covers can obtain additional functions. The upholstery-integrated electronics can be:

- Relatively large because textile materials cover relatively large surfaces;

- Durable because upholstery is not washed and is protected by a cover layer (glass-laminate panels in airplanes);

- Reliable because integrated communication busses or sensor networks are supported by a planar, firm surface of a vehicle.

The role of the main building block of textile-integrated electronics is played by textile-integrated waveguides (TIW). In the *State of the Art*, the progress in the TIW-based integration of microwave components was documented, and particular manufacturing options were discussed comprising screen printing, inkjet printing and embroidering. In order to create side walls of TIW, various approaches were presented including metal eyelets, conductive threads or conductive textiles. Advanced circuits were shown to be implemented by the combinations of conventional substrates, integrated buttons and elementary semiconductor elements.

The PhD thesis was aimed to meet three main objectives:

Objective 1

The methodology of designing the transition between a microstrip line on a conventional substrate and a textile-integrated waveguide was presented in Chapter 3. The transition was constructed using a current probe placed into the waveguide. The transition is similar to the transition between a coaxial connector and a SIW.

In the thesis, two transitions were proposed. The first transition was optimized for the ISM frequency band 5.8 GHz and the second one for the UWB frequency band 8 GHz. Results indicate that the transitions are suitable for narrowband applications. The attenuation of transitions (including SMA connectors) was 3.32 dB for the 5.8 GHz ISM band and varied from 1.1 dB to 4.3 dB for in the band group 6 UWB band.

Objective 2

The methodology of designing a textile-integrated waveguide switch was presented in Chapter 4. The switch was based on a T divider completed by PIN diodes playing the role of control elements. The divider was optimized for the textile integration. Achieved parameters were worse than those available in [41, 42]. This result was caused by larger manufacturing tolerances, by the use of PIN diodes with a larger package and stronger parasitic properties. The improper transition between the SMA connector and the TIW is another disadvantage.

The divider was designed for the working frequency 5.8 GHz and was manufactured by screen printing. The following parameters were measured: reflection from the input port −14.60 dB, transmission to the open port −6.21 dB and transmission to the closed port −14.92 dB.

Objective 3

The methodology of designing a circularly polarized antenna for operation frequencies 5.8 GHz and 24 GHz was described in Chapter 5. Two versions of the antenna were implemented – the first one was manufactured using a copper foil and the second one was produced by screen-printing. Properties of both the antennas were experimentally verified. Antennas achieved gains ranging from 4 to 6 dBi. The circular polarization of the antennas was proven by measuring the axial ratio, which was 1 dB in the minimum.

In case of antennas optimized for the frequency 24 GHz and manufactured by screen printing, the resonant frequency was shifted due to the manufacturing limitations.

References

[1]   HUGHES-RILEY, T., DIAS, T., CORK, C. A Historical Review of the Development of Electronic Textiles. *Fibers* [online]. 2018, **6**(2), 34. doi: 10.3390/fib6020034

[2]   GU, J., GORGUTSA, S., SKOROBOGATIY, M. A fully woven touchpad sensor based on soft capacitor fibers. 2011, 20.

[3]   AN, X., STYLIOS, G. A Hybrid Textile Electrode for Electrocardiogram (ECG) Measurement and Motion Tracking. *Materials (Basel, Switzerland)* [online]. 2018, **11**(10). ISSN 1996-1944. doi: http://dx.doi.org/10.3390/ma11101887

[4]   BOUWSTRA, S., CHEN, W., OETOMO, S. B., FEIJS, L. M. G., CLUITMANS, P. J. M. Designing for reliable textile neonatal ECG monitoring using multi-sensor recordings. In: *2011 Annual International Conference of the IEEE Engineering in Medicine and Biology Society* [online]. 2011, p. 2488–2491. doi: 10.1109/IEMBS.2011.6090690

[5]   PARADISO, R., LORIGA, G., TACCINI, N. A wearable health care system based on knitted integrated sensors. *IEEE Transactions on Information Technology in Biomedicine* [online]. 2005, **9**(3), 337–344. ISSN 1089-7771. doi: 10.1109/TITB.2005.854512

[6]   CARPI, F., ROSSI, D. D. Electroactive polymer-based devices for e-textiles in biomedicine. *IEEE Transactions on Information Technology in Biomedicine* [online]. 2005, **9**(3), 295–318. ISSN 1089-7771. doi: 10.1109/TITB.2005.854514

[7]   WIJESIRIWARDANA, R., MITCHAM, K., HURLEY, W., DIAS, T. Capacitive fiber-meshed transducers for touch and proximity-sensing applications. *IEEE Sensors Journal* [online]. 2005, **5**(5), 989–994. ISSN 1530-437X. doi: 10.1109/JSEN.2005.844327

[8]   SERGIO, M., MANARESI, N., TARTAGNI, M., GUERRIERI, R., CANEGALLO, R. A textile based capacitive pressure sensor. In: *2002 IEEE SENSORS* [online]. 2002, p. 1625–1630 vol.2. doi: 10.1109/ICSENS.2002.1037367

[9]   WIJESIRIWARDANA, R., MITCHAM, K., DIAS, T. Fibre-meshed transducers based real time wearable physiological information monitoring system. In: *Eighth International Symposium on Wearable Computers* [online]. 2004, p. 40–47. doi: 10.1109/ISWC.2004.20

[10]   QIN, Y., WANG, X., WANG, Z. Microfibre–nanowire hybrid structure for energy scavenging. *Nature* [online]. 2008, **451**(7180), 809–813. ISSN 0028-0836, 1476-4687. doi: 10.1038/nature06601

[11]   CUI, N., LIU, J., GU, L., BAI, S., CHEN, X., QIN, Y. Wearable Triboelectric Generator for Powering the Portable Electronic Devices. *ACS Applied Materials & Interfaces*

[online]. 2015, **7**(33), 18225–18230. ISSN 1944-8244, 1944-8252. doi: 10.1021/am5071688

[12] VELTEN, J., KUANYSHBEKOVA, Z., GÖKTEPE, Ö., GÖKTEPE, F., ZAKHIDOV, A. Weavable dye sensitized solar cells exploiting carbon nanotube yarns. *Applied Physics Letters* [online]. 2013, **102**(20), 203902. ISSN 0003-6951. doi: 10.1063/1.4807891

[13] UDDIN, M. J., DAVIES, B., DICKENS, T. J., OKOLI, O. I. Self-aligned carbon nanotubes yarns (CNY) with efficient optoelectronic interface for microyarn shaped 3D photovoltaic cells. *Solar Energy Materials and Solar Cells* [online]. 2013, **115**, 166–171. ISSN 0927-0248. doi: 10.1016/j.solmat.2013.03.025

[14] LIU, Y., GORGUTSA, S., SANTATO, C., SKOROBOGATIY, M. Flexible, Solid Electrolyte-Based Lithium Battery Composed of LiFePO4 Cathode and Li4Ti5O12 Anode for Applications in Smart Textiles. *Journal of The Electrochemical Society* [online]. 2012, **159**(4), A349–A356. ISSN 0013-4651, 1945-7111. doi: 10.1149/2.020204jes

[15] JOST, K., DION, G., GOGOTSI, Y. Textile energy storage in perspective. *Journal of Materials Chemistry A* [online]. 2014, **2**(28), 10776–10787. ISSN 2050-7496. doi: 10.1039/C4TA00203B

[16] OSMAN, M., RAHIM, M., SAMSURI, N., ALI, M. Compact and embroidered textile wearable antenna. In: *2011 IEEE International RF Microwave Conference* [online]. 2011, p. 311–314. doi: 10.1109/RFM.2011.6168756

[17] WANG, Z., ZHANG, L., PSYCHOUDAKIS, D., VOLAKIS, J. L. Flexible textile antennas for body-worn communication. In: *2012 IEEE International Workshop on Antenna Technology (iWAT)* [online]. 2012, p. 205–208. doi: 10.1109/IWAT.2012.6178647

[18] KAUFMANN, T., FUMEAUX, I., FUMEAUX, C. Comparison of fabric and embroidered dipole antennas. In: *2013 7th European Conference on Antennas and Propagation (EuCAP)*. 2013, p. 3252–3255.

[19] SEAGER, R. D., CHAURAYA, A., VARDAXOGLOU, J. C., DEMAAGT, P. Towards a compact low frequency woven antenna. In: *2009 IEEE Antennas and Propagation Society International Symposium* [online]. 2009, p. 1–4. doi: 10.1109/APS.2009.5171742

[20] CHAURAYA, A., ZHANG, S., WHITTOW, W., ACTI, T., SEAGER, R., DIAS, T., VARDAXOGLOU, Y. C. Addressing the challenges of fabricating microwave antennas using conductive threads. In: *2012 6th European Conference on Antennas and Propagation (EUCAP)*: *2012 6th European Conference on Antennas and Propagation (EUCAP)* [online]. 2012, p. 1365–1367. doi: 10.1109/EuCAP.2012.6205910

[21] IVSIC, B., BONEFACIC, D., BARTOLIC, J. Considerations on Embroidered Textile Antennas for Wearable Applications. *IEEE Antennas and Wireless Propagation Letters* [online]. 2013, **12**, 1708–1711. ISSN 1536-1225. doi: 10.1109/LAWP.2013.2297698

[22] TUDOR, J., VARDAXOGLOU, J., TORAH, R., LI, Y., WHITTOW, W., CHAURAYA, A., BEEBY, S., YANG, K. Inkjet printed dipole antennas on textiles for wearable

communications. *IET Microwaves, Antennas & Propagation* [online]. 2013, **7**(9), 760–767. ISSN 1751-8725, 1751-8733. doi: 10.1049/iet-map.2013.0076

[23] LI, Y., TORAH, R., BEEBY, S. P., TUDOR, J. Inkjet printed flexible antenna on textile for wearable applications. 2012.

[24] KARIMI, M. A., SHAMIM, A. A flexible inkjet printed inverted-F antenna on textile. In: *2016 IEEE Middle East Conference on Antennas and Propagation (MECAP)* [online]. 2016, p. 1–2. doi: 10.1109/MECAP.2016.7790101

[25] KRYKPAYEV, B., FAROOQUI, M., BILAL, R. M., VASEEM, M., SHAMIM, A. A wearable tracking device inkjet-printed on textile. *Microelectronics Journal* [online]. 2017, **65**, 40–48. ISSN 0026-2692. doi: 10.1016/j.mejo.2017.05.010

[26] KAZANI, I., HERTLEER, C., DE MEY, G., SCHWARZ, A., GUXHO, G., VAN LANGENHOVE, L. Electrical conductive textiles obtained by screen printing. *Fibres & Textiles in Eastern Europe*. 2012, **20**(1), 57–63.

[27] KAZANI, I., DECLERCQ, F., SCARPELLO, M. L., HERTLEER, C., ROGIER, H., GINSTE, D. V., MEY, G. D., GUXHO, G., LANGENHOVE, L. V. Performance Study of Screen-Printed Textile Antennas after Repeated Washing. *Autex Research Journal* [online]. 2014, **14**(2), 47–54. doi: 10.2478/v10304-012-0049-x

[28] KELLOMÄKI, T., VIRKKI, J., MERILAMPI, S., UKKONEN, L. Towards washable wearable antennas: a comparison of coating materials for screen-printed textile-based UHF RFID tags. *International Journal of Antennas and Propagation*. 2012, **2012**.

[29] BOZZI, M., MOSCATO, S., SILVESTRI, L., DELMONTE, N., PASIAN, M., PERREGRINI, L. Innovative SIW components on paper, textile, and 3D-printed substrates for the Internet of Things. In: *2015 Asia-Pacific Microwave Conference (APMC)* [online]. 2015, p. 1–3. doi: 10.1109/APMC.2015.7411615

[30] MORO, R., BOZZI, M., AGNEESSENS, S., ROGIER, H. Compact cavity-backed antenna on textile in substrate integrated waveguide (SIW) technology. In: *2013 European Microwave Conference* [online]. 2013, p. 1007–1010. doi: 10.23919/EuMC.2013.6686830

[31] MORO, R., AGNEESSENS, S., ROGIER, H., DIERCK, A., BOZZI, M. Textile Microwave Components in Substrate Integrated Waveguide Technology. *IEEE Transactions on Microwave Theory and Techniques* [online]. 2015, **63**(2), 422–432. ISSN 0018-9480, 1557-9670. doi: 10.1109/TMTT.2014.2387272

[32] VASINA, P., LACIK, J. Textile linear polarization reconfigurable ring slot antenna for 5.8 GHz band. In: *2017 Conference on Microwave Techniques (COMITE)* [online]. 2017, p. 1–4. doi: 10.1109/COMITE.2017.7932311

[33] KAUFMANN, T., XU, Z., FUMEAUX, C. Wearable substrate-integrated waveguide with embroidered vias. In: *The 8th European Conference on Antennas and Propagation (EuCAP 2014)* [online]. 2014, p. 1746–1750. doi: 10.1109/EuCAP.2014.6902130

[34] XU, Z., KAUFMANN, T., FUMEAUX, C. Wearable Textile Shielded Stripline for Broadband Operation. *IEEE Microwave and Wireless Components Letters* [online]. 2014, **24**(8), 566–568. ISSN 1531-1309. doi: 10.1109/LMWC.2014.2321060

References

[35]   AGNEESSENS, S., LEMEY, S., VERVUST, T., ROGIER, H. Wearable, Small, and Robust: The Circular Quarter-Mode Textile Antenna. *IEEE Antennas and Wireless Propagation Letters* [online]. 2015, **14**, 1482–1485. ISSN 1536-1225. doi: 10.1109/LAWP.2015.2389630

[36]   MORO, R., AGNEESSENS, S., ROGIER, H., BOZZI, M. Wearable textile antenna in substrate integrated waveguide technology. *Electronics Letters*. 2012, **48**(16), 985–987.

[37]   LEMEY, S., AGNEESSENS, S., ROGIER, H. Textile SIW antennas as hybrid energy harvesting and power management platforms. In: *2015 European Microwave Conference (EuMC)* [online]. 2015, p. 20–23. doi: 10.1109/EuMC.2015.7345689

[38]   KAUFMANN, T., FUMEAUX, C. Wearable Textile Half-Mode Substrate-Integrated Cavity Antenna Using Embroidered Vias. *IEEE Antennas and Wireless Propagation Letters* [online]. 2013, **12**, 805–808. ISSN 1536-1225. doi: 10.1109/LAWP.2013.2270939

[39]   WEI, S., YANG, C., CHEN, Y., CHEN, T., CHANG, C. V- and W-Band Substrate Integrated Waveguide (SIW) Mechanical Switch. *IEEE Transactions on Microwave Theory and Techniques* [online]. 2018, **66**(6), 3090–3098. ISSN 0018-9480. doi: 10.1109/TMTT.2018.2825381

[40]   GHIOTTO, A., ADHIKARI, S., WU, K. Ferrite-Loaded Substrate Integrated Waveguide Switch. *IEEE Microwave and Wireless Components Letters* [online]. 2012, **22**(3), 120–122. ISSN 1531-1309. doi: 10.1109/LMWC.2012.2183859

[41]   LIM, I., LIM, S. Substrate-Integrated-Waveguide (SIW) Single-Pole-Double-Throw (SPDT) Switch for X-Band Applications. *IEEE Microwave and Wireless Components Letters* [online]. 2014, **24**(8), 536–538. ISSN 1531-1309. doi: 10.1109/LMWC.2014.2321065

[42]   NUMAN, A. B., FRIGON, J., LAURIN, J. Single-Pole Single-Throw Switch for Substrate-Integrated Waveguide. *IEEE Microwave and Wireless Components Letters* [online]. 2018, **28**(3), 221–223. ISSN 1531-1309. doi: 10.1109/LMWC.2018.2804259

[43]   XU, R. F., IZQUIERDO, B. S., YOUNG, P. R. Switchable Substrate Integrated Waveguide. *IEEE Microwave and Wireless Components Letters* [online]. 2011, **21**(4), 194–196. ISSN 1531-1309. doi: 10.1109/LMWC.2011.2108274

[44]   CHEN, H., CHE, W., ZHANG, T., CHAO, Y., FENG, W. SIW SPDT switch based on switchable HMSIW units. In: *2016 IEEE International Workshop on Electromagnetics: Applications and Student Innovation Competition (iWEM)* [online]. 2016, p. 1–3. doi: 10.1109/iWEM.2016.7504980

[45]   KLEMM, M., LOCHER, I., TROSTER, G. A novel circularly polarized textile antenna for wearable applications. In: *7th European Conference on Wireless Technology, 2004.* 2004, p. 285–288.

[46]   RAIS, N. H. M., SOH, P. J., MALEK, F., AHMAD, S., HASHIM, N. B. M., HALL, P. S. A review of wearable antenna. In: *2009 Loughborough Antennas Propagation Conference* [online]. 2009, p. 225–228. doi: 10.1109/LAPC.2009.5352373

References

[47] PINAPATI, S. P., KAUFMANN, T., LINKE, I., RANASINGHE, D., FUMEAUX, C. Connection strategies for wearable microwave transmission lines and antennas. In: *2015 International Symposium on Antennas and Propagation (ISAP)*. 2015, p. 1–4.

[48] CHEN, S. J., KAUFMANN, T., RANASINGHE, D. C., FUMEAUX, C. A Modular Textile Antenna Design Using Snap-on Buttons for Wearable Applications. *IEEE Transactions on Antennas and Propagation* [online]. 2016, **64**(3), 894–903. ISSN 0018-926X. doi: 10.1109/TAP.2016.2517673

[49] SEAGER, R. D., FLINT, J. A., FONSECA, D. S. Textile-to-rigid microstrip transition using permanent magnets. *Electronics Letters* [online]. 2015, **51**(9), 709–710. ISSN 0013-5194, 1350-911X. doi: 10.1049/el.2014.4361

[50] SUNTIVES, A., ABHARI, R. Transition Structures for 3-D Integration of Substrate Integrated Waveguide Interconnects. *IEEE Microwave and Wireless Components Letters* [online]. 2007, **17**(10), 697–699. ISSN 1531-1309. doi: 10.1109/LMWC.2007.905592

[51] CHAHAT, N., ZHADOBOV, M., MUHAMMAD, S. A., COQ, L. L., SAULEAU, R. 60-GHz Textile Antenna Array for Body-Centric Communications. *IEEE Transactions on Antennas and Propagation* [online]. 2013, **61**(4), 1816–1824. ISSN 0018-926X. doi: 10.1109/TAP.2012.2232633

[52] LOCHER, I., KLEMM, M., KIRSTEIN, T., TRSTER, G. Design and Characterization of Purely Textile Patch Antennas. *IEEE Transactions on Advanced Packaging* [online]. 2006, **29**(4), 777–788. ISSN 1521-3323. doi: 10.1109/TADVP.2006.884780

[53] BOZZI, M., GEORGIADIS, A., WU, K. Review of substrate-integrated waveguide circuits and antennas. *Antennas Propagation IET Microwaves* [online]. 2011, **5**(8), 909–920. ISSN 1751-8725. doi: 10.1049/iet-map.2010.0463

[54] POZAR, D. M. *Microwave Engineering*. 4 edition. Hoboken, NJ: Wiley, 2011. ISBN 978-0-470-63155-3.

[55] MIKULASEK, T., GEORGIADIS, A., COLLADO, A., LACIK, J. 2x2 Microstrip Patch Antenna Array Fed by Substrate Integrated Waveguide for Radar Applications. *IEEE Antennas and Wireless Propagation Letters* [online]. 2013, **12**, 1287–1290. ISSN 1536-1225, 1548-5757. doi: 10.1109/LAWP.2013.2283731

[56] DESLANDES, D. Design equations for tapered microstrip-to-Substrate Integrated Waveguide transitions. In: *2010 IEEE MTT-S International Microwave Symposium* [online]. 2010, p. 704–707. doi: 10.1109/MWSYM.2010.5517884

[57] IWASAKI, H. A circularly polarized small-size microstrip antenna with a cross slot - IEEE Journals & Magazine. *IEEE Transactions on Antennas and Propagation* [online]. 1996, **44**(10), 1399–1401. doi: 10.1109/8.537335

[58] KIN-LU WONG, CHIEN-CHIN HUANG, WEN-SHAN CHEN. Printed ring slot antenna for circular polarization. *IEEE Transactions on Antennas and Propagation* [online]. 2002, **50**(1), 75–77. ISSN 1558-2221. doi: 10.1109/8.992564

[59] CUPAL, M., DŘÍNOVSKÝ, J., GÖTTHANS, T., HERMÁNY, R., KOKOLIA, M., LÁČÍK, J., PAŘÍZEK, T., PRÁŠEK, J., RAIDA, Z., ŠPŮREK, J., KRÁČALOVÁ, D., LÉDROVÁ, Z., PROCHÁZKA, J., KRUTÍLEK, D., ŘEZNÍČEK, D. Textile-integrated

electronics for small airplanes. In: *12th European Conference on Antennas and Propagation (EuCAP 2018)* [online]. 2018, p. 1–5. doi: 10.1049/cp.2018.0845

[60]   COLLIER, A. M. *A Handbook of Textiles*. 2Rev Ed edition. Oxford; Toronto: ELSEVIER, 1975. ISBN 978-0-08-018057-1.

List of Figures

List of Tables

List of Symbols

f	frequency
ε_r	relative permittivity
f_c	critical frequency
f_{off}	cutoff frequency
C	capacity
L	inductance
R	resistivity
λ_g	wavelength inside waveguide
c	speed of light
δ	dielectric loss

List of Abbreviations

3D	Three dimensions
AR	Axial Ratio
BT	Bluetooth
ECG	Electrocardiogram
ECT	Electrically conductive textile
EEG	Electroencephalography
EM	Electromagnetic
HMSIW	Half mode substrate integrated waveguide
ISM	Industrial, Scientific and Medical
LFSIW	L-folded substrate integrated switch
LHCP	Left Hand Polarization
MCG	Magnetocardiogram
MCU	Micro-Controller Unit
MTL	Microstrip transmission line
PCB	Printed circuit board
PEC	Perfect electric conductor
PET	Polyethylene terephthalate
PIFA	Planar Inverted F Antenna
PIN	P intrinsic N diode
PU	Polyurethane
RF	Radio frequency
RFID	Radio frequency identification
RHCP	Right hand polarization
SIFW	Substrate integrated folded waveguide
SIW	Substrate integrated waveguide
SMA	sub miniature version A
SPDT	Single pole double through
TIE	Textile integrated electronics

TIW	Textile integrated waveguide
UHF	Ultra height frequency
UV	Ultra-violet
UWB	Ultra wide band
VNA	Vector analyzer

Curriculum Vitae

Miroslav Cupal

Družstevní 890   email: xcupal02@phd.feec.vutbr.cz
572 01 Polička   phone: +420 736 616 695
Czech Republic

Education

2015 – current	Brno University of Technology, Brno, Czech Republic Ph.D., Electronics and Communication Research topic: Textile-integrated electronics
2013 – 2015	Brno University of Technology, Brno, Czech Republic MSc., Electronics and Communication Diploma thesis: In-car wireless power transfer
2010 – 2013	Brno University of Technology, Brno, Czech Republic BSc., Electronics and Communication Bachelor thesis: Implantable antennas for biomedical telemetry

Working experience and research stays

3/2012 to 8/2012	OMKO Digital, a.s. Service technician of satellite receivers
7/2014 to 8/2014	RETIA, .a.s. Technician of antenna systems
9/2014 to 12/2020	SIX Research Centre PhD researcher
01/2020 to present	Brno University of Technology
09/2020 to present	SINTEX, a.s. Designer of textile integrated electronics

Research projects

2017 to 2019	Interdisciplinary research of wireless technologies Ministry of Education, Youth and Sports, LO1401

2016 to 2017	Tools for the synthesis of antennas and sensors Technology Agency of the Czech Republic, TA04010457
10/2016 to present	Intelligent upholstery of vehicles (INTELUP) Ministry of Industry and Trade, FV10087
07/2019 to present	Textile electronics for homecare and professional use (TED) Ministry of Industry and Trade, FV40385

Language

English

Software skills

CST Microwave Studio,
MATLAB,
Python,
ANSYS Electromagnetic Desktop,
PSpice

Author's Publications

[01] **CUPAL, M.**, RAIDA, Z.; Textile integrated waveguide switch for ISM band 5.8 GHz. *Microwave and Optical Technology Letters*, 2020. ISBN: 0895-2477. doi: https://doi.org/ 10.1002/mop.32242.

[02] **CUPAL, M.**, RAIDA, Z.; Textile-integrated microwave components: State of the Art. *Materials*, 2020. ISSN 1996-1944. Submitted.

[03] **CUPAL, M.**, RAIDA, Z.; Circularly polarized textile-integrated slot antenna: 5.8 GHz versus 24 GHz ISM band. *IEEE Transactions on Antennas and Propagation*, 2020. ISSN: 0018-926X. Submitted.

[04] **CUPAL, M.**; RAIDA, Z.; Frequency limits of textile-integrated components. In *International Conference on Microwave, Radar and Wireless Communications* MIKON 2020. Vilnius (Lithuania): Microwave and Radiolocation Foundation, 2020. Submitted.

[05] DŘÍNOVSKÝ, J.; LÁČÍK, J.; RAIDA, Z.; **CUPAL, M.**; KRUTÍLEK, D.; In-plane textile electronics: selection of optimum operation bands. In *International Conference on Microwave, Radar and Wireless Communications* MIKON 2020. Vilnius (Lithuania): Microwave and Radiolocation Foundation, 2020. Submitted.

[06] KRÁČALOVÁ, D.; PROCHÁZKA, J.; LÉDROVÁ, Z.; RAIDA, Z.; LÁČÍK, J.; DŘÍNOVSKÝ, J.; **CUPAL, M.**; Textile microwave substrates: Special types of 3D knitted materials. In *International Conference on Microwave, Radar and Wireless Communications* MIKON 2020. Vilnius (Lithuania): Microwave and Radiolocation Foundation, 2020. Submitted.

[07] LÁČÍK, J.; RAIDA, Z.; DŘÍNOVSKÝ, J.; **CUPAL, M.**; KRÁČALOVÁ, D.; PROCHÁZKA, J.; LÉDROVÁ, Z.; Characterization of 3D knitted substrates. In *International Conference on Microwave, Radar and Wireless Communications* MIKON 2020. Vilnius (Lithuania): Microwave and Radiolocation Foundation, 2020. Submitted.

[08] PROUZA, J.; **CUPAL, M.**; RAIDA, Z.; Qi standard-based textile-integrated wireless charger. In *International Conference on Microwave, Radar and Wireless Communications* MIKON 2020. Vilnius (Lithuania): Microwave and Radiolocation Foundation, 2020. Submitted.

[09] RAIDA, Z.; LÁČÍK, J.; DŘÍNOVSKÝ, J.; **CUPAL, M.**; PRÁŠEK, J.; KRÁČALOVÁ, D.; PROCHÁZKA, J.; LÉDROVÁ, Z.; Textile-integrated electronics: state of the art. In *International Conference on Microwave, Radar and Wireless Communications* MIKON 2020. Vilnius (Lithuania): Microwave and Radiolocation Foundation, 2020. Submitted.

[10] **CUPAL, M.**; LÁČÍK, J.; RAIDA, Z.; DŘÍNOVSKÝ, J.; GÖTTHANS, T.; PRÁŠEK, J. Textile integrated transmit unit. In *European Conference on Multifunctional Structures*. Barcelona (Spain): CIMNE, 2019, p. 142-146. ISBN: 978-8-4949-1944-2.

[11] **CUPAL, M.**; DŘÍNOVSKÝ, J.; GÖTTHANS, T.; HERMÁNY, R.; KOKOLIA, M.; LÁČÍK, J.; PAŘÍZEK, T.; PRÁŠEK, J.; RAIDA, Z.; ŠPŮREK, J.; KRÁČALOVÁ, D.; LEDROVÁ, Z.; PROCHÁZKA, J.; KRUTÍLEK, D.; ŘEZNÍČEK, Z. Textile-integrated electronics for small airplanes. In *European Conference on Antennas and Propagation EuCAP 2018*. London (United Kingdom): European Association on Antennas and Propagation, 2018. ISBN: 978-1-5090-3742-1.

[12] KUŘÁTKO, D.; RAIDA, Z.; **CUPAL, M.**; LAČÍK, J.; WÓJCIK, D.; KOUDELKA, V.; VEJMOLA, Č.; PIORECKÁ; V.; JIŘÍČEK, S.; PÁLENÍČEK, T.; BRUNOVSKÝ, M.

Electromagnetic modeling of rat's brain: comparison of models and solvers. In *International Workshop on Computing, Electromagnetics, and Machine Intelligence CEMi 2018*. Stellenbosch (South Africa): Stellenbosch University, 2018. ISBN: 978-1-5386-7845-9.

[13] LÁČÍK, J.; KOUDELKA, V.; RAIDA, Z.; **CUPAL, M.**; KUŘÁTKO, D.; WÓJCIK, D., JIŘÍČEK, S.; PIORECKÁ, V.; VEJMOLA, C.;PÁLENÍČEK, T.;BRUNOVSKÝ, M. EEG forward problem modeling: comparison of FieldTrip-SimBio and CST EM Studio. In *International Workshop on Computing, Electromagnetics, and Machine Intelligence CEMi 2018*. Stellenbosch (South Africa): Stellenbosch University, 2018. ISBN: 978-1-5386-7845-9.

[14] MRNKA, M.; **CUPAL, M.**; RAIDA, Z.; PIETRIKOVÁ, A.; KOCUR, D. Millimeter-wave dielectric resonator antenna array based on directive LTCC elements. *IET Microwaves Antennas & Propagation*, 2018, vol. 12, no. 5, p. 662-667. ISSN: 1751-8725.

[15] **CUPAL, M.**; RAIDA, Z. Textile integrated waveguide switch. In *International Conference on Broadband Communications for Next Generation Networks and Multimedia Applications CobCom 2018*. Graz (Austria): IEEE, 2018. ISBN: 978-1-5386-4157-6.

[16] **CUPAL, M.**; RAIDA, Z. Circularly polarized substrate integrated textile antenna for ISM band 24 GHz. In *International Conference on Electromagnetics in Advanced Applications ICEAA 2017*. Verona (Italy): IEEE, 2017, p. 1154-1157. ISBN: 978-1-5090-4450-4.

[17] **CUPAL, M.**; RAIDA, Z.; VÉLIM, J. Transition adapters for 3D textile substrates. In *Microwave and Radio Electronics Week MAREW 2016*. Brno: IEEE, 2017. ISBN: 978-1-5090-4594-5.

[18] **CUPAL, M.**; LÁČÍK, J.; MRNKA, M.; RAIDA, Z.; VÉLIM, J. Wireless body area networks: numerical, experimental and approximate characterization. In *International Conference on Mathematical Methods in Electromagnetic Theory MMET 2016*. Lvov: IEEE East Ukraine Joint Chapter, 2016, p. 130-133. ISBN: 978-1-5090-1956-4.

[19] ŠPŮREK, J.; VÉLIM, J.; **CUPAL, M.**; RAIDA, Z.; PRÁŠEK, J.; HUBÁLEK, J. Slot loop antennas printed on 3D textile substrate. In *International Conference on Microwave, Radar and Wireless Communications MIKON 2016*. Krakow (Poland): Microwave and Radiolocation Foundation, 2016. ISBN: 978-1-5090-2213-7.

[20] **CUPAL, M.**; RAIDA, Z. H-plane SIW horn antenna for on-body communication. In *International Conference RADIOELEKTRONIKA 2016*. Brno (Czech Republic): IEEE, 2016, p. 427-432. ISBN: 978-1-5090-1673-0.

[21] MRNKA, M.; **CUPAL, M.**; RAIDA, Z.; PIETRIKOVÁ, A.; KOCUR, D. Millimeter- wave directive dielectric resonator antenna based on LTCC. In *Loughborough Antennas and Propagation Conference LAPC 2016*. Loughborough (United Kingdom): IEEE, 2016. ISBN: 978-1-5090-0783-7.

[22] RAIDA, Z.; VÉLIM, J.; **CUPAL, M.**; KRUTÍLEK, D. Wireless power transmission in small airplanes. In *Wireless Power Transfer Conference WPTC 2016*. Aveiro (Portugal): University of Aveiro, 2016. ISBN: 978-1-4673-7986-1.